

AD-A213 793

DTIC FILE COPY

ESL-TR-87-23

# A LITERATURE REVIEW OF GEOTECHNICAL CENTRIFUGE MODELING WITH PARTICULAR EMPHASIS ON ROCK MECHANICS

P.J. JOSEPH, H.H. EINSTEIN, R.V. WHITMAN

MASSACHUSETTS INSTITUTE OF TECHNOLOGY  
DEPARTMENT OF CIVIL ENGINEERING  
CAMBRIDGE, MASSACHUSETTS 02139

JUNE 1988

FINAL REPORT

APRIL 1986 - DECEMBER 1986

DTIC  
ELECTE  
OCT 30 1989  
S D

APPROVED FOR PUBLIC RELEASE: DISTRIBUTION UNLIMITED



ENGINEERING & SERVICES LABORATORY  
AIR FORCE ENGINEERING & SERVICES CENTER  
TYNDALL AIR FORCE BASE, FLORIDA 32403

89 10 27 180

NOTICE

PLEASE DO NOT REQUEST COPIES OF THIS REPORT FROM  
HQ AFESC/RD (ENGINEERING AND SERVICES LABORATORY).

ADDITIONAL COPIES MAY BE PURCHASED FROM:

NATIONAL TECHNICAL INFORMATION SERVICE  
5285 PORT ROYAL ROAD  
SPRINGFIELD, VIRGINIA 22161

FEDERAL GOVERNMENT AGENCIES AND THEIR CONTRACTORS  
REGISTERED WITH DEFENSE TECHNICAL INFORMATION CENTER  
SHOULD DIRECT REQUESTS FOR COPIES OF THIS REPORT TO:

DEFENSE TECHNICAL INFORMATION CENTER  
CAMERON STATION  
ALEXANDRIA, VIRGINIA 22314

UNCLASSIFIED

SECURITY CLASSIFICATION OF THIS PAGE

## REPORT DOCUMENTATION PAGE

Form Approved  
OMB No. 0704-0188

1a. REPORT SECURITY CLASSIFICATION UNCLASSIFIED			1b. RESTRICTIVE MARKINGS		
2a. SECURITY CLASSIFICATION AUTHORITY			3. DISTRIBUTION / AVAILABILITY OF REPORT		
2b. DECLASSIFICATION / DOWNGRADING SCHEDULE			Approved for public release Distribution unlimited		
4. PERFORMING ORGANIZATION REPORT NUMBER(S)			5. MONITORING ORGANIZATION REPORT NUMBER(S)		
			ESL-TR-87-23		
6a. NAME OF PERFORMING ORGANIZATION Massachusetts Institute of Technology		6b. OFFICE SYMBOL (If applicable)	7a. NAME OF MONITORING ORGANIZATION		
			Air Force Engineering and Services Center		
6c. ADDRESS (City, State, and ZIP Code)			7b. ADDRESS (City, State, and ZIP Code)		
Department of Civil Engineering Cambridge, Massachusetts 02139			HQ AFESC/RDCS Tyndall Air Force Base, Florida 32403-6001		
8a. NAME OF FUNDING / SPONSORING ORGANIZATION		8b. OFFICE SYMBOL (If applicable)	9. PROCUREMENT INSTRUMENT IDENTIFICATION NUMBER		
			Contract # DACA88-86-D-0013		
8c. ADDRESS (City, State, and ZIP Code)			10. SOURCE OF FUNDING NUMBERS		
			PROGRAM ELEMENT NO.	PROJECT NO.	TASK NO.
			6.2	2673	0074
					WORK UNIT ACCESSION NO.
					N/A
11. TITLE (Include Security Classification)					
A Literature Review of Geotechnical Centrifuge Modeling with Particular Emphasis on Rock Mechanics					
12. PERSONAL AUTHOR(S)					
P. G. Joseph, H. H. Einstein, R. V. Whitman					
13a. TYPE OF REPORT		13b. TIME COVERED		14. DATE OF REPORT (Year, Month, Day)	
Final		FROM Apr 86 to Dec 86		June 1988	
				15. PAGE COUNT	
				120	
16. SUPPLEMENTARY NOTATION					
Availability of this report is specified on reverse of front cover.					
17. COSATI CODES			18. SUBJECT TERMS (Continue on reverse if necessary and identify by block number)		
FIELD	GROUP	SUB-GROUP			
			Geotechnical Centrifuge Modeling      Rock Mechanics		
			Small-Scale Modeling                      Literature Review		
19. ABSTRACT (Continue on reverse if necessary and identify by block number)					
<p>Small-scale modeling of structural and geotechnical problems has a long history. Centrifuge modeling plays an increasingly important role in this context. This report summarizes geotechnical centrifuge work which has been done up to now with particular emphasis on rock mechanics. The reader will first be familiarized with the basic principles of small-scale and centrifuge modeling. In particular, the scaling relations based on first principles and on dimensional analysis are discussed in detail. Problematic aspects are mentioned and possible solutions are described. The second chapter is the summary of geotechnical centrifuge work. While the soils work is mentioned, it is in the form of an overview; in contrast rock mechanics and associated centrifuge research are more completely described. The report then provides the reader with a good background in the principles and application of geotechnical centrifuge modeling, while simultaneously creating the basis for the parallel report in which scaling relations for rock centrifuge modeling are established.</p>					
20. DISTRIBUTION / AVAILABILITY OF ABSTRACT			21. ABSTRACT SECURITY CLASSIFICATION		
<input checked="" type="checkbox"/> UNCLASSIFIED/UNLIMITED <input type="checkbox"/> SAME AS RPT. <input type="checkbox"/> DTIC USERS			UNCLASSIFIED		
22a. NAME OF RESPONSIBLE INDIVIDUAL			22b. TELEPHONE (Include Area Code)		22c. OFFICE SYMBOL
STEVEN T. KOENNEN, 2Lt, USAF			(904) 283-6298		HQ AFESC/RDCS

## PREFACE

This report was submitted as a dissertation to Massachusetts Institute of Technology, funded under Job Order Number 26730074 by the Air Force Engineering and Services Center, Engineering and Services Laboratory, Tyndall AFB, Florida 32403-6001.

This dissertation is being published in its original format by this laboratory because of its interest to the worldwide scientific and engineering community. This dissertation covers work performed between April 1986 and December 1986. AFESC/RD project officers were Paul L. Rosengren, Jr., and 1Lt Steven T. Kuennen.


This report has been reviewed by the Public Affairs Officer (PA) and is releasable to the National Technical Information Service (NTIS). At NTIS, it will be available to the general public, including foreign nationals.

This technical report has been reviewed and is approved for publication.

  
STEVEN T. KUENNEN, 2Lt, USAF  
Project Officer

  
WILLIAM S. STRICKLAND, GM-14  
Chief, Facility Systems and  
Analysis Branch

  
ROBERT J. MAJKA, Lt Col, USAF  
Chief, Engineering Research Division

  
JAMES R. VAN ORMAN  
Deputy Director of Engineering  
and Services Laboratory

INSPECTED  
4

1	2	3	4	5	6	7	8	9	10
11	12	13	14	15	16	17	18	19	20
21	22	23	24	25	26	27	28	29	30
31	32	33	34	35	36	37	38	39	40
41	42	43	44	45	46	47	48	49	50
51	52	53	54	55	56	57	58	59	60
61	62	63	64	65	66	67	68	69	70
71	72	73	74	75	76	77	78	79	80
81	82	83	84	85	86	87	88	89	90
91	92	93	94	95	96	97	98	99	100

A-1

## Table of Contents

	<u>Page Number</u>
Chapter 1	Model Testing Using the Centrifuge
1.1	Introduction
1.2	The Theory of Centrifuge Modeling
1.3	Advantages of Centrifuge Testing
1.4	Use of Scaled Model Tests
1.5	Relationship between Prototype and Model
1.6	Summary
Chapter 2	Geotechnical Applications of the Centrifuge
2.1	Introduction
2.2	Soil Mechanics
2.3	Rock Mechanics
2.4	Ice Mechanics
2.5	Tectonics
2.6	Conclusion
References	

(The reverse of this page is blank.)

## Chapter 1

### Model Testing Using the Centrifuge

#### 1.1 Introduction

Small scale models are a relatively inexpensive and convenient way of studying prototype behaviour. Consequently, they have been used extensively in various fields of engineering. In certain prototypes, however, stresses due to self weight play a major role, and so, should be reproduced to scale in the model. This can be done by placing the model in a centrifuge.

Probably the earliest mention of a centrifuge to simulate self weight effects was by Phillips (1869) who suggested that it be used to simulate self weight stresses in structural beams. As this was a relatively minor problem, the use of a centrifuge for modelling was not further pursued until Bucky (1931) used the centrifuge to study mining problems. Independently of Bucky, two Russian scientists, Pokrovsky (1933) and Davidenkov (1933) came up with the same idea. In the following decades, only a few centrifuge research projects were pursued in the U.S., namely, those by Panek (1949) and Clark (late fifties and early sixties), in Rock Mechanics. In Russia, however, the centrifuge seems to have seen frequent use, although oriented toward specific design problems rather than providing basic input.

Early centrifuge work outside the U.S. and Russia was done by Ramberg (1963) in Sweden, to study gravity tectonics, and by Hoek (1965) in South Africa, to study the effect of gravitational force fields in mine models. In England, Professor Schofield and his colleagues at the University of Cambridge built a prototype machine in 1966. Professor Schofield continued his work at the University of Manchester Institute of Science and Technology where he built a 1.5 m centrifuge in 1969. In the early 1970's, Professor Peter Rowe built a much larger capacity machine also at the University of

Manchester, in the Simon Engineering laboratory. In the meantime, Professor K. H. Roscoe at Cambridge University had been given £40,000 towards the construction of a centrifuge with a 10 m rotor arm. In 1974, Professor Schofield rejoined Cambridge University and took charge of the group. Thereafter, centrifuge testing of problems involving soil started in earnest, with various professors from other countries visiting Cambridge to study the centrifuge technique. During this period, Japan, Denmark, Sweden, Netherlands and France developed centrifuge modelling facilities.

In the midseventies, in the U.S.A., there was a renewed interest in centrifuge modeling of geotechnical problems. Professor R.F. Scott was active in centrifuge modeling in 1975. The University of California at Davis obtained a 1 meter radius centrifuge in 1976. Dr. R.M. Schmidt of Boeing started cratering experiments on a 1-meter centrifuge in 1976. In 1979, the National Science Foundation funded the modification of a large centrifuge located at NASA Ames Research Centre, Mountain View, California, for use in research in geotechnical engineering. As of this date, the centrifuge is not yet ready. When complete, it will have a nominal radius of 30 feet and carry 6,000 lbs. of soil at 300 g's and with subsequent modification, 40,000 lbs. at 100 g's, thus making it the largest capacity centrifuge in the U.S.A. As of now, several universities in the U.S. have developed or are in the process of developing centrifuge facilities for geotechnical research. The University of California at Davis has been proposed as a center for Geotechnical Centrifuge modeling. The goals of this center will be to foster centrifuge modeling in the U.S.A. and to serve as a resource for experimenters in this field.

This report will cover the principles, advantages, and problems of centrifuge testing. It will discuss the use of scaled model tests, the various relationships between the model and prototype, and how to obtain them. It will examine the various uses that the centrifuge has been put to, for modelling soil, rock and ice behaviour, and for studying gravity tectonics.



## 1.2 The Theory of Centrifuge Modelling

This section will examine the basic theory on which centrifuge modelling is based. The underlying principle is that stresses at geometrically similar points in prototype and model should be the same. Bucky (1931) suggested a method for doing this: "To produce at corresponding points in a small scale model, the same unit stresses that exist in a full scale structure, the weight of the material of the model must be increased in the same ratio that the scale of the model is decreased with respect to the full scale structure. The effect of an increase in weight may be obtained by the use of centrifugal force, the model being placed in a suitable revolving apparatus." If the model and prototype are made of materials with identical mechanical properties, then the strains in the model and prototype will also be identical. In other words, if a  $\frac{1}{N}$  scale model of a prototype is spun at  $Ng$  on the centrifuge, then the model's behaviour is thought to be similar to the prototype's behaviour. For this to hold true, three assumptions must be satisfied. These are: 1) that the model is a correctly scaled version of the prototype; 2) that the  $\frac{1}{N}$  scaled model when subject to an ideal  $Ng$  gravity field (such as that acting on the surface on an  $Ng$  planet), behaves like the prototype at  $1g$ ; and 3) that the centrifuge produces this ideal gravitational field. These three assumptions will be examined in detail in the following sections. Emphasis will be placed on commenting on the effects which result from not fully satisfying the assumptions.

### 1.2.1 Assumption One

This assumption is that the model is an exactly scaled version of the prototype, which requires that the scaling relations between the model and prototype be satisfied. Such scaling relationships are obtained from either a

dimensional analysis of the relevant variables, or from consideration of the governing equation. The details of the two scaling approaches will be discussed later, while a summary is provided here:

If the suffixes 'p' and 'm' stand for prototype and model respectively, and  $L_p$  and  $L_m$  represent the length of the prototype and the length of the model respectively, then the relation

$$\frac{L_p}{L_m} = N \quad (1.1)$$

is a scaling relation and 'N' is the scale factor. Analogous scaling relations can be established for other properties i.e.: unit weight, velocity, acceleration, etc., whose scale factors may be the same as the scale factor for length, or may be different. In many cases however, exact similitude between model and prototype is not possible. In such cases, variables whose effects are known or which influence the behaviour in a relatively minor way, are allowed to deviate from their scaled values.

Scaling down a prototype, especially with large scale factors, may result in a loss of prototype detail. In some cases this may not be of importance, while in others, it may be crucial. For example, i.e. centrifuge modelling of gravity tectonics processes, the value of the scale factor 'N' is of the order of  $10^4$  [Ramberg (1965)]. In such a situation, modelling of a rock layer a few feet thick is not possible for reasons of practicality. However, since the structures being modelled have dimensions in the order of miles, this departure from exactness is not likely to influence results. In other cases, however, this may not be true. For example, thin seams in the prototype may control the behaviour being studied, and consequently will have to be correctly scaled and included in the model.

Scaling down a prototype may also result in parameters, which do not have an effect on prototype behaviour, significantly influencing model behaviour. These effects are known as scale effects since they arise as a result of scaling done to the prototype. For example, in studies of footing behavior using the centrifuge, the soil material is usually not scaled in grain size. In such a case, the model footing may be scaled down to the extent that the individual size of the grains would begin to affect the footing behaviour. Scale effects occur to some extent in all models. Their effects are reduced, by building the model as large as possible. One way to guard against scale effects is to check what is called the 'Internal Consistency' of the experiment using the 'Modelling of Models' technique. This technique consists of modelling the same prototype at different scales, by choosing the g level for each scale such that the product of each scale factor and its corresponding g level is always the same. So, if the results of a  $\frac{1}{100}$  scale model of a particular prototype, tested at 100g are the same as those of a  $\frac{1}{20}$  scale model of the same prototype tested at 20g, then one can conclude that the scale effects are not significant. Examples of parameters that could result in scale effects are grain size and surface roughness.

Apart from loss of prototype detail and scale effects, it may not be possible to model certain prototype characteristics. For example, the crystal structure of model ice may differ from that of the arctic sea ice being modelled. In such cases it has been suggested that results from the tests using model ice be modified analytically to account for the difference in ice crystal structure [Vinson (1982)].

### 1.2.2 Assumption Two

This assumption is that the  $\frac{1}{N}$  scale model when subject to an ideal  $Ng$  gravity field (such as that acting on the surface of an  $Ng$  planet), behaves like the prototype at  $1g$ . This assumption requires that for a correctly scaled model (see 1.2.1), the model material at  $Ng$  has the same material properties as the model material at  $1g$  since the scaling is done on the basis of the material properties at  $1g$ . It also requires that the phenomena that occur in the prototype at  $1g$  occur in the model at  $Ng$ . Each of these conditions can be examined in greater detail:

Schofield (1980) states that whatever the model material, its material properties do not change as the  $g$  level changes. Material properties, apart from the self-weight, are determined by the electron shells of the atoms of the materials involved. When the  $g$  field changes, the effects are felt at the centre of the mass of the atom, and not at the electron shells. Consequently, though the unit weight of the material may change, the material properties at  $Ng$  remain unaltered from those at  $1g$ .

While the material properties may remain unaltered, phenomena that occur in a prototype at  $1g$  may not always be reproduced in a correctly scaled model at  $Ng$ . Tan and Scott (1985) examined the case of a soil particle moving in a fluid and, as will be explained later, showed that behaviour in the  $Ng$  field was not the same as in a  $1g$  field.

### 1.2.3 Assumption Three

This assumption is that the centrifuge produces an ideal  $Ng$  gravitational field. An ideal gravitational field is considered to be the gravitational

field acting on the surface of an Ng planet. The earth can be considered an Ng planet, where N=1. Any mass resting on the surface of such a planet is subject to two forces that give it its weight. One force is the centrifugal force due to rotation of the planet about its axis while the other is due to gravity and is given by Newton's law of universal gravity. Thus the force acting on a body on the surface of a planet like the earth is given as

$$F = \frac{G m_1 m_2}{r^2} - m_1 \omega^2 r \quad (1.2)$$

where

F = Force acting on the mass resting on or in the earth

$m_1$  = Mass of the body on or in the earth

$m_2$  = Mass of the earth

r = The radius of the earth at that point

$\omega$  = Angular velocity of rotation of the earth

G = The universal gravitational constant.

In comparison with the quantity  $\frac{G m_1 m_2}{r^2}$ , the quantity  $m_1 \omega^2 r$  is so

small that it can be neglected. Also, it can be seen that the gravitational field on a planet is not a constant, but varies with distance from the center of the earth. However, up to depths normally encountered in geotechnical engineering, this change is so small that it can be neglected. Consequently, for normal civil engineering purposes, the acceleration due to gravity is considered constant, throughout the prototype.

The direction of the gravity field also changes on the surface as it acts towards the earth's center. However, for civil engineering projects, this change in direction is too small to consider. Hence, simulation of an ideal gravity field requires that the  $g$  level does not change in both magnitude and direction at all points within the model. As will be shown later, the centrifuge, while it does not provide an exact replication of the above conditions, comes very close to doing so. How it does this is discussed in the following paragraphs.

Let a mass 'M' be placed on the arm of the centrifuge at a distance of 'R' meters from the axis of rotation, and spun at an angular velocity of  $\omega$  rad/sec. There are two ways of looking at this body as it rotates in the centrifuge. One way is from a fixed external frame of reference, while the other is from a reference frame that rotates with the body. Any force that occurs in the rotating frame but not in the fixed frame is a pseudo force. Examples of pseudo forces are the centrifugal force and the coriolis force, both of which are discussed in the following paragraphs.

The tangential velocity of the mass as it rotates about the axis is given by  $\omega R$ . If the mass were unrestrained, it would shoot out with this velocity along a path tangential to the circumference of rotation. Viewed externally, the mass is pulled out from this straight line and around a curve of radius 'R' meters. When the rotation is uniform, it can be shown [see for example, Fundamentals of Physics by Halliday and Resnick (1981)], that there is an acceleration  $A = \omega^2 R$  that is always directed radially inward. This acceleration is called the centripetal acceleration. This centripetal acceleration acting on the rotating mass results in a force called the

centripetal force. Since this force acts in a fixed frame, it is a real force. When the reference frame rotates with the mass on the centrifuge, there will be a force acting radially outwards that is equal in magnitude to the centripetal force, but opposite in direction. This is the centrifugal force, and since it exists only in a moving reference frame, it is a pseudo force. The various forces are shown in Figure 1.1.

As explained previously, ideal conditions in an artificial  $g$  field require that the acceleration does not change in magnitude and direction at any point in the model. For the M.I.T. centrifuge (Figure 1.2), a typical model extends for a distance of about 0.15 times the radius, and subtends an arc of about  $\pm 0.15$  radians. This results in the acceleration vector not having the same magnitude and direction at all points in the model, and results in a model stress error, which, as will be shown, might be large enough to significantly influence results.

First the effect of model depth will be studied. Consider a model rotating at a distance ' $R$ ' from the center of rotation, at an angular velocity of  $\omega$  rad/sec. All points in the model are not equidistant from the axis of rotation and consequently, the acceleration field in the rotating model increases linearly with depth. The effect of this linearly varying  $g$  field is that the self weight stresses vary non linearly as shown in Figure 1.3, as opposed to the prototype case where stress variation is linear. This error in stress can be quantified [Schofield (1980)] as shown below.

At the upper surface, both the model and prototype have zero total stress. Now consider a point at a distance  $R$  from the axis of rotation, and at a depth ' $aR$ ' below the surface of the model. The acceleration at this point is  $\omega^2 R = Ng$  and consequently the scale factor at this point is  $N$ .

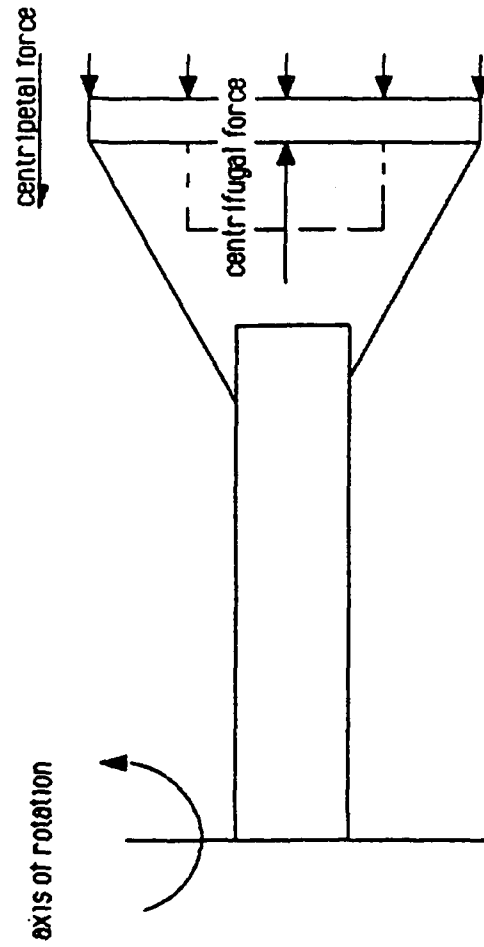


Fig. 1.1 Forces acting on a body rotating about an axis.



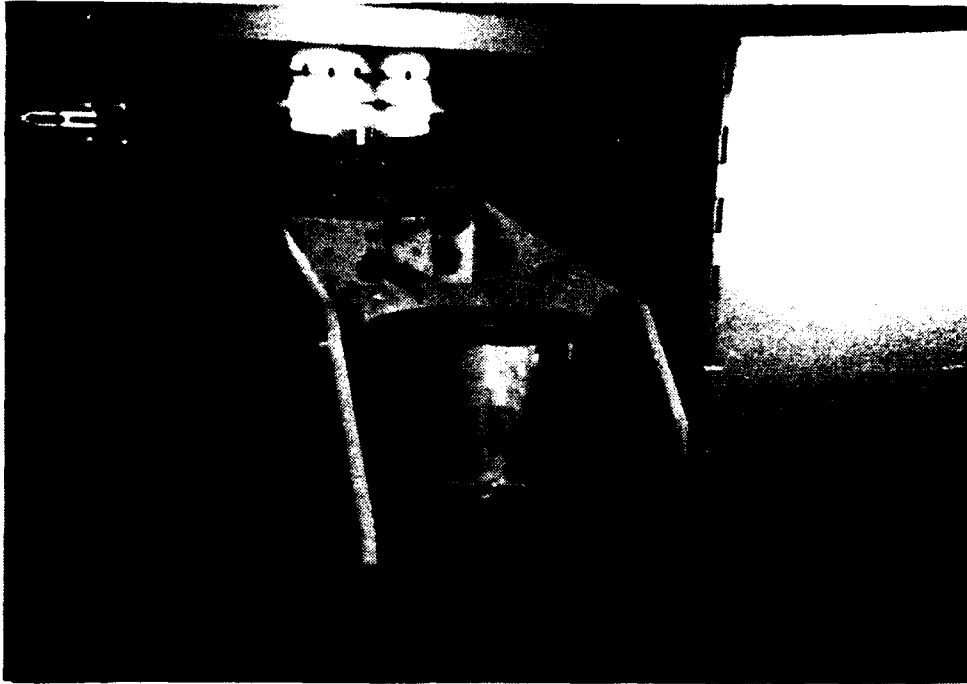


Fig.1.2. The M.I.T. Centrifuge

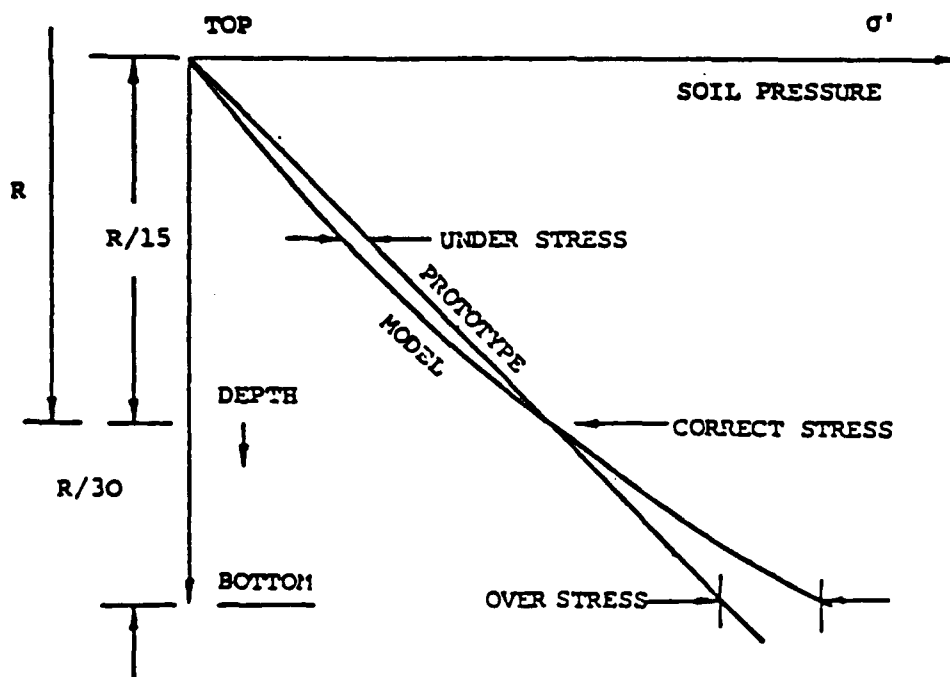


Fig.1.3. Model stress error with depth. From. Schofield (1980)

For the prototype, this point would correspond to a point at a depth  $NaR$ . The vertical stress at this point in the prototype would be

$$\sigma_v = \rho g N a R \quad (1.3)$$

where  $\rho$  is the mass density of the prototype material.

For the model in the centrifuge, however, the vertical stress at this point is given by an integration to the depth 'aR', since the acceleration field from  $R-aR = R(1-a)$  (the radius to the ground surface) to  $R$  is not constant. Consequently, the stress at this point in the model is given by

$$\begin{aligned} \sigma_v &= \int_{R(1-a)}^R \rho \omega^2 r \, dr \\ &= \frac{\rho \omega^2}{2} [r^2]_{R-aR}^R \\ &= \frac{\rho \omega^2}{2} [R^2 - (R-aR)^2 + 2aR^2 - a^2R^2] \\ &= \frac{\rho \omega^2}{2} a R^2 (2-a) \end{aligned} \quad (1.4)$$

Equating 1.3 and 1.4

$$\rho g N a R = \frac{\rho \omega^2 a R^2}{2} (2-a)$$

or

$$\frac{Ng}{\omega^2 R} = \frac{2-a}{2} \quad (1.5)$$

This relationship will be used in the following derivation.

Now, for points in the model at depths less than  $aR$ , there will be an understress in the model as compared to the prototype, and for points at depths greater than  $aR$ , there will be an overstress compared to the prototype. In other words, while stress in the prototype varies linearly as shown in Fig. 1.3, it varies parabolically in the model. The depth below the model surface at which they intersect is given by the reference depth  $aR$  and is the only depth in the model where the model stresses are exactly equal to the prototype stresses.

As indicated above, at all points between the surface and the point at depth  $aR$ , there is an understress. At depth  $\frac{aR}{2}$ , the model pressure is given by

$$\begin{aligned}
 \sigma_v &= \int_{R(1-a)}^{R(1-a/2)} \rho \, r \, \omega^2 \, dr = \left[ \frac{\rho \omega^2}{2} r^2 \right]_{R(1-a)}^{R(1-a/2)} \\
 &= \frac{\rho \omega^2}{2} R^2 \left( 1 + \frac{a^2}{4} - a - 1 - a^2 + 2a \right) \\
 &= \frac{\rho \omega^2}{2} R^2 a \left( 1 - \frac{3a}{4} \right) \quad (1.6)
 \end{aligned}$$

At the corresponding prototype depth, the stress is

$$\sigma_v = \rho \, g \, N \, a \, \frac{R}{2} \quad (1.7)$$

and consequently, the model error is

$$\begin{aligned}
 &\frac{\rho \, g \, N \, a \, R/2}{\rho \omega^2 R^2 a \left( \frac{4-3a}{4} \right)/2} - 1 \\
 &= \left( \frac{Ng}{\omega^2 R} \frac{4}{4-3a} \right) - 1 \quad (1.8)
 \end{aligned}$$

Substituting equation 1.5 into 1.8, we get the model understress as

$$\left( \frac{2-a}{2} \frac{4}{4-3a} \right) - 1 = \left( \frac{a}{4-3a} \right) \quad (1.9)$$

If for example  $a = \frac{1}{15}$ , then the error is less than 2%, which is negligible.

Below the depth  $aR$ , there is an overstress. For instance, at a depth  $\frac{3aR}{2}$ , it can be shown that the overstress is given by  $\frac{a}{4-a}$ . Hence, for a total model depth of  $\frac{3aR}{2} = \frac{R}{10}$ , with  $a = \frac{1}{15}$ , the stress error is less than  $\pm 2\%$ , which is insignificant.

For the MIT centrifuge, a typical radius is 47", and a typical model depth is  $\frac{R}{6}$ . For a total model depth of  $\frac{3aR}{2} = \frac{R}{6}$ , with  $a = \frac{1}{9}$ , the model stress error at depth  $\frac{aR}{2}$  below the model surface is about 3% and at depth  $\frac{3aR}{2}$  it is less than 3%. Thus, it is clear that the centrifuge very closely simulates the prototype body stresses, with any differences being so small as to be negligible.

Any rotating Ng planet or rotating model, when referenced to a moving framework, demonstrates effects due to a force called the Coriolis force. Since this force exists only with reference to an accelerating (non-Newtonian) framework, it too (like the centrifugal force) is a pseudo force. For a civil engineering prototype on a planet such as earth, the reference frame rotates so slowly that for all purposes it can be considered as fixed. Consequently, prototype civil engineering structures are not effected by the Coriolis force.\* For the model on the centrifuge, the model reference frame (which rotates with the centrifuge) is very much non-Newtonian, and consequently it may be that

---

\* Some projects with which civil engineers deal with may involve currents in bodies of air or water and can be influenced by Coriolis forces.

Coriolis forces play a role, resulting in a violation of assumption three. In order to determine if the resulting error is significant, it is necessary to derive an expression for the Coriolis force and see if it is significant when compared to the centrifugal force.

By Newton's second law, the rate of change of momentum is directly proportional to the change in force. For rotating bodies, the equivalents of linear momentum and force are angular momentum and torque. Thus, a change in angular momentum will be directly proportional to the change in torque.

Consider a particle of mass 'm' on a model rotating at a radius R with an angular velocity of  $\omega$  rad/sec, in a centrifuge. The angular momentum L of this particle is

$$L = m(\omega R) (R) = m \omega R^2 \quad (1.10)$$

Now, if this particle is made to move radially (inwards or outwards) its distance from the axis of rotation i.e. R, would change and consequently its angular momentum would change. The rate of change of angular momentum is given as

$$\frac{dL}{dt} = \frac{d}{dt} (m \omega R^2) = 2 m \omega R \frac{dR}{dt} = 2m \omega R V_R \quad (1.11)$$

where  $V_R$  is the velocity of the particle in the radial direction. This change in angular momentum results in a torque T given as

$$T = F_{CR} \cdot R = \frac{dL}{dt} = 2 m \omega R V_R \quad (1.12)$$

where  $F_{CR}$  is the Coriolis force, and is given by  $2 m \omega V_R$ . For a particle moving in the radial direction, the direction of the Coriolis force at any instant is tangential to the circle passing through the particle, and having its centre at the axis of rotation.

The Coriolis force also occurs if the particle moves around the circumference of a circle. Consequently, for tests involving dynamic shaking in the plane of rotation, the additional velocity in the circumferential

direction will result in a Coriolis force. The velocity in this case being tangential, the direction of the Coriolis force is radial. Since the direction of shaking reverses during one cycle of shaking, the model will feel an oscillating radial Coriolis force. The Coriolis force is always in the same direction relative to the velocity, irrespective of the direction of the velocity. It is at right angles to the velocity and of magnitude  $2m \omega V$ , where  $V$  is the velocity of the particle.

The Coriolis acceleration is given by

$$\frac{F_{CR}}{m} = 2\omega V \quad (1.13)$$

For a particle moving radially with a velocity  $V_R$  the ratio of

Coriolis acceleration to centrifuge acceleration is given by 
$$\frac{2 \omega V_R}{\omega^2 R} = \frac{2 V_R}{\omega R}$$

or, in other words,

$$\frac{\text{Coriolis Acceleration}}{\text{Centrifuge Acceleration}} = \frac{2 \times \text{Radial Velocity of Particle of Model}}{\text{Tangential Velocity of Model}} \quad (1.14)$$

If  $N = 100g$  and  $R = 1.2$  m, then  $\omega$  is about 29 rad/sec and the tangential velocity is about 35 m/sec. If for instance, in a seepage experiment the flow velocity (radial) is about  $\frac{1}{2}$  m/sec, then the error involved due to the Coriolis acceleration is  $2 \times \frac{1}{2} / 35 = 2.9\%$ . Hence, for most applications, the Coriolis force can be neglected, though for certain modelling situations where velocities are very high - for example, when modelling explosions in the centrifuge, account must be taken of the Coriolis force.

Assumption three also requires that the acceleration field be uniform in direction. In the centrifuge this is not the case, as the acceleration acts radially outwards. In figure 1.4, the resultant acceleration at point A acts radially outward and consequently can be resolved into two components  $Ng_V$  and  $Ng_H$ . The resultant acceleration at A is  $\omega^2(OA)$ .

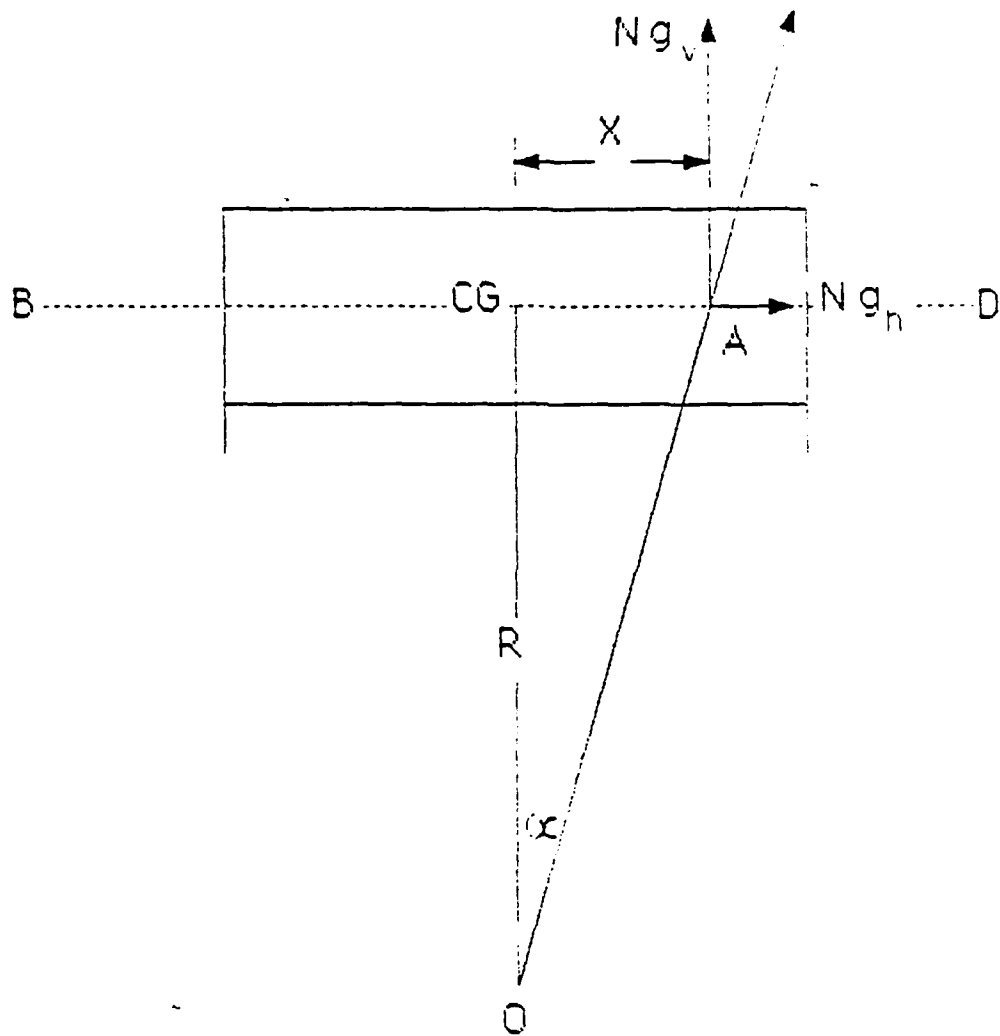


Fig. 1.4. Components of the  $g$  field.

Hence,  $Ng_V = \omega^2(OA) \cos \alpha$  and  $Ng_H = \omega^2(OA) \sin \alpha$

Now  $\cos \alpha = \frac{R}{OA}$  and  $\sin \alpha = \frac{X}{OA}$

Substituting for  $\cos \alpha$  and  $\sin \alpha$  in the expressions for  $Ng_V$  and  $Ng_H$  respectively, results in

$$Ng_V = \omega^2 R = Ng$$

$$\text{and} \quad Ng_H = \omega^2 X$$

In other words, the vertical component of acceleration  $Ng_V$  remains constant along BD, while the horizontal component of acceleration  $Ng_H$  varies linearly. Along a normal to BD, the reverse holds true, with the horizontal component of acceleration remaining constant, and the vertical component varying linearly [Andersen (1987)]. The horizontal acceleration  $Ng_H$  varies with g level and could effect the behaviour of the model in the centrifuge. For example, a slope that is stable at 1g should be stable at any higher g level, if the model material is purely frictional, with a constant friction angle. However, the presence of a horizontal force that increases with g level could result in instability at higher g levels. A series of braced excavation tests were run at M.I.T. For these tests, a typical value of R was 47" and the horizontal distance of the centroid of the failure wedge to the center of gravity of the package was about 3.7". At  $Ng = 120g$ ,  $\omega$  is about 31.4 rad/sec and consequently, at 3.7",

$$Ng_H = \omega^2 X = 3650 \text{ inches/sec}^2 \text{ or } 9.4g,$$

which is about 8% of  $Ng$ . Consequently, for these tests, the effect of  $Ng_H$  had to be taken into account.

Other sources of error arise from improper orientation of the platform and from the time required to reach the desired acceleration (known as spin up time or SUT). These two errors are discussed below.



For reasons of convenience, many geotechnical centrifuges have platforms that swing up. A few, such as Hoek's (1965) centrifuge (Fig. 1.5), and that at the Simon Engineering Laboratory at the University of Manchester, have platforms that are rigidly fixed, perpendicular to the axis of the centrifuge arm. The Cambridge centrifuge (Fig. 1.6) was initially a fixed platform type, but was later modified to a hybrid type with the platform swinging up, and then locking in the vertical position. The acceleration acting on the centrifuge platform or any mass resting on it is the resultant of the centrifugal acceleration and the earth's gravitational acceleration. Consequently, the resultant acceleration vector makes an angle  $\theta = \tan^{-1} \frac{g}{N_g}$  with the horizontal. A platform that is free to swing will rotate upwards until a line from the center of rotation to the CG of the the platform and package is parallel to the resultant acceleration vector. Friction at the pivots may cause under-rotation of the bucket. Similarly, during the test, if the center of gravity changes, then the bucket orientation will change. Either of these situations will result in the acceleration vector and the geostatic stresses being no longer perpendicular to the model ground surface. This error can be corrected [Bloomquist et al, (1984)] by designing the bucket to over rotate and then restraining it in the vertical direction by means of a restraining bracket, or by using an accelerometer and a small motor to make slight changes in the platform orientation. The second error is due to the startup time or 'SUT'. This is the time required by the centrifuge to reach the desired acceleration, when starting from rest. Some problems studied on the centrifuge do not depend on time or depend on time to a very small extent and consequently are not affected by the startup time. However, some problems, such as large strain consolidation, seepage, etc. are time dependent and consequently, neglecting the effect of the SUT could result in errors. Bloomquist et al, (1984), detail correction procedures. (Since the error is usually small, the correction procedure is not discussed in this report.)

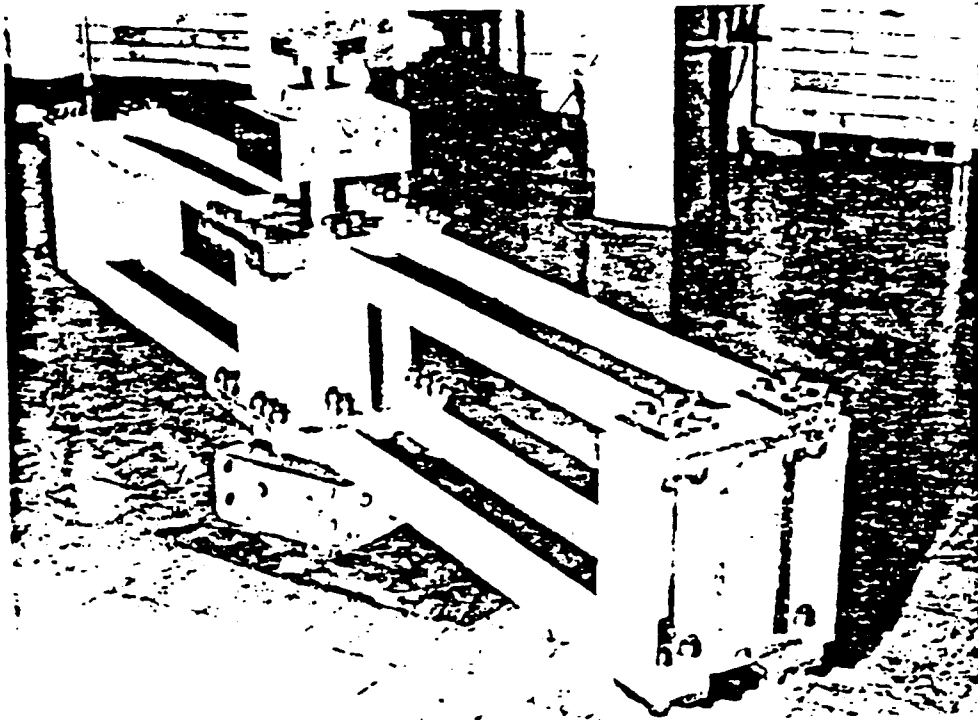


Fig.1.5. Photograph showing the principal constructional features of the CSIR centrifuge rotor. From Hoek (1965)

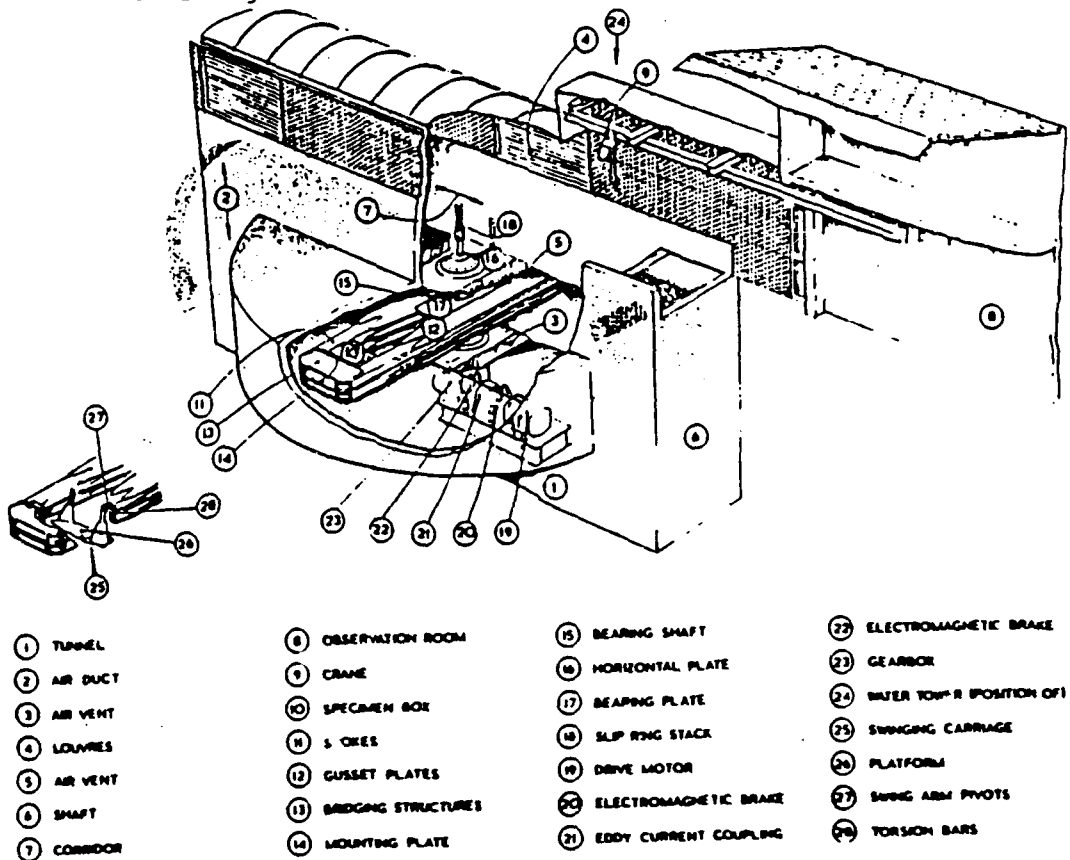


Fig.1.6. The Cambridge centrifuge. From Schofield (1980)

Finally, the centrifuge model container is a possible source of errors [Anandarajah et al (1985)]. The rigid boundaries of the container distort the stress distribution. For dynamic tests, waves are transmitted from side walls to the soil model through contact areas. Further, reflection of waves at the boundaries occur, possibly generating standing waves.

In view of all these errors, it may appear that the centrifuge does not produce the ideal  $N_g$  gravity field. However, most of the errors listed are small and can either be neglected or corrected. In other words, for all practical purposes, the centrifuge can be considered to produce a good simulation of an  $N_g$  field.

### 1.3 Advantages of Centrifuge Testing

If, through the use of correct prototype modelling and centrifuge procedure, the three assumptions discussed previously are satisfied, with acceptable approximation, then the technique offers significant advantages over modelling at  $1g$ , for problems in which gravity is a dominant factor in prototype behavior.

Modeling at  $1g$  does not produce the same stresses at corresponding points in the model and prototype. Most geotechnical materials are non-linear, as regards material properties and so the strains at these stress levels are not the same as those of the prototype. In other words, modeling at  $1g$  does not results in good model-prototype similitude. The basic principle of centrifuge modeling is that the stresses at various points in the model are approximately the same as those of corresponding points in the prototype. Consequently, if the same materials are used in the prototype, then the strains will be the same, resulting in an increased model-prototype similitude as regards observed model behaviour. Further, techniques to measure the material properties at low stresses need not be developed, since the stresses imposed on the materials are the actual prototype stresses. These are some of the major advantages of centrifuge testing.

Model studies using the centrifuge, if done correctly demonstrate behaviour that is close to prototype behaviour. Consequently, such test data can be used to validate existing theoretical models. Once the model is verified on the basis of centrifuge tests, then it can be used to run parametric studies of the prototype. If no theoretical model exists, then the data from the tests may provide added insight into the phenomenon, perhaps leading ultimately to the development of a theoretical model. This ability to provide realistic data for the verification/development of theoretical models is an important advantage of the centrifuge.

For these reasons, the centrifuge has been used extensively for the verification of theories, for the study of deformation and failure, for the study of problems involving the flow of water, as well as for various dynamic problems such as pile driving, earthquake effects, etc. Direct modeling of a particular prototype is sometimes suggested but as of yet, more research and development must be done before this can be successfully accomplished. For the reasons cited above, the centrifuge has been used to study a wide variety of problems in soil mechanics, rock mechanics, ice mechanics and gravity tectonics.

#### 1.4 Use of Scaled Model Tests

Before going into the details of obtaining scaling relations, it is worth considering under what circumstances centrifuge tests should be run and why. There are two basic approaches to centrifuge testing: 1) One uses well defined physical models for centrifuge testing, in order to generate data regarding prototype behavior. The data are compared to the results of a theoretical analysis of the prototype. If the results do not compare well, and if the physical modelling is correct, then the analytical (or numerical) model is modified until agreement with the centrifuge model data is obtained. Once this agreement is obtained, then for reasons of economy, the numerical model is

used to run parametric studies for the prototype. 2) In some cases however, not enough is known about the prototype phenomenon, so much so that no theoretical model exists. In such situations, models of the prototype which are as representative as possible are made and studied in the centrifuge to gain more insight into the phenomena of interest. As information about the phenomenon is collected, a better understanding of the processes involved is obtained. The link between theoretical or computer modelling and centrifuge simulation is shown in Fig. 1.7.

Whitman (1984) points out that only very rarely is centrifuge testing used directly for parametric studies in geotechnical engineering, as it is difficult to obtain exact similitude with a specific prototype. He suggests that centrifuge model tests be thought of as "small scale tests with full scale stress conditions rather than as exact replica model tests." In view of the limited data that often exist concerning prototype behavior, the centrifuge is potentially a useful tool, that must be used in combination with other techniques such as numerical methods, analytical methods, and field observations, in order to predict prototype behavior.

### 1.5 Relationship between Prototype and Model

Any relationship between a model and a prototype is called a scaling relationship. Scaling relationships are required for a) building a correctly scaled model of the prototype, and b) for converting the observed model behavior to prototype behavior. There are two ways of obtaining these scaling relationships. One way consists of using the governing equation of the phenomenon to be modelled, while the other employs the method of dimensional analysis.

#### 1.5.1 Method using the Governing Equation

Any physical phenomenon is governed by various physical factors which interact with one another. In some cases, enough is known about the phenomenon

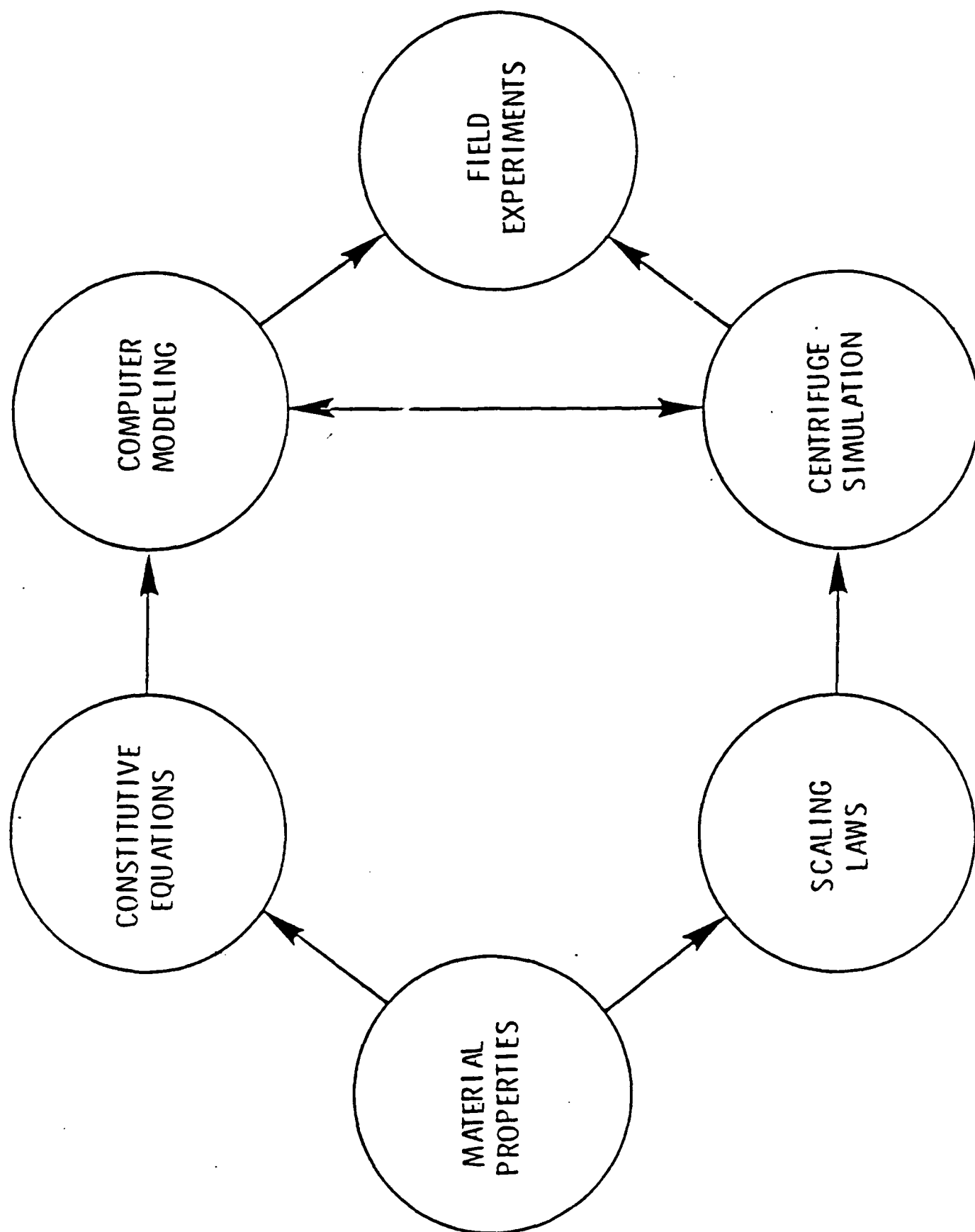


Fig. 1.7. Link between computer modelling and centrifuge simulation. From Sutherland (1982).

so that the physical factors involved can be identified and expressed in a relationship (often a differential equation) that expresses the way in which they interact, and which consequently models the phenomenon. If the governing governing equation is written for the model in terms of the model parameters expressed as a function of the prototype parameters, and compared with the prototype governing equation, then the scaling relation for the phenomena will be obtained. This can best be described by an example taken from Cheney (1982). The equation being modelled is the diffusion equation for a porous medium which is

$$\frac{du}{dt} = \frac{k}{a(1+e)\gamma} \left( \frac{\partial^2 u}{\partial x^2} + \frac{\partial^2 u}{\partial y^2} + \frac{\partial^2 u}{\partial z^2} \right) \quad (1.15)$$

where,  $u$  = excess pore water pressure

$e$  = void ratio

$k$  = permeability

$a$  = coefficient of compression

$\gamma$  = unit weight of pore fluid

Let the subscript 'p' refer to the prototype and the subscript 'm' to the model, and let the relationships between prototype and model dimensions be as follows

$$x_p = N x_m, \quad y_p = N y_m, \quad z_p = N z_m$$

Let the pore pressure, unit weight, time and permeability in the model and prototype be scaled as

$$u_p = \alpha_u u_m$$

$$\gamma_p = \alpha_\gamma \gamma_m$$

$$t_p = \alpha_t t_m$$

$$k_p = \alpha_k k_m$$

where the  $\alpha$ 's are scaling factors whose form is to be determined.

The differential equation of the prototype can be expressed in terms of the model parameters as

$$\frac{\partial \alpha_u u_m}{\partial \alpha_t t_m} = \frac{\alpha_k k_m}{a(1+e) \alpha_\gamma \gamma_m} \left[ \frac{\partial^2 (\alpha_u u_m)}{\partial (N x_m)^2} + \frac{\partial^2 (\alpha_u u_m)}{\partial (N y_m)^2} + \frac{\partial^2 (\alpha_u u_m)}{\partial (N z_m)^2} \right]$$

$$\text{i.e. } \frac{\alpha_u}{\alpha_t} \frac{\partial u_m}{\partial t_m} = \frac{\alpha_k k_m}{a(1+e) \alpha_\gamma \gamma_m} \frac{\alpha_u}{N^2} \left[ \frac{\partial^2 u_m}{\partial x_m^2} + \frac{\partial^2 u_m}{\partial y_m^2} + \frac{\partial^2 u_m}{\partial z_m^2} \right]$$

$$\text{i.e. } \frac{\partial u_m}{\partial t_m} = \frac{\alpha_t}{\alpha_u} \frac{\alpha_k}{\alpha_\gamma} \frac{\alpha_u}{N^2} \frac{k_m}{a(1+e) \gamma_m} \left[ \frac{\partial^2 u_m}{\partial x_m^2} + \frac{\partial^2 u_m}{\partial y_m^2} + \frac{\partial^2 u_m}{\partial z_m^2} \right]$$

$$\text{or } \frac{\partial u_m}{\partial t_m} = \frac{\alpha_t}{N^2} \frac{\alpha_k}{\alpha_\gamma} \frac{k_m}{a(1+e) \gamma_m} \left[ \frac{\partial^2 u_m}{\partial x_m^2} + \frac{\partial^2 u_m}{\partial y_m^2} + \frac{\partial^2 u_m}{\partial z_m^2} \right]$$

So, for similarity between the model and prototype equations,

$$\frac{\alpha_k \alpha_t}{N^2 \alpha_\gamma} = 1 \quad (1.16)$$

Now  $k = \frac{K\gamma}{\eta}$  where  $K$  is the physical permeability of the solid,  $\gamma$  the unit weight of the pore fluid and  $\eta$  the pore fluid viscosity. Let the relationships between the model and the prototype for the viscosity and physical permeability be

$$\eta_p = \alpha_\eta \eta_m$$

$$K_p = \alpha_K K_m$$

$$\text{Now } k_p = \alpha_k k_m = \frac{K_p \gamma_p}{\eta_p} = \frac{\alpha_K \alpha_\gamma}{\alpha_\eta} \frac{K_m \gamma_m}{\eta_m}$$

$$\text{i.e. } \alpha_k k_m = \frac{\alpha_K \alpha_\gamma}{\alpha_\eta} k_m$$

$$\text{or } \alpha_k = \frac{\alpha_K \alpha_\gamma}{\alpha_\eta} \quad (1.17)$$



Substituting this value of  $\alpha_K$  in Equation 1.16, we get

$$\frac{\alpha_K \alpha_\gamma \alpha_t}{N^2 \alpha_\gamma \alpha_\eta} = 1$$

$$\text{or} \quad \frac{\alpha_K \alpha_t}{N^2 \alpha_\eta} = 1 \quad (1.18)$$

In centrifuge modelling of geotechnical prototypes involving soil, it is usual to use the prototype soil in the model as the model soil then has the same material properties as the prototype soil. Scale effects do not arise unless, as previously discussed, the model is so small as to include only a few grains of soil. Consequently, if, in the modelling of diffusion, the model and prototype materials (solids and pore fluid) are the same, then

$$K_p = K_m \text{ or } \alpha_K = 1$$

and

$$\eta_p = \eta_m \text{ or } \alpha_\eta = 1$$

substituting these values of  $\alpha_K$  and  $\alpha_\eta$  in equation 1.18, we get

$$\alpha_t = N^2 \quad \text{or} \quad \frac{t_m}{t_p} = \frac{1}{N^2} \quad (1.19)$$

In other words, if model dimensions are  $\frac{1}{N}$  times prototype dimensions, and if both model and prototype materials are the same, then pore pressure dissipates  $N^2$  times faster in the model when compared with the prototype.

Scott and Morgan (1977) provide a set of scaling relations which were obtained with this approach. The only difficulty with this approach is that the governing equation of the phenomenon must be known. In some cases the governing equation may be based on assumptions that may not be really justified. In other cases, the phenomenon may be so complex that the

governing equation is not known. In such cases, the second approach, i.e. dimensional analysis should be used.

### 1.5.2 Method Using Dimensional Analysis

This method is more general than the governing equation method and is used where not enough is known about the prototype to formulate an equation that describes its behavior. The method will be briefly explained in this section with an example taken from Hoek (1965), showing how he modelled intact rock. While the general theory is described in detail by Langhaar (1951), here the basic procedure of dimensional analysis is summarized:

- a) Identify the independent variables that play a role in determining how the prototype behaves.
- b) Arrange these independent variables to form dimensionless products.
- c) Try and reproduce these dimensionless products in the model.

Thus the first step is to identify the variables involved. In order to do this, enough must be known about the problem so that it is understood, conceptually, whether and to what degree a variable influences the behavior. Hoek (1965) analysed an elastic material in thermal equilibrium. His approach was as follows: The behavior of a point in the structure, defined by coordinates  $x$ ,  $y$  and  $z$ , depends on the geometry of the structure, the material properties and the applied force field.

Let the geometry of the structure be defined as

$L$  = A typical length dimension, for example the diameter of a tunnel opening

$r^L$  = A set of dimensional ratios relating other dimensions of the structure to  $L$ .

Let the material properties of the prototype at this point  $(x, y, z)$  be defined as

$\rho$  = the density of the material

$E$  = the Young's modulus of the material

$\nu$  = the Poisson's ratio of the material

The material properties at any point in the structure depend on the state of stress, the direction of the bedding planes and, the material at that point. Consequently, the material properties at various points in the structure may not be the same as those at point  $x, y, z$ . If this is the case, then let the properties at the various points be related to the properties at point  $x, y, z$  by the set of dimensionless ratios  $r^{\rho}$ ,  $r^E$  and  $r^{\nu}$ .

The remaining area where similitude is required is in the applied stress conditions. The stresses imposed on the model consist of those that are applied externally, and those that are internal, such as a tectonic stress or a stress due to gravitational body forces. Let the applied loads, stresses, displacements and accelerations at point  $(x, y, z)$  be

$Q$  = an externally applied load

$P$  = an externally applied stress

$\sigma_0$  = an internal stress, due for example to tectonic stress

$g$  = an acceleration to which the entire body is subject to, and which results in self-weight body forces

$U_0$  = a displacement imposed directly on point  $x, y, z$  of the structure as a result of a force

$\gamma$  = an acceleration imposed directly on point  $x, y, z$  of the structure.

The applied loads, stresses, displacements and accelerations at other points may not be the same as those at point  $x, y, z$ . In this case, let them be related to those at the point  $x, y, z$  by a set of dimensionless ratios  $r^Q$ ,  $r^P$ ,  $r^{\sigma_0}$ ,  $r^{U_0}$ ,  $r^{\gamma}$ .

Now, the displacement ' $u$ ' or the stress ' $\sigma$ ' at point  $x, y, z$  is some function of the above variables, i.e. they are each defined by some at present unknown interaction among the above variables. Thus,

$$u = f(x, y, z, t, L, \rho, E, Q, P, \sigma_0, g, v, r^L, \dots, r^V) \quad (1.20)$$

and

$$\sigma = f(x, y, z, t, L, \rho, E, Q, P, \sigma_0, g, v, r^L, \dots, r^V) \quad (1.21)$$

Each variable in the above functions has dimensions which are some combination of the basic system of units, namely mass (M), length (L) and time (t). By suitably arranging these terms, dimensionless products can be formed, as follows.

a) Any dimensionless product  $\pi_i$  can be written as

$$\pi_i = u^{k_1} \sigma^{k_2} x^{k_3} y^{k_4} z^{k_5} t^{k_6} F^{k_7} \rho^{k_8} g^{k_9} P^{k_{10}} U_0^{k_{11}} \sigma_0^{k_{12}} L^{k_{13}} Q^{k_{14}} Y^{k_{15}} \quad (1.22)$$

Many dimensionless products can be written from these variables, but only a few will be independent of each other. By using the following procedure, a complete set of dimensionless products can be obtained. A set of dimensionless products of given variables is complete if each product in the set is independent of the others in the set, and any other dimensionless product of the variables, not in the set, is a product of powers of dimensionless products in the set.

b) Each variable can be written in terms of its basic dimensions as follows

$$\sigma^{k_2} = \left(\frac{M}{LT^2}\right)^{k_2} = \frac{M^{k_2}}{L^{k_2} T^{2k_2}} = \frac{M^{a_2} k_2}{L^{b_2 k_2} T^{c_2 k_2}}$$

$$\rho^{k_8} = \left(\frac{M}{L^3}\right)^{k_8} = \frac{M^{k_8}}{L^{3k_8}} = \frac{M^{a_8} k_8}{L^{b_8 k_8}}$$

and so on, where  $a_i$ ,  $b_i$  and  $c_i$  are constants.

c) For a product of several variables to be dimensionless, the condition is

$$\begin{array}{c}
 \begin{array}{cccccccccccccccc}
 1 & 2 & . & . & . & . & . & . & . & . & . & . & . & . & 15 \\
 u & \sigma & & & & & & & & & & & & & \gamma
 \end{array} \\
 \begin{array}{l}
 L \\
 M \\
 T
 \end{array}
 \begin{bmatrix}
 a_1 & a_2 & \dots & a_{15} \\
 b_1 & b_2 & \dots & b_{15} \\
 c_1 & c_2 & \dots & c_{15}
 \end{bmatrix}
 \begin{bmatrix}
 k_1 \\
 k_2 \\
 \vdots \\
 k_{15}
 \end{bmatrix}
 = 0
 \end{array}$$

For the case of Hoek's elastic solid, the variables can be written in the above form as follows.

$$\begin{array}{c}
 \begin{array}{cccccccccccccccc}
 1 & 2 & 3 & 4 & 5 & 6 & 7 & 8 & 9 & 10 & 11 & 12 & 13 & 14 & 15 \\
 u & \sigma & x & y & z & t & E & \rho & g & P & U_o & \sigma_o & L & Q & \gamma
 \end{array} \\
 \begin{array}{l}
 L \\
 M \\
 t
 \end{array}
 \begin{bmatrix}
 1 & -1 & 1 & 1 & 1 & 0 & -1 & -3 & 1 & -1 & 1 & -1 & 1 & 1 & 1 \\
 0 & 1 & 0 & 0 & 0 & 0 & 1 & 1 & 0 & 1 & 0 & 1 & 0 & 1 & 0 \\
 0 & -2 & 0 & 0 & 0 & 1 & -2 & 0 & -2 & -2 & 0 & -2 & 0 & -2 & -2
 \end{bmatrix}
 \begin{bmatrix}
 k_1 \\
 k_2 \\
 \vdots \\
 k_{15}
 \end{bmatrix}
 = 0
 \end{array}
 \quad (1.23)$$

Langhaar (1951) suggests that in general, the columns of this matrix be arranged so that the variables that appear first are the dependent variables. After the dependent variables, should come the variables that are easiest to regulate experimentally, and so on, until finally come the variables over which there is little or no control. In some cases, this arrangement may lead to a situation in which the dimensional matrix does not contain a nonzero determinant of order  $r$  in the right-hand  $r$  columns. The variables in the dimensional matrix should then be rearranged without altering the recommended arrangement more than necessary. By

arranging the variables in this way, the dimensionless products will fall out such that each of the original variables that can be regulated, occur in only one dimensionless product. So, for example, if  $E$  can be regulated easily, then it should occur in only one dimensionless product. Of the several variables listed in equations 1.20 and 1.21, only these fifteen have been chosen since the remaining variables are dimensionless by themselves and consequently cannot be meaningfully included in the analysis. The number of independent dimensionless products that make up a complete set is equal to the total number of variables less the rank of their dimensional matrix. In this case, the rank of the dimensional matrix is three, and consequently, the number of independent dimensionless products that make up a complete set is  $15 - 3 = 12$ .

d) There are 15 unknowns and 3 equations. Consequently, the set of solutions is possible if the values of the first twelve unknowns are set and the equations solved for the remaining three unknowns. An orderly way to do this is to let  $k_1 = 1$  and  $k_2 = k_3 = \dots = k_{12} = 0$ . Putting these values into Equation 1.23, we get

$$1 + k_{13} + k_{14} + k_{15} = 0 \quad (\text{corresponding to the } L \text{ terms in Equation 1.23})$$

$$k_{14} = 0 \quad (\text{corresponding to the } M \text{ terms in Equation 1.23})$$

and  $-2k_{14} - 2k_{15} = 0 \quad (\text{corresponding to the } T \text{ terms of Equation 1.23})$

Solving these three equations for the three unknowns  $k_{13}$ ,  $k_{14}$ ,  $k_{15}$ , we get  $k_{13} = -1$ ,

$k_{14} = k_{15} = 0$ . So, one-dimensionless product is given by  $\pi_1 = \frac{u}{L}$ . For the next

product, set  $k_2 = 1$  and  $k_{1,3,4,\dots,12} = 0$  and find  $k_{13}$ ,  $k_{14}$  and  $k_{15}$ .

The complete solution can be written in matrix form as

	1	2	3	4	5	6	7	8	9	10	11	12	13	14	15
	u	$\sigma$	x	y	z	t	E	$\rho$	g	P	$U_o$	$\sigma_o$	L	Q	$\gamma$
$\pi_1$	1	0	0	0	0	0	0	0	0	0	0	0	-1	0	0
$\pi_2$	0	1	0	0	0	0	0	0	0	0	0	0	2	-1	0
$\pi_3$	0	0	1	0	0	0	0	0	0	0	0	0	-1	0	0
$\pi_4$	0	0	0	1	0	0	0	0	0	0	0	0	-1	0	0
$\pi_5$	0	0	0	0	1	0	0	0	0	0	0	0	-1	0	0
$\pi_6$	0	0	0	0	0	1	0	0	0	0	0	0	-1/2	0	1/2
$\pi_7$	0	0	0	0	0	0	1	0	0	0	0	0	2	-1	0
$\pi_8$	0	0	0	0	0	0	0	1	0	0	0	0	3	-1	1
$\pi_9$	0	0	0	0	0	0	0	0	1	0	0	0	0	0	-1
$\pi_{10}$	0	0	0	0	0	0	0	0	0	1	0	0	2	-1	0
$\pi_{11}$	0	0	0	0	0	0	0	0	0	0	1	0	-1	0	0
$\pi_{12}$	0	0	0	0	0	0	0	0	0	0	0	1	2	-1	0

From this, the set of dimensionless products can be written as

$$\frac{u}{L}, \frac{\sigma L^2}{Q}, \frac{x}{L}, \frac{y}{L}, \frac{z}{L}, \frac{t \gamma^{1/2}}{L^{1/2}}, \frac{E L^2}{Q}, \frac{\rho \gamma L^3}{Q}, \frac{g}{\gamma}, \frac{P L^2}{Q}, \frac{U_o}{L} \text{ and } \frac{\sigma_o L^2}{Q}$$

It is seen that every product in this set is independent of the other products in the set. Further it can be shown that any dimensionless product of these variables, not in this set, can be expressed as a product of the dimensionless products in the set. For example

$$\frac{\rho g L}{E} \text{ has units } \left( \frac{M}{L^3} \right) \left( \frac{L}{T^2} \right) (L) / \left( \frac{M}{L T^2} \right)$$

or is dimensionless. However, it can also be expressed in terms of the previous dimensional products. i.e.

$$\frac{\rho g L}{E} = \frac{\rho \gamma L^3}{Q} \cdot \frac{g}{\gamma} \cdot \frac{Q}{E L^2}$$

In other words, the set of dimensionless products that has been obtained is complete, since it satisfies the definition of completeness.

As stated before, the displacement 'u' and the stress 'σ' at points x, y, z can be expressed as functions of all the variables involved as in equations 1.20 and 1.21, namely,

$$u = f(x, y, z, t, L, \rho, E, Q, P, \sigma_0, g, v, r^L, \dots r^v) \quad (1.20)$$

$$\text{and} \quad \sigma = f'(x, y, z, t, L, \rho, E, Q, \rho, \sigma_0, g, v, r^L \dots r^v) \quad (1.21)$$

Buckingham's Theorem (also called the  $\pi$  theorem) states that if an equation is homogenous, it can be reduced to a relationship among a complete set of dimensionless products. In other words, displacement u or stress σ, in the form of a dimensionless product, can be related to all the other variables when expressed as a complete set of dimensionless products. Using the complete set just obtained, the following relations result.

$$\frac{u}{L} = F \left[ \frac{x}{L}, \frac{y}{L}, \frac{z}{L}, \frac{t \gamma^{1/2}}{L^{1/2}}, \frac{E L^2}{Q}, \frac{\rho \gamma L^3}{Q}, \frac{g}{\gamma}, \frac{P L^2}{Q}, \frac{U_0}{L}, \frac{\sigma_0 L^2}{Q}, v, r^L, r^E, r^v, r^Q, r^P, r^{U_0}, r^\rho, r^{\sigma_0}, r^\gamma \right] \quad (1.24)$$

and

$$\frac{\sigma L^2}{Q} = F' \left[ \frac{x}{L}, \dots r^\gamma \right] \quad (1.25)$$

where F and F' are functions expressing the relation among the dimensionless terms.



These dimensionless products provide a means of ensuring that model behavior simulates prototype behavior. For complete similitude between the model and prototype, the dimensionless products of the model should be the same as the corresponding products of the prototype. In other words, for complete similitude between model and prototype,

$$\pi_i \text{ Model} = \pi_i \text{ Prototype for all } i\text{'s.} \quad (1.26)$$

This similitude between model and prototype will hold true only if all the relevant variables in the prototype have been included in the dimensional analysis.

Another use of this complete set of dimensionless products is that the terms in the set can be manipulated to form other dependent dimensionless products that are of use either because they describe model behavior well, or because they relate model behavior to prototype behavior in a better manner. Thus the dependent

dimensionless product  $\frac{\rho L^2}{E t^2}$  can be obtained as follows:

$$\frac{\rho L^2}{E t^2} = \frac{\rho \gamma L^3}{Q} \cdot \frac{Q}{E L^2} \cdot \frac{L^{1/2}}{t \gamma^{1/2}} \cdot \frac{L^{1/2}}{t \gamma^{1/2}} \quad (1.27)$$

If subscripts 'm' and 'p' stand for model and prototype respectively, then the left hand side of equation 1.27 can be written for model and prototype. For similitude between model and prototype, these two products should be equal or

$$\frac{\rho_m L_m^2}{E_m t_m^2} = \frac{\rho_p L_p^2}{E_p t_p^2}$$

or

$$\frac{t_m}{t_p} = \left[ \frac{\rho_m E_p}{\rho_p E_m} \right]^{1/2} \cdot \frac{L_m}{L_p} \quad (1.28)$$

i.e. by manipulating the independent dimensionless products a dependent product has been obtained which expresses the scaling relationship for time between the model and the prototype in terms of the respective material properties and lengths.

Dimensional analysis is a powerful tool in modelling. For example, it does not matter if  $E_p$  is not equal to  $E_m$ , as long as the dimensionless products that contain  $E_p$  and  $E_m$  are equal, i.e.,  $\frac{E L^2}{Q}$  is the same for both model and prototype. Perhaps the most important part of the analysis is the identification of the relevant independent variables. Once the independent variables have been identified and the dimensionless products formed, then every attempt is made to reproduce the values of these dimensionless products in the model. Complete similitude is usually not possible, in which case variables whose effects are minor are allowed to deviate from their theoretically correct values. If the effect of a variable is fully known, and, its scaled value is not reproduceable in the model, then the variable is allowed to depart from its correct value, and a correction is later made for its effect on the results. Once equality of the dimensionless products is achieved, then by equating the dimensionless products of the prototype to those of the model, scaling relationships such as the scaling relationship given by equation 1.28 can be obtained.

### 1.5.3 Scaling Relationships

This section establishes various basic scaling relationships, deriving them from first principles, for the case of a model subject to  $N_g$  in the centrifuge, and made up of the same material as the prototype. As noted previously, either the governing equation approach or the dimensional analysis approach or both can be used to obtain the relationships. The derivations of the scaling relationships are given in the subsequent sections and are summarized in Table 1.1.

Table 1.1

Equation Number	Quantity	Symbol	<u>Model Dimension</u> <u>Prototype Dimension</u>
<u>1. For All Events</u>			
1.29	Length	L	$\frac{1}{N}$
1.29	Displacement	U	$\frac{1}{N}$
1.30	Area	A	$\frac{1}{N^2}$
1.31	Volume	V	$\frac{1}{N^3}$
1.32	Mass	M	$\frac{1}{N^3}$
1.33	Density	$\rho$	1
1.34	Strain	$\epsilon$	1
1.35	Force	F	$\frac{1}{N^2}$
1.36	Stress	$\sigma$	1
1.37	Energy	$\Pi$	$\frac{1}{N^3}$
1.38	Energy Density	$\pi$	1

2. For Dynamic Events

1.39	Acceleration	a	N
1.40	Time	t	$\frac{1}{N}$
1.41	Velocity	v	1
1.42	Frequency	f	N
1.43	Strain Rate	$\dot{\epsilon}$	N

3. For Self Weight

1.44	Acceleration	a	N
------	--------------	---	---

4. For Diffusion Events

1.45	Time	t	$\frac{1}{N^2}$
1.46	Velocity	v	N
1.47	Acceleration	a	$N^3$
1.48	Strain Rate	$\dot{\epsilon}$	$N^2$

5. For the Laminar Flow of Water Through Soil

1.49	Permeability	k	N
1.50	Head	L	$\frac{1}{N}$
1.51	Pressure	p	1
1.52	Hydraulic Gradient	i	1
1.53	Velocity	v	N
1.54	Flow Quantity	Q	$\frac{1}{N}$

1.56	Capillary Rise D		$\frac{1}{N}$
1.57	Time	t	$\frac{1}{N^2}$

6. For Viscous Effects

1.35	Force	F	$\frac{1}{N^2}$
1.59	Time	t	1
1.60	Velocity	v	$\frac{1}{N}$
1.61	Acceleration	a	$\frac{1}{N}$

### 1. For All Events

For a model rotated at  $Ng$ , in order to satisfy the condition of geometric similarity with the prototype, it is required that lengths  $L$  and displacements  $U$  be scaled as follows

$$\frac{L_m}{L_p} = \frac{U_m}{U_p} = \frac{1}{N} \quad (1.29)$$

Now area  $A$  has dimensions  $L^2$  and so scales as

$$\frac{A_m}{A_p} = \frac{L_m^2}{L_p^2} = \frac{1}{N^2} \quad (1.30)$$

and volume  $V$  as

$$\frac{V_m}{V_p} = \frac{L_m^3}{L_p^3} = \frac{1}{N^3} \quad (1.31)$$

Mass =  $\rho L^3$ , scales as

$$\frac{M_m}{M_p} = \frac{\rho_m L_m^3}{\rho_p L_p^3} = \frac{1}{N^3} \quad (1.32)$$

Density by definition is independent of  $g$  and so

$$\frac{\rho_m}{\rho_p} = 1 \quad (1.33)$$

Strain  $\epsilon$  scales as

$$\frac{\epsilon_m}{\epsilon_p} = \frac{\frac{\Delta L_m}{L_m}}{\frac{\Delta L_p}{L_p}} = \frac{\Delta L_m}{\Delta L_p} \times \frac{L_p}{L_m} = \frac{1}{N} \cdot N = 1 \quad (1.34)$$

Force =  $F$  scales as  $\frac{F_m}{F_p} = \frac{M_m g_m}{M_p g_p} = \frac{1}{N^3} \cdot N = \frac{1}{N^2} \quad (1.35)$

Consequently stress  $\sigma$  scales as  $\frac{\sigma_m}{\sigma_p} = \frac{F_m/A_m}{F_p/A_p} = \frac{1}{N^2} \cdot N^2 = 1 \quad (1.36)$

Potential energy  $\Pi$  scales as  $\frac{\Pi_m}{\Pi_p} = \frac{M_m g_m h_m}{M_p g_p h_p} = \frac{1}{N^3} \cdot N \cdot \frac{1}{N} = \frac{1}{N^3} \quad (1.37)$

Energy density  $\pi$  is energy/unit volume and scales as

$$\frac{\pi_m}{\pi_p} = \frac{M_m g_m h_m / L_m^3}{M_p g_p h_p / L_p^3} = \frac{1}{N^3} \cdot N \cdot \frac{1}{N} \cdot N^3 = 1 \quad (1.38)$$

## 2. For Dynamic Events

The inertia force  $F = Ma$  and scales as

$$\frac{F_m}{F_p} = \frac{M_m a_m}{M_p a_p}$$

From 1.35 we know that any force scales as  $\frac{F_m}{F_p} = \frac{1}{N^2}$ . Also from 1.32 we know that

$\frac{M_m}{M_p} = \frac{1}{N^3}$ . Substituting for  $F$  and  $M$  in the scaling relation for force, we get

$$\frac{a_m}{a_p} = N \quad (1.39)$$

$$\text{Now } \frac{a_m}{a_p} = \frac{L_m t_m^{-2}}{L_p t_p^{-2}} = \frac{1}{N} \frac{t_p^2}{t_m^2} = N$$

$$\text{i.e. } \frac{t_p^2}{t_m^2} = N^2 \text{ or } \frac{t_m}{t_p} = \frac{1}{N} \quad (1.40)$$

$$\text{Velocity } V \text{ scales as } \frac{V_m}{V_p} = \frac{L_m t_m^{-1}}{L_p t_p^{-1}} = \frac{1}{N} \cdot N = 1 \quad (1.41)$$

$$\text{As } \frac{t_m}{t_p} = \frac{1}{N}, \text{ it follows that frequency } f \text{ scales as } \frac{f_m}{f_p} = N \quad (1.42)$$

in order to maintain the same number of cycles in the model per unit of prototype time.

Strain rate  $\dot{\epsilon}$  scales as

$$\frac{\dot{\epsilon}_m}{\dot{\epsilon}_p} = \frac{\frac{\Delta L_m}{L_m t_m}}{\frac{\Delta L_p}{L_p t_p}} = \frac{\Delta L_m}{\Delta L_p} \cdot \frac{L_p}{L_m} \cdot \frac{t_p}{t_m} = \frac{1}{N} \cdot N \cdot N = N \quad (1.43)$$

### 3. For Self Weight

Acceleration on the model is increased to  $Ng$  by controlling the rotational speed of the centrifuge so that  $\omega^2 R = Ng$  and

$$\frac{a_m}{a_p} = N \quad (1.44)$$



#### 4. For Diffusion Events

By analysis of the diffusion equation in section 1.5.1, it was shown that when the model materials and prototype materials are the same, then time  $t$  scales as

$$\frac{t_m}{t_p} = \frac{1}{N^2} \quad (1.45)$$

Velocity  $V$  scales in this case as 
$$\frac{V_m}{V_p} = \frac{L_m t_m^{-1}}{L_p t_p^{-1}} = \frac{1}{N} \cdot N^2 = N \quad (1.46)$$

Acceleration  $a$  scales as

$$\frac{a_m}{a_p} = \frac{L_m t_m^{-2}}{L_p t_p^{-2}} = \frac{1}{N} \cdot N^4 = N^3 \quad (1.47)$$

Strain rate  $\dot{\epsilon}$  scales as

$$\frac{\dot{\epsilon}_m}{\dot{\epsilon}_p} = \frac{\frac{\Delta L_m}{L_m \Delta t_m}}{\frac{\Delta L_p}{L_p \Delta t_p}} = \frac{\Delta L_m}{\Delta L_p} \cdot \frac{L_p}{L_m} \cdot \frac{\Delta t_p}{\Delta t_m} = \frac{1}{N} \cdot N \cdot N^2 = N^2 \quad (1.48)$$

It is seen that time, velocity, acceleration and strain rate scale differently for diffusion events and dynamic events.

#### 5. For the Laminar Flow of Water through Soil

Permeability  $k$  is given by  $k = \frac{K \gamma}{\eta}$  where  $K$  is the physical permeability,  $\gamma$  is the unit weight and  $\eta$  is the viscosity. As previously explained, if prototype material and model material are the same, then

$$K_m = K_p \text{ and } \eta_m = \eta_p$$

$$\text{Now} \quad \frac{k_m}{k_p} = \frac{\frac{K_m \gamma_m}{\eta_m}}{\frac{K_p \gamma_p}{\eta_p}} = \frac{\gamma_m}{\gamma_p} = \frac{\rho_m g_m}{\rho_p g_p} = N \quad (1.49)$$

$$\text{Head } h \text{ scales as } \frac{h_m}{h_p} = \frac{1}{N} \quad (1.50)$$

Fluid pressure  $p$  for a fluid of density  $\rho_f$  scales as

$$\frac{p_m}{p_p} = \frac{\rho_f g_m h_m}{\rho_f g_p h_p} = N \cdot \frac{1}{N} = 1 \quad (1.51)$$

i.e. fluid pressure and stress scale the same, as they have the same units.

$$\text{Hydraulic gradient } i \text{ scales as } \frac{i_m}{i_p} = \frac{h_m/L_m}{h_p/L_p} = \frac{1}{N} \cdot N = 1 \quad (1.52)$$

$$\text{Velocity of flow } V \text{ scales as } \frac{V_m}{V_p} = \frac{k_m i_m}{k_p i_p} = N \cdot 1 = N \quad (1.53)$$

Flow quantity  $Q$  scales as

$$\frac{Q_m}{Q_p} = \frac{k_m i_m A_m}{k_p i_p A_p} = N \cdot 1 \cdot \frac{1}{N^2} = \frac{1}{N} \quad (1.54)$$

It can be shown by dimensional analysis [Cargill and Ko (1983)] that capillary rise  $D$  scales as

$$\frac{D_m}{D_p} = \frac{S_m \rho_p g d_p}{S_p \rho_m N g d_m} \quad (1.55)$$

where  $S$  is the surface tension and  $d$  is the effective diameter of the inter-particle voids. Since model and prototype are made of the same material,  $\rho_p = \rho_m$ ,  $d_p = d_m$  and  $S_p = S_m$  so that

$$\frac{D_m}{D_p} = \frac{1}{N} \quad (1.56)$$

In a model, the distance between two points is  $\frac{1}{N}$  times the distance between two geometrically similar points in the prototype. Further, the velocity of flow in the model is  $N$  times the velocity of flow in the prototype (equation 1.53). Pokrovsky and Fyodorov (1936) predicted that because of this time would scale as

$$\frac{t_m}{t_p} = \frac{1}{N^2} \quad (1.57)$$

## 6. Viscous Effects

The viscous force ' $F$ ' acting on a small area ' $A$ ' can be defined as

$$F = \mu_s \frac{dv}{dn} A, \quad (1.58)$$

where  $\mu_s$  is the viscosity of the soil skeleton, and  $dv$  is the differential of the soil velocity with respect to the normal ' $n$ ' to the flow direction. Hence

$$\frac{F_m}{F_p} = \frac{\mu_{sm}}{\mu_{sp}} \cdot \frac{dv_m}{dv_p} \cdot \frac{dn_p}{dn_m} \cdot \frac{A_m}{A_p}$$

Viscosity  $\mu$  is independent of gravity and so, for the same material in the model and prototype,  $\mu_{sm} = \mu_{sp}$ . Consequently, the drag force scales as

$$\begin{aligned} \frac{F_m}{F_p} &= \frac{dv_m}{dv_p} \cdot \frac{dn_p}{dn_m} \cdot \frac{A_m}{A_p} \\ &= \frac{L_m t_m^{-1}}{L_p t_p^{-1}} \cdot \frac{L_p}{L_m} \cdot \frac{L_m^2}{L_p^2} \\ &= \frac{t_m^{-1}}{t_p^{-1}} \cdot \frac{1}{N^2} \end{aligned}$$

Since any force scales as  $\frac{1}{N^2}$ , for the viscous force one obtains

$$\frac{1}{N^2} = \frac{t_m^{-1}}{t_p^{-1}} \cdot \frac{1}{N^2} \quad \text{or,}$$

$$\frac{t_m}{t_p} = 1 \quad (1.59)$$

$$\text{Velocity } V \text{ scales as } \frac{V_m}{V_p} = \frac{L_m t_m^{-1}}{L_p t_p^{-1}} = \frac{1}{N} \cdot 1 = \frac{1}{N} \quad (1.60)$$

Acceleration 'a' scales as

$$\frac{a_m}{a_p} = \frac{L_m t_m^{-2}}{L_p t_p^{-2}} = \frac{1}{N} \cdot 1 = \frac{1}{N} \quad (1.61)$$

The various scaling relations that have been derived are shown in Table 1.1.

#### 1.5.4 Discussion of Scaling Relationships

The scaling relations described in the previous section are valid only if the model and prototype materials are the same. On examining the scaling relationships, it is clear that it may not be possible to satisfy all the similitude requirements, leading to possibly significant errors, especially at high values of the model factor 'N'. A number of cases are possible:

One case is where two or more parameters with conflicting scaling relations play a significant role in the phenomenon being modelled. An example of this situation would be the case of modelling ice-structure interaction, where both velocity and strain rate play a role. From the previous section it is seen that for dynamic events, velocity scales at 1:1 (model: prototype), while strain rate scales at  $N:1$ . Now the strength of ice is significantly strain rate dependent, while the forces exerted on the ice flow are functions of the velocity of movement. Consequently, if the velocity is scaled correctly, then the model strain rate is  $N$  times the prototype strain rate. In this case one solution is to model the velocity, and, knowing the strength of the model ice at the resulting model strain rate, input these values into a theoretical model and check to see if the results from the theoretical model correspond with the results from the centrifuge tests [Vinson (1982)].

The second case is when the same parameter or variable has a different scaling relationship depending on the process with which it is associated and two or more such processes occur within the same phenomenon. A classic example of this is liquefaction. The initial part of the phenomenon - the collapse of the soil structure and the generation of pore pressures - is associated with dynamic shaking while the latter part - the dissipation of the excess pore pressure - is a diffusion type process. For a dynamic event, time scales as  $\frac{t_m}{t_p} = \frac{1}{N}$ , while for the case of

diffusion, time scales as  $\frac{t_m}{t_p} = \frac{1}{N^2}$ . Often, in such cases the approach used would

be to model the two processes separately. Thus the time scale for the initial

portion of the phenomenon i.e. till liquefaction occurs, is  $\frac{t_m}{t_p} = \frac{1}{N}$ , while the

time scale for the subsequent dissipation of excess pore pressure is  $\frac{1}{N^2}$ . Tan and

Scott (1985) showed that the correct approach in this case is to use one time scale for modelling the whole process. This can be done by using a model fluid that is N times as viscous as the prototype fluid.

Tan and Scott (1985) analyzed a sphere settling in a field in uniform Ng conditions. Their analyses showed, among other things, that a) consistency required that only one time scale be applied to the governing equation of the sphere and b) that for soil particles larger than 0.1mm, the behaviour of a particle in a uniform Ng field is not similar to that in a 1g field. Their analysis is as follows:

The governing equation of a particle with no initial velocity relative to the fluid is

$$V_s (\rho_s - \rho_1) Ng - \frac{1}{2} C_D \rho_1 \pi a^2 \left(\frac{dx}{dt}\right)^2$$

$$= \left(\frac{2}{3} \pi a^3 \rho_1 + \frac{4}{3} \pi a^3 \rho_s\right) \frac{d^2x}{dt^2} \quad (1.62)$$

where, a = radius of the particle

$C_D$  = Drag coefficient

$Re$  = Reynolds number

$V_s$  = Volume of the particle

$\rho_s$  = Density of the sphere

$\rho_1$  = Density of the fluid and

$\rho_w$  = Density of water

The value  $C_D$  depends on the value of the Reynolds number  $Re$ . For the model, equation 1.62 can be written as

$$A N g + (C_D)_m B \left( \frac{dx_m}{dt_m} \right)^2 = C \frac{d^2 x_m}{dt_m^2} \quad (1.63)$$

where  $A = V_s (\rho_s - \rho_l)$  ,  $B = -\frac{1}{2} \rho_l \pi a^2$  and,

$C = \frac{2}{3} \pi a^3 (\rho_l + 2\rho_s)$  and have the same values as in the prototype.

For the prototype,  $N = 1$  and the corresponding equation is

$$A g + (C_D)_p B \left( \frac{dx_p}{dt_p} \right)^2 = C \frac{d^2 x_p}{dt_p^2} \quad (1.64)$$

For the model,  $\frac{x_m}{x_p} = \frac{1}{N}$  or  $x_m = \frac{x_p}{N}$

Substituting this in equation 1.63, and dividing by  $N$ , gives

$$A g + (C_D)_m B \frac{1}{N^3} \left( \frac{dx_p}{dt_m} \right)^2 = \frac{C}{N^2} \frac{d^2 x_p}{dt_m^2} \quad (1.65)$$

For no fluid,  $C_D = 0$  or  $B = 0$  and equations 1.64 and 1.65 reduce to

$$A g = C \frac{d^2 x_p}{dt_p^2} \quad (1.64a)$$

and

$$A g = \frac{C}{N^2} \frac{d^2 x_p}{dt_m^2} \quad (1.65a)$$

Consequently, for similitude between Equations 1.64a and 1.65a,  $t_m = \frac{1}{N} t_p$  (1.66)

For the case with a fluid,  $C_D \neq 0$  and  $B \neq 0$ , and similitude between model and prototype requires equations 1.64 and 1.65 to be equivalent. For them to be equivalent, the following conditions should be met

$$t_m = \frac{1}{N} t_p \quad (1.67)$$

$$\text{and} \quad (C_D)_m = N(C_D)_p \quad (1.68)$$

For low Reynolds number ( $R_e < 1.0$ ),

$$R_e = \frac{2\rho_1 a}{\mu} \frac{dx}{dt} \quad (1.69)$$

$$\text{and} \quad C_D = \frac{24}{R_e} = \frac{24 \mu}{2\rho_1 a \, dx/dt} \quad (1.70)$$

where  $\mu$  is the fluid viscosity.

$$\text{Using equation 1.67,} \quad \frac{dx_p}{dt_p} = \frac{N dx_m}{N dt_m} = \frac{dx_m}{dt_m} \quad (1.71)$$

Substituting equation 1.70 in equations 1.64 and 1.65, the following equations are obtained.

From equation 1.64 (Prototype),

$$A g + \mu_p \frac{24B}{2\rho_1 a} \frac{dx_p}{dt_p} = C \frac{d^2 x_p}{dt_p^2} \quad (1.72)$$

and from Equation 1.65 (Model), with  $t_m = \frac{1}{N} t_p$

$$A g + \frac{\mu_m}{N} \frac{24B}{2\rho_1 a} \frac{dx_p}{dt_p} = C \frac{d^2 x_p}{dt_p^2} \quad (1.73)$$



So, for Equation 1.73, which represents conditions in the model, to be identical with Equation 1.72, which represents conditions in the prototype,  $\mu_m$  should be equal to  $N \mu_p$ . When  $\mu_m = N \mu_p$ , the phenomena in the model will be the same as in the prototype with time scaling as  $\frac{t_m}{t_p} = \frac{1}{N}$ . A glycerine-water mixture or silicone oil can be used to obtain the required viscosity, while at the same time, a correction must be made to account for any difference in densities. Further, when  $R_e$  in the prototype exceeds 1, then the drag force is no longer a linear function of velocity in the prototype. In the model however, since  $\mu_m = N \mu_p$  the correspondingly scaled  $R_e$  for the model is  $\frac{(R_e)_p}{N}$ , which may be less than 1 up to the terminal velocity. Consequently the drag force on the particle in the centrifuge at  $Ng$  will be a linear function of the velocity and there will no longer be similitude between the model and the prototype. In other words, behavior at  $Ng$  in the model need not be the same as behavior at  $1g$  in the prototype.

Certain scaling relations have caused considerable discussion and debate. One case is the laminar flow of water through a porous medium. The velocity of flow between two points in the model is  $N$  times the corresponding flow velocity between the two corresponding points in the prototype. Schofield (1980) states that this increased velocity is due to the fact that by spinning the model at  $Ng$ , the driving head in the model is the same as that in the prototype. The distance between two points in the model however is  $\frac{1}{N}$  the distance between the two corresponding points in the prototype and consequently the gradient and the velocity of flow between two points in the model is  $N$  times the velocity of flow between the two corresponding points in the prototype. Tan and Scott (1985) say that the hydraulic gradient is the same in both model and prototype, as shown below.

At  $1g$  in the model,

$$h_{m_{1g}} = \frac{1}{N} h_p \quad \text{and} \quad x_{m_{1g}} = \frac{1}{N} x_p$$

At  $Ng$ ,

$$h_{m_{Ng}} = h_p \quad \text{and} \quad x_{m_{Ng}} = x_p$$

And consequently

$$i_m = \frac{\partial h_{m_{Ng}}}{\partial x_{m_{Ng}}} = \frac{\partial h_p}{\partial x_p} = i_p \quad (1.74)$$

They attribute the change in velocity to the fact that the permeability  $k$  is not a material constant, but since it is defined as

$$k = \frac{\gamma K}{\mu},$$

it depends on the unit weight  $\gamma$  and consequently on the  $g$  field, i.e. permeability scales as

$$\frac{k_m}{k_p} = \frac{\gamma_m k_m}{\mu_m} / \frac{\gamma_p k_p}{\mu_p}$$

Now, if the same materials are used in the model and prototype, then

$$\mu_m = \mu_p, \quad K_m = K_p \quad \text{and} \quad \gamma_m = N \gamma_p$$

or

$$\frac{k_m}{k_p} = \frac{\gamma_m}{\gamma_p} = \frac{\rho_m g_m}{\rho_p g_p} = N \quad (1.75)$$

i.e.  $k_m = N k_p$  and consequently

$$V_m = k_m i_m = N k_p i_p = N V_p. \quad (1.76)$$

Note that this derivation is exactly the same as that given in section 1.5.3, under laminar flow of water through soil.

Goodings (1984) says that some researchers prefer to consider Darcy's coefficient of permeability,  $k$ , as a material constant since in the normal geotechnical context, a change in  $k$ , implies a change in the material structure. From this view point, the increase in self-weight must be reflected by a corresponding increase in hydraulic gradient. This increased hydraulic gradient is argued for on the basis that the rate of loss of water pressure occurs at a rate  $N$  times faster in the centrifuge model.

Tan and Scott (1985) have shown clearly that  $k$  is not a material constant, but changes with the unit weight of the permeant. Further, consistent applications of the scaling laws shows that the hydraulic gradients in both model and prototype are the same. Consequently, it appears that the arguments presented by Tan and Scott (1985), are more correct. However, regardless of the reason, it is commonly accepted that the velocity of the flow in the model is  $N$  times the corresponding flow velocity in the prototype. Consequently, flow that is laminar in the prototype, could be turbulent in the model.

Once the model and the scaling relations have been chosen, it is desirable, that in view of the above uncertainties, a check be run to see if behavior similar to that of the prototype is obtained. Prototype behavior however is not known, and further, extrapolation of results to prototype dimensions may not be justified. In such cases, the technique of 'modeling of models', which was previously described, is used. If the results of a  $\frac{1}{100}$  scale model tested at 100g are the same as those of a  $\frac{1}{20}$  model run at 20g, then one can conclude with reasonable justification that these results are also representative of the unscaled model at 1g. This modeling of models' technique establishes the 'internal consistency of the experiment' or the range within which the scaling relations apply.

Rather than viewing a test as modelling a prototype, a test may be viewed as a real event in itself, with no attempt being made to simulate any exact prototype condition. Theories, which can be later applied to 1g situations, can be tested on these real events. Finally, a possibility exists that some feature of the prototype is too complex to be exactly scaled. In ice-structure interaction problems for example, it may not be possible to model the complex arctic ice structure. One way that has been suggested [Vinson (1982)] is to apply a correction, to the results of centrifuge tests, which analytically accounts for the more complex structure of the arctic ice.

### 1.6 Summary

This section summarizes the problems that may be encountered in centrifuge testing and methods that are of use in correcting for them. The problems can be classified in two general categories - problems associated with the centrifuge and problems associated with scaling.

Problems associated with the centrifuge are discussed in section 1.2.3. The ideal gravity field for modeling is an  $Ng$  field whose magnitude and direction does not change from point to point. In the centrifuge, the  $g$  field varies linearly with depth and, consequently, the effective stresses vary parabolically through the model depth in contrast with the prototype where the variation is linear. The difference in stresses generally being less than 2%, it is neglected.

The centrifuge gravity field acts radially and so if the model surface is not curved to the centrifuge radius, then the model stresses at two points at the same depth will not be the same, but the difference being less than the difference due to the first error (parabolic as opposed to linear stress variation) it is neglected. Since the acceleration field acts radially, there exists a horizontal component of acceleration that could be significant in some problems, e.g. slope stability, and consequently should be considered. Finally, improper orientation of the platform and

also the time required to reach the desired g level may also cause minor errors, but these errors can be corrected for.

Successful centrifuge testing requires that the scaling relations between the model and prototype be understood and satisfied. Successful testing also requires that the model behave at  $N_g$  as the prototype behaves at  $l_g$ . Scaling relations were examined in detail and it was shown that if the governing equation of the phenomenon is known, these relations can be obtained from the equation. If the governing equation is not known, however, then the more general method of dimensional analysis can be used. The success of this method depends on correctly choosing the independent variables, which in turn requires at least some understanding of the problem. Using either of these methods, a number of basic scaling relations were obtained for various situations, in each of which the model material was the same as the prototype material. Exact scaling of a phenomenon is sometimes not possible, as the various prototype features may be difficult to model.

In conclusion, the centrifuge is a useful tool, and if properly used, can provide useful information about the prototype.

## 2. Geotechnical Applications of the Centrifuge

### 2.1 Introduction

Centrifuge research in geotechnical engineering encompasses many areas, notably, soil mechanics, rock mechanics, ice mechanics and gravity tectonics. This section provides an overview of the research that has been performed in these areas and gives an idea of the breadth of research that is possible using the centrifuge. In the sections on soil, ice and gravity tectonics, only a brief review of the research done is presented. whereas, more details are provided for work done in the area of rock mechanics. Most of the recent geotechnical work that has been done on the centrifuge deals with soil models, while relatively little work has been done in the remaining areas, the reason being that soil lends itself more easily to centrifuge testing rather than rock, ice, or models of tectonic structures.

### 2.2 Soil Mechanics

This section summarizes work that has been done in soil mechanics, with the centrifuge. Since a relatively large amount of work has been done, it is described under the following headings: Flow of Water Through Soils, Soil-Structure Interaction, Underground Construction, Dynamics and Miscellaneous.

#### 2.2.1 Flow of Water Through Soils

Many geotechnical problems involve water movement through or on soil. The problems fall into the following broad categories: a) Steady flow of water through soils; b) Diffusion of excess pore water pressure; c) Erosion, river basin flooding, and similar problems. Liquefaction though involving water is treated under the section on dynamics.

The steady flow of water through soils is central to the study of many geotechnical problems involving seepage. The flow of water may be either laminar or turbulent. Many researchers have worked on laminar flow and have derived the

scaling laws required for modeling, for example: Laut (1975), Goodings (1979), (1984), Cargill and Ko (1983), etc. The phreatic surface for steady state seepage through homogenous embankment dams for laminar flow has been successfully modeled by Goodings (1979). Turbulent seepage however does not appear to have been modeled on the centrifuge, though Goodings (1984) has derived the appropriate scaling relations. She, however, says that the validity of some of the equations on which these scaling relations are based have not been established at lg.

The diffusion of excess pore pressure has been successfully modeled in the centrifuge by Croce et al (1984) who modeled the self-weight consolidation of a thick layer of soft clay, using the centrifuge. They were able to verify the scaling relations for diffusion, including the scaling for time, i.e.  $\frac{t_m}{t_p} = \frac{1}{N^2}$ . By comparing centrifuge test results with various theories, they showed that conventional small strain consolidation theory was inadequate for studying the self-weight behavior of soft clays, but that finite strain consolidation theory provided an accurate prediction of prototype response.

Various other problems involving the interaction of water and soil have been studied. Padfield and Schofield (1983) modeled a flood embankment made of clay and built on a clay foundation layer which in turn overlay a pervious gravel layer. By applying high water pressures to the pervious layer, they simulated high uplift pressures on the embankment, and were able to model the failure process. In another similar study, Schofield (1980) modeled underwater flow slides that occur as a result of erosion of the underlying clay layers, and proposed a failure hypothesis based on the test results.

### 2.2.2 Soil-Structure Interaction

The centrifuge has been extensively used to study soil-structure interaction problems. This section lists some of the major areas that have been studied.

The centrifuge at the Peter W. Rowe Laboratory at the University of Manchester, England, has been used extensively to study coastal and offshore gravity structures. Model studies were conducted for the design of the Oosterschelde storm surge barrier in the Netherlands. A field model experiment was undertaken at one-third full scale and both this experiment and the projected prototype were modeled in a series of centrifuge experiments [Rowe and Craig (1976)]. The centrifuge tests gave realistic results. Rowe and Craig (1978) later studied the effect of variations in weight and shape of the structure. George and Shaw (1976) and Rowe and Craig (1980) also investigated the stability of an already designed concrete gravity structure to be placed in a gas field in the North Sea. Failures by surface sliding and/or associated shakedown settlements were reported by Rowe (1975) when the prevalent analyses assumed deep seated failure mechanisms. Centrifuge tests have consistently shown that whether founded on cohesionless soil, on cohesive soil or on mixed strata, the failure of models under cyclic loading has always been observed at or close to the mudline on essentially flat-bottomed structures [Rowe and Craig (1980)], or close to the level of the tips of surface penetrating skirts [Craig and Al-Saodi (1981)].

In America, Prevost et al (1981) used the technique to study foundations of off-shore gravity structures. A model off-shore platform was machined out of aluminum and sand glued to its bearing surface, to simulate in-situ conditions. As in the prototype, the model was provided with skirts. Vertical and horizontal loads were applied, and the resulting movements measured. The effect of cyclic loads on the platform was also studied. Prevost et al (1981) concluded that centrifuge simulation was possible and suggested that further experiments be run to assess the reliability of alternative design or analysis techniques.



Scott (1971a, 1979b, 1981) did a considerable amount of centrifugal testing of piles in sands. He investigated the behavior of piles subject to cyclic loading. Discrepancies were observed between field and model tests, which were attributed to the fact that the piles were not driven under field stress conditions and that, consequently, the sand around the model pile was not as dense as the sand around the prototype pile. Sabagh (1984) ran cyclic axial load tests in piles in sand and found that the magnitude of cyclic load at failure was controlled by the existing static load, the size of the load increment and the number of cycles. Oldham (1984) investigated the lateral loading of single piles in sand. To model field conditions, he drove the piles in flight. The load-deflection curve showed reasonable agreement with published field values, though the experimental values showed slightly more flexible behavior in the initial part of the load deflection curve, as compared to field behavior. Finn et al (1984) studied the dynamic lateral response of pile foundations and found that their numerical technique gave adequate information for design for seismic loads. Nunez and Randolph (1984) modeled tension piles in soft clay. Instrumented piles of various flexibilities were driven in flight into carefully prepared clay samples. Craig (1984), did installation studies for model piles and concluded that it may not be possible to simulate pile group installation in the centrifuge. Barton (1984) studied the response of pile groups to lateral loading. From the various test programs done on piles, it can be concluded that accurate modeling requires that the piles be driven in flight to simulate field conditions. This makes successful instrumentation of the model pile difficult. Once the instrumented pile is driven in sand or clay, then its behavior can be studied using various loading mechanisms. Modeling pile groups, however, is not straightforward, due to interaction effects between individual piles.

The centrifuge has been used in tests to predict the behavior of footings on cohesionless soil. Oveson (1975) at the Danish Engineering Academy ran model footing tests as cohesionless soils. He found that scale effects occurred for model footings with diameters less than about fifteen times the average grain size and that the diameter of the model container had to be at least five times the diameter of the model footing. Kimura et al (1985), experimentally obtained load-deformation curves and ultimate bearing capacities of footings on cohesionless soil, and compared the results with various theoretical models. Kimura et al (1984) studied the behavior of footing on clay, in the centrifuge, and compared the resulting pore-pressure distributions with those predicted by theory. Gemperline and Ko (1984) studied footings on steep slopes of cohesionless material and compared the results with existing theories. The tests showed that selection of the type of analysis and the friction angle had to be done with care.

Retaining walls too, have been studied in the centrifuge. Lyndon and Pearson (1984) studied the pressure distribution on a rigid retaining wall in cohesionless material. Their results compared well with the theory used and with available prototype data. Bolton and Steedman (1984) investigated the behavior of fixed cantilever walls subject to lateral shaking. They were able to verify the theoretical model they had developed earlier [Bolton and Steedman (1982)]. Their 'modeling of models' program using different bumpy tracks was also quite successful. Work is underway at M.I.T. to study the behavior of a tilting gravity retaining wall subject to base shaking. In general, centrifuge tests on retaining walls have resulted in a better understanding of the pressures acting behind the wall as the wall rotates, translates or does both. It is also a cost effective method of verifying theoretical models.

The centrifuge has been used to study the behavior of buried flexible pipes (Trott et al 1984). Both full scale prototypes and small scale centrifuged models were tested, and good agreement was found between the model and prototype strain distributions and bending movement. Bolton (1984) studied multi-anchor earth retention systems, by modeling them on the centrifuge. Various configurations of reinforcement were studied and an optimum design developed.

Modeling of soil-structure interaction problems is one of the major advantages of the centrifuge technique. If a theoretical model exists for the interaction problem, then a comparison can be made between the theoretical and experimental results and the theoretical model either validated or improved. If the interaction problem is a new one, then an increased understanding is obtained, which can ultimately lead to the development and verification of a theoretical model. Prototype behavior before failure is rarely known, whereas, by correct simulation on the centrifuge, behavior till failure can be observed, at a relatively low cost.

### 2.2.3 Dynamics, Underground Construction and Other Uses

With an increase in the sophistication of data acquisition systems used in centrifuge testing, there has been an associated increase in the use of the centrifuge for dynamic testing. The advantage of dynamic testing on the centrifuge is that unlike normal dynamic testing of models at 1g, dynamic model testing can be done on the centrifuge at the g level at which self-weight model stresses are the same as in the prototype.

The centrifuge technique has been used to study problems in geotechnical earthquake engineering. A review of the equipment and instrumentation required for shaking the models, of developments in the theory and practice of centrifuge testing using ground motion simulation and of suggestions for future experiments involving ground motion has been made by Whitman (1984). Also included in this paper is an appendix that summarizes the work done in earthquake simulation, by various

centrifuge laboratories all over the world. There are several ways of simulating ground motion. These are: the piezoelectric shaking system, the explosive simulator, the bumpy road and the hydraulic simulator. Each method of simulation has its own advantages and disadvantages. The major areas where work has been done are the liquefaction of saturated sand below a level surface, the development of excess pore pressures in saturated sand in earth dams and below structures, forces on retaining walls and soil-structure interaction, amplification of ground motion through the soil and the permanent deformation of earth dams. Whitman (1984) concluded that the results of these programs were of value to geotechnical engineering research and that they provided information regarding the theory of dynamic centrifuge testing itself, i.e. problems such as soil containment, scaling relations, and rate effects. He also makes suggestions for future work.

The centrifuge has also been used to study explosive cratering. On the basis of tests run on the centrifuge, Schmidt and Holsapple (1980) developed a unified theory for cratering dynamics. Further details can be found in Section 2.3.4.

When designing a tunnel, shaft, or excavation in soft soil several decisions regarding the use of temporary support such as compressed air or pressurized slurry need to be made. If such support is required, the question of the amount of support arises. Once a stable tunnel is designed, there is a need to know how much deformation will occur. These and other related questions can be addressed through model studies on the centrifuge. Extensive work has been done on both sands and clays at Cambridge University. Details can be found in Atkinson and Potts (1977), Mair (1979), Kusakabe (1982), Phillips (1982), (1984), Taylor (1974), (1979), Schofield (1980) and Mair et al (1984). The conclusions reached were that the stability ratio  $T_c$  defined by

$$T_c = \frac{\sigma_v - \sigma_{tc}}{c_u} \quad (2.1)$$

where  $\sigma_v$  = total overburden pressure at the tunnel axis

$\sigma_{tc}$  = tunnel support pressure at collapse

$c_u$  = undrained shear strength of the clay

for tunnels in clay lies between 3 and 9 and not necessarily at 6 as has often been assumed. Tests on model tunnels at different scales (modeling of models) showed good agreement. For a given clay, immediate surface deformations above the tunnel were found to be related to the inverse of the factor of safety. There was close agreement between predicted and observed failure mechanisms for shaft and trench excavation. As strains increased and soil strength progressively mobilized, the pattern of ground deformation around the tunnel or excavation remained unchanged. Time dependent deformations were found to be due not to any viscous effect, but due to changes in the effective stress as the excess pore pressures generated by tunneling dissipate. In the first phase, all the pore pressures drop as the excavation occurs. Subsequently, settlements continue as the pore pressures increase with time. These deformations are often referred to by tunnelers as "squeeze" and it is often wrongly concluded that the movement is due to viscous ground behavior. Centrifuge tests coupled with effective-stress analyses using finite elements show that the movements are uniquely related to effective stress changes in the clay. For tunnels in clay or sand, with support conditions similar to those found in construction, centrifuge test results were closely bracketed by the result of theoretical studies based on upper and lower bound plasticity theorems.

The centrifuge has also been used to study the slope stability of overconsolidated clays [Fragaszy and Cheney (1981)]. The centrifuge they used differs from conventional centrifuges in that it is a drum centrifuge, consisting of a drum that rotates about its vertical axis. The advantage of this type of centrifuge is that the model embankment occupies the entire circumference of the drum

and so forms an endless model. The tests showed that there was a combination of prototype height and g level, beyond which only long term failure (after 1 to 8 hours of spinning) took place.

Al-Hussaini et al (1981) modeled coal waste embankments using the centrifuge. Various geometries were studied, and, based on the tests, it was found that estimates of the phreatic surface based on finite element seepage analysis and Dupuit's theory agreed with the observed results. Sutherland and Richard (1984) investigated the development of the phreatic surface in a stable tailings dam. It was found that the phreatic surface was only slightly affected by truncating the upstream part of the model. Below 100g, scaling effects were minimized and the experimental results agreed well with the theoretical results. Almeida et al (1984) studied the staged construction of embankments on soft clay, with and without reinforcement. Their results showed that large lateral deformations indicated low factors of safety and that the strengthening effect of granular reinforcement columns was less important than their effect of increasing the rate of pore pressure dissipation.

Ferguson and Ko (1984) used the centrifuge to model cone penetrometer tests. Their results indicated that there was no unique relationship between the CPT data and the relative density. They found that additional work was required to increase the accuracy of predicting liquefaction potential using the cone. Moisture effects were found to play a role in the results. Relationships among various soil properties could be established only on a soil by soil basis. However, the results indicated that the centrifuge could model in-situ tests.

This discussion of centrifuge research in soil mechanics is not intended to be complete, but is provided so as to have an idea about its breadth.

### 2.3 Rock Mechanics

This section describes the centrifuge work that has been done in rock

mechanics. Most of the research was performed in the fifties and sixties, after which the emphasis of centrifuge testing shifted to soils. Clark (1981) reviewed research done with the centrifuge in rock mechanics, up till 1981. This review is reported here along with more recent work. The review is broken into four sections. The first deals with work on beams, the second with work on layered roofs, subsidence problems, underground openings and excavations, the third with rock slopes and rock fill dams and the fourth with miscellaneous topics.

### 2.3.1 Beams

Much has been done in modeling beams, since a section of a mine roof can be represented as a beam. Bucky (1931) ran a number of centrifuge tests on simple beams, made up of artificial material (a mixture of sand, cement and water), and of rock (sandstone). Two series of tests were run, the first series to verify the scaling laws and the second to show that the failure pattern obtained by self-weight (internal) loading in the centrifuge was considerably different from the failure pattern obtained by external pressure loading, in terms of deformations, fracture pattern and amount of arching. As previously mentioned, this appears to have been the first use of a centrifuge for model studies.

Caudel and Clark (1955) analyzed the stress distribution in a simple beam subject to three different loading conditions: a) a uniformly distributed load b) loaded by self-weight and c) loaded in a centrifuge. Two types of end conditions were studied - a) simply supported beams and b) beams with restrained ends. The various combinations are shown in Fig. 2.1. Their theoretical analysis showed that the critical stresses in these simple beams could be approximated by any one of the three types of loading, when the ratio of the length of the body to its thickness was greater than 5. When this ratio was less than 5, then the combination of stresses under multiple  $g$  loading caused arching rather than typical beam failure.

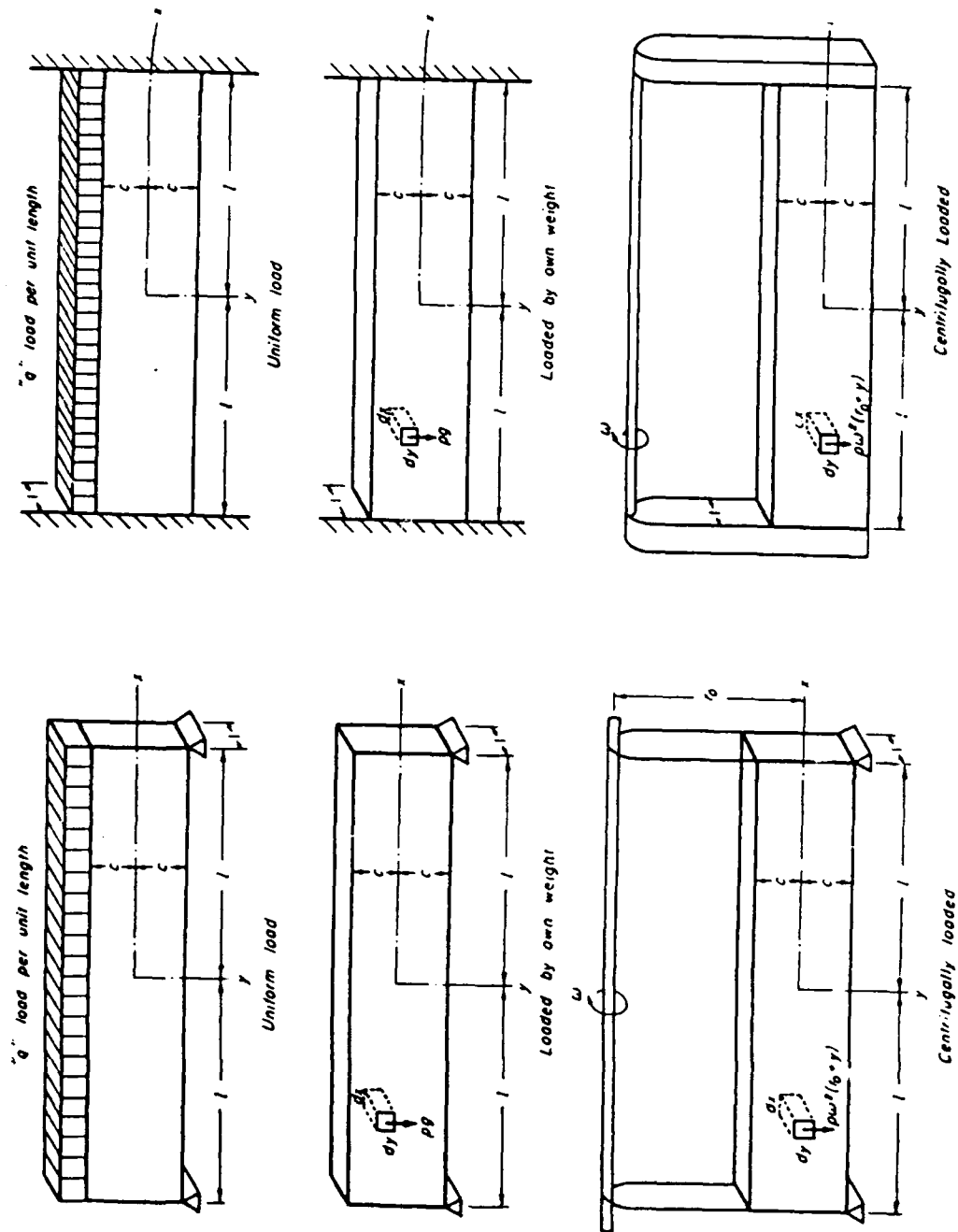


Fig.2.1. The end conditions and loading conditions analyzed. From Clark (1981).



They suggested that, for simple beams, the value of centrifugal testing lies not in determining the stress distribution per se, but in finding the failure mechanism which is different for self-weight loading as compared to external loading. Their conclusion was that centrifuge testing would also be of use in finding the stress distributions after failure, the post failure behavior, the stress distribution and failure behavior of unsymmetric beams with or without rock bolts, etc.

Chan (1960) attempted to model beams using models made of gypsum rock. The beams were 12 inches long, 2 inches wide, with thicknesses varying between 1 and 1.5 inches. The ends of the beam were clamped in a model holder, placed in a centrifuge and rotated up to failure. The behavior of the beam was observed from first fracture to failure, using a stroboscope. The rpm at fracture varied from 360 to 630, with the corresponding scale factors varying from 124 to 383. Prototype beams with dimensions equal to those of the model multiplied by the corresponding scale factor at failure, and having the same material properties, would thus theoretically fail due to self-weight, with the same stresses as in the model. Values of prototype beam length at failure when plotted versus prototype beam thickness at failure, were found to fall on a straight line in a log-log plot.

Wang et al (1967) tested simple and multiple-layer beams, simply supported or restrained, in a 2 foot diameter centrifuge that was capable of producing up to 2700 g's. The beams were made of Bedford limestone and the bi-refringement-coating method of photoelastic analysis used to determine the stress distributions. The fixed beams were restrained at their ends by pouring molten type metal into end holders and allowing it to solidify. However, this metal shrinks as it cools, and, has a lower yield strength than rock. Consequently, the ends of the beam were probably not rigidly fixed. This could explain why the stresses observed for these beams were different from the theoretical values. Results for the simply supported beams agreed well with the theory.

Esser (1962) used the centrifugal-photoelastic technique to study the stress distributions in unsymmetric beams subject to self-weight loading in multiple g-fields. Typical models that he studied are shown in Fig. 2.2. The semi-cured photoelastic model with the roof bolts installed was placed in the centrifuge and spun for four hours at the desired g level, within which time full curing of the photoelastic material was completed. The model was taken down and the thickness reduced with a metal shaper to  $\frac{1}{2}$ " and later  $\frac{3}{8}$ " in order to obtain more distinct fringe patterns. The most well-defined fringes were, however, not clear enough for a precise quantitative analysis but nevertheless made some interpretation possible. Initially, symmetrically loaded unbolted models were studied. During this series, it was found that open bolt holes did not influence the fringe pattern significantly, compared to a model with no bolt holes. In tests on unsymmetric unbolted beams, one abutment was made more rigid than the other. It was found that shearing stresses increased over the rigid abutment and decreased over the flexible abutment. In the next series, symmetrical beams with roof bolts were tested. The bolts were found to reduce the bending stresses as well as the stress concentrations in the corners and in the area around the abutment. In subsequent tests, the rigidity of one abutment was progressively reduced. This produced larger bending stresses in the beam. Various bolt patterns were tried using three bolts oriented at various angles. It was found that a bolt pattern could either reduce stresses, or, if installed without regard to the existing stress distribution, could result in an adverse effect. As a result of the tests, a final bolt pattern, as shown in Fig. 2.3, was developed, which resulted in an overall reduction of stresses in the beams.

As seen above, modeling of beams with various geometries and materials, with or without bolting, can be done using the centrifuge. The research described above, is applicable to mine roofs.



a) Fringe pattern of an unsymmetrical model.



b) Fringe pattern of an unsymmetrical model with three vertical roof bolts.



c) Fringe pattern of an unsymmetrical model with three holes (45, 60, and 90°).



d) Fringe pattern of an unsymmetrical model with three roof bolts (90, 60, and 45°).

Fig.2.2. Results of tests on bolted unsymmetrical beams. From Clark (1981).

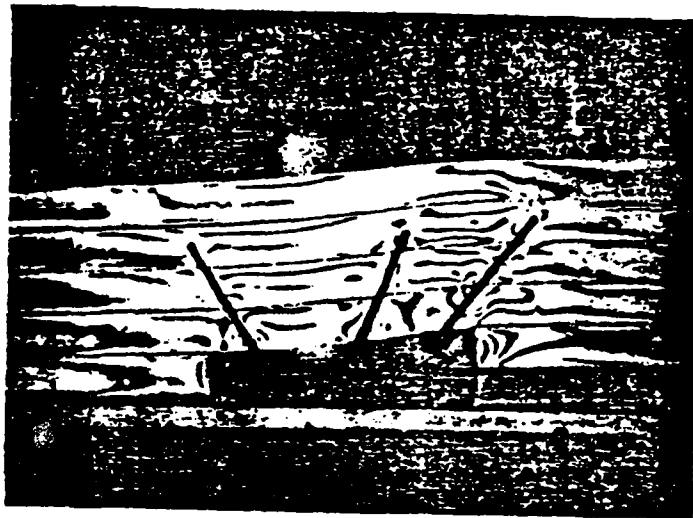


Fig. 2.3. Fringe pattern of an unsymmetrical model with three roof bolts (45, 60, and 60°). From Clark (1981)

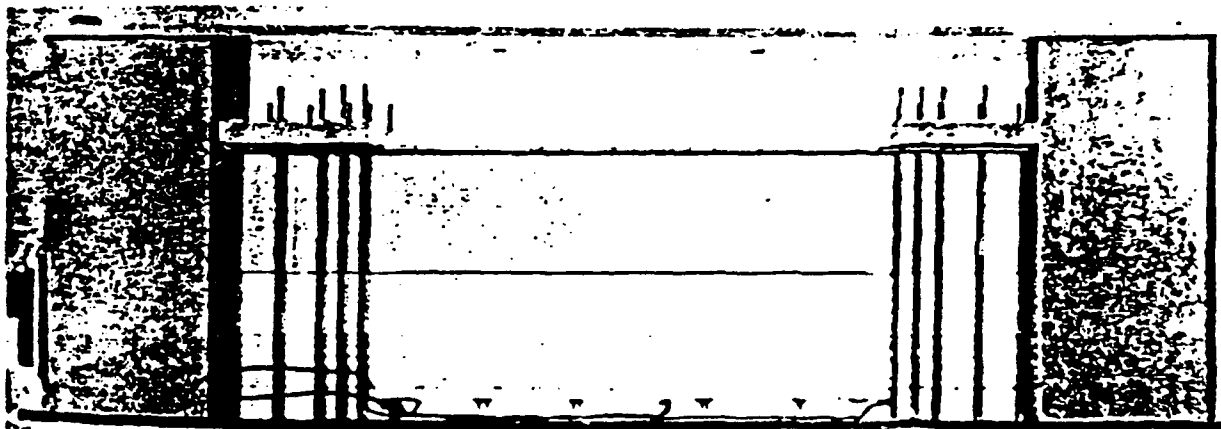


Fig. 2.4. Typical roof model mounted in holder (12 inch span).

### 2.3.2 Layered Mine Roofs, Subsidence Problems, Underground Openings and Excavations

Panek conducted what remains one of the most extensive investigations in rock mechanics using the centrifuge. In this program, he designed a 6 foot diameter centrifuge, which he enclosed in an evacuated tank [Panek (1952a, 1952b)]. He applied dimensional analysis to the problem of bedded mine roofs reinforced by rock bolts. The role of bolts in increasing interbed friction, in suspending the strata and the combined effect of suspension and interbed friction were studied. Using dimensional analysis, he was able to express the strain as a function of seventeen  $\Pi$  terms. It was found during the analysis that the diameter, weight, Young's Modulus and Poisson's ratio of the bolt and the Poisson's ratio of the rock had secondary effects and that consequently the number of  $\Pi$  terms could be reduced from seventeen to six. The resulting similitude equation was

$$(\epsilon_x)_i = f \left( \frac{Nw_i L}{E_i}, \frac{P_o}{E_i L^2}, \frac{P_a}{P_r}, \frac{L}{t_i}, \frac{L}{b}, \frac{h}{t_{avg}}, k, F, a, U_i \right)$$

where  $N$  = centrifugal loading ratio

$h$  = bolt length

$E_i$  = Young's Modulus of rock of  $i^{\text{th}}$  bed

$b$  = bolt spacing

$(\epsilon_x)_i$  = strain in  $i^{\text{th}}$  roof bed

$k$  = number of bolts per set across opening

$t$  = bed thickness

$w_i$  = unit weight of rock of  $i^{\text{th}}$  bed

$P_o$  = bolt pre-tension

$P_r$  = least value of bolt tension that will prevent strata separation at the bolt positions

$P_a$  = actual bolt tension

$L$  = length of beams

$a$  = coefficient from the theory of bending

$F$  = coefficient of bedding plane friction for bolted beds

$U_i$  = function of the relative flexural rigidity of the bolted roof beds

A series of tests were run with the variables taking values typically encountered in practice. It was found that friction between the beddings reduces the bending of all the beds in the unit. This interbed friction increases with the use of tensioned bolts. If the bolts are not tensioned, then their effect is only to suspend the less rigid layers. Hence, a pre-tensioned bolt increases the friction between the bedded planes and also suspends the beds (layers). Specifically, Panek (1956) investigated the frictional effect between layers of beds, while later [Panek (1962a)] he gave details concerning the effects of suspension. The final report of the series, Panek (1962b), documents the combined effect of friction and suspension.

A typical model of a bolted roof is shown in Fig. 2.4. Panek's tests on the centrifuge provided considerable insight into roof bolting and resulted in a quantitative solution for roof bolting design. The conclusions of the study were that the friction effect reduces the bending of all the beds in the bolted unit. As a result of the suspension effect, the maximum outer-fibre bending stress in a bed increases or decreases according to whether the flexural rigidity of that bed is greater or less than the average for all the beds in the bolted unit. The net effect of friction and suspension in a given layer was found to depend on the bedding sequence and the bolt pre-tension. The results of Panek's research conclusively demonstrated the usefulness of the centrifuge in solving rock structure problems.

More recently, Stephansson (1971, 1982) conducted centrifuge tests at high  $g$  levels (4000  $g$ 's) on layers of slabs of dimensions 20 cm x 20 cm, to study the behavior of single openings in horizontally bedded rock. The various types of roof

geometries, layer stiffnesses and the types of contact between the layers (free movement between layers vs. layers bonded together) are shown in Fig. 2.5. Once again, the rigidity of the abutments was found to strongly influence the stresses and deflections about the opening. The values of maximum stress in and the deflection of a single layer roof were between those of a simply supported beam and a fixed beam. A double layer roof, with the upper layer stiffer than the lower layer, gave rise to separation between the layers. As the thickness of the upper layer increased, behavior shifted towards that of a single layer roof, with compression of the abutments under loading strongly influencing the stresses and deformations around the openings. Results from finite element studies showed good agreement with the centrifuge tests. For a layer with a low flexural rigidity resting on a stiffer layer, the upper layer was found to carry part of its weight, with the rest of its load being carried by the underlying rigid layer. Double layer roofs made up of different materials and bonded together could be treated as equivalent single layer T-cross-sections made up of the same material as the lower layer.

From the result of his tests, Stephansson (1982) was able to formulate a theory to calculate the deflections and stresses in a mine roof area supported by pillars. The theory was applied to the Laisvall lead mine, where detailed observations of roof movements over a number of years are available, and good agreement between theory and results was found.

Sutherland et al (1982) investigated subsidence over coal mines as a result of a "longwall" operation. Such an operation is one in which a panel of coal roughly 440 yards wide by half a mile long, is removed from a coal seam, making the roof unstable until it finally collapses. The effects of the failure migrate to the surface, eventually creating a surface depression. Nevada Tuff, being linear up to failure, was chosen as the model material. Each layer was 10.5 inches long, 1/8

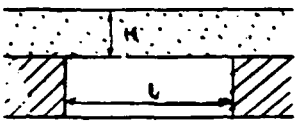
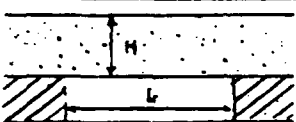
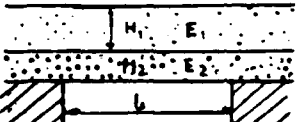
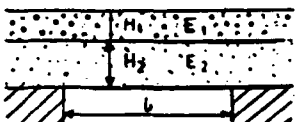
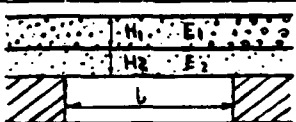
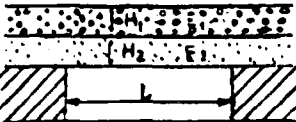
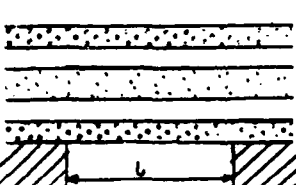
SINGLE-LAYER ROOF	I		$H < \frac{L}{5}$
	II		$\frac{L}{2} > H > \frac{L}{5}$ Including shear stress in the layer
DOUBLE-LAYER ROOF	III		$E_1 I_1 > E_2 I_2$ Free slip along the contacts Detaching
	IV		$E_1 I_1 < E_2 I_2$ Free slip along the contacts No detaching
	V		$E_1 < E_2$ Welded contact
	VI		$E_1 > E_2$ Welded contact
MULTI-LAYER ROOF	VII		Welded contacts

Fig.2.5. Types of roof configurations. From Stephannson (1982).



inch thick and 1 inch wide. As shown in Fig. 2.6, these layers were supported on rigid abutments so as to simulate an opening, and then spun to failure. Three distinct processes were observed. First, failure of the rock mass above the opening occurred, with material falling into the opening. Second, as the number of broken strata increased, the volume of the opening decreased as a result of broken material falling into it, and third, the top of the failure zone formed an arch which progressively moved upwards. The shape and size of this arch was found to determine the surface deflections (Fig. 2.7). By using the centrifuge, considerable insight into the reasons for surface subsidence was gained, and the capabilities and limitations of various numerical models in predicting this phenomenon were explored.

Howell and Jenkins (1984) studied a similar problem: subsidence features, in areas underlain by rock salt, caused by the progressive removal of the underlying salt through solution mining. The chief feature of the subsidence is the very rapid formation of a crater on the surface. Centrifuge tests were used to study the development of these craters. The model consisted of a box, the upper part of which contained dry sand representing the material overlying the rock salt beds. The lower portion of the box was empty, representing the void formed as a result of the progressive solution of the rock salt. The sand was separated from the void by a partition with trap doors. For a given trap door opening sand trickled into the lower zone from the upper zone, with considerable readjustment of the sand in the upper zone, no subsidence being observed at the surface. If the trap door was widened further, inducing more material to fall into the underlying void, a critical stage would be reached in the body of sand above the trap door and a plume of disturbed material would extend from the cavity to the so far undisturbed surface, causing a crater to rapidly develop. The centrifuge tests were found to resemble the field events and provided information that seemed to account for the previously unexplained speed at which these craters develop.

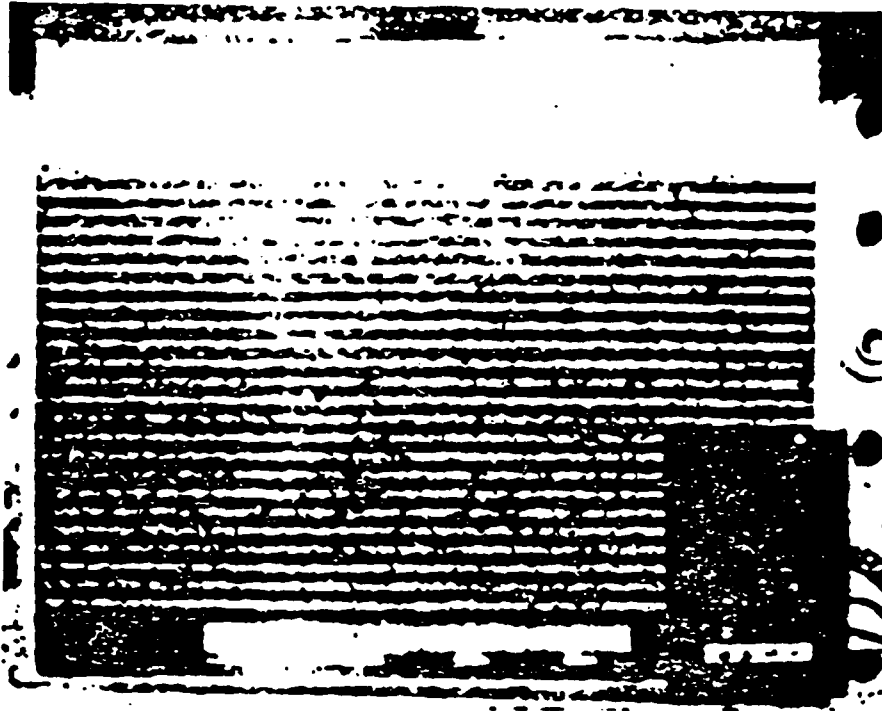


Fig.2.6. Model of layered mine roof. From Sutherland (1982).

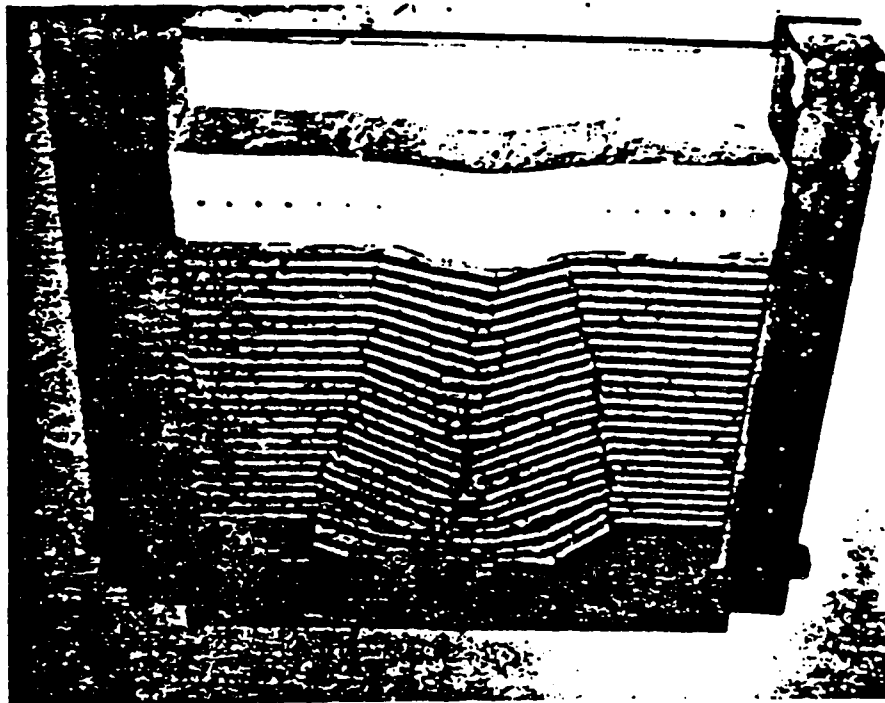


Fig. 2.7. Fractured layers sharing the shape of the arch.  
From Sutherland (1982).

The centrifuge has been used in rock mechanics to study tunnels and other underground openings. Oudenhoven (1962) used the centrifuge to study tunnel liners. One of the major purposes of a tunnel liner is to support all or part of the load of the overlying rock formation. Analytical solutions are available for stresses in circular tunnels and shaft linings. The centrifugal technique also offers a method of determining these stresses. Oudenhoven (1962) studied the effect of tunnel liners on the stress distribution in the surrounding rock, by modeling them as openings in plates made of photoelastic materials. The openings were lined with materials of various stiffnesses, placed in a centrifuge and spun. The combinations used were

Case 1: A circular opening without a liner

Case 2: Openings in a plate of low elastic modulus, with liners of constant thickness to radius ratio and having elastic moduli greater than the surrounding plate, the elastic moduli of the liners being the variable.

Case 3: Openings in a plate of low elastic modulus with liners having a constant elastic modulus higher than that of the surrounding plate, the liner thickness being the variable.

Results for these three cases are as follows:

Case 1: The fringe pattern for the model loaded by its self-weight (the centrifugal model) was shifted downwards as compared to the theoretical stress distribution for loading by an externally applied uniaxial load. Also, for uniaxial loading, there theoretically is tension at the top and bottom of the opening and the stress concentration factor at the springline is three, whereas for the centrifuged model there was no tension at the top and bottom of the opening, and the stress concentration at the springline was 2.5. These differences were caused both by the vertical stress gradient and by the plate holder frame which prevented the plate model from expanding laterally, thereby inducing a small side pressure.

Case 2: For these tests, it was found, as shown in Fig. 2.8, that the load was transferred to the liner through narrow regions of high stress, the remaining plate material surrounding the liner being relatively unstressed. The stress concentration factors were found to increase with increase in the elastic modulus of the liner.

Case 3: In this series, it was found that the stress concentration decreased with an increase in liner thickness, as shown in Fig. 2.9.

More detailed studies along the above lines would result in more information about the interaction between the liner and the rock, which could be used in the development of better theoretical models and design methods.

Haycocks (1962) studied the stress distribution around underground openings of various shapes, using photoelastic methods. Most of the stresses around underground openings are due to the weight of the overlying rock, and so the centrifuge technique is a useful way of studying them. Haycocks used semi-cured photoelastic models into which he froze the stresses. Fig. 2.10 shows some of the openings that were studied: (1) a circular opening; (2) a horizontal rectangular opening (see fig. 2.10a); (3) a horizontal rectangular opening with a vertical fault running down the center and two fracture extending from its two upper corners at an angle of about  $15^\circ$  from the vertical; (4) an opening with a high parabolic arch with a vertical fault and two inclined fractures (see fig. 2.10b); and (5) a flatter parabolic arch, with fault and fractures.

For the circular opening, the stress pattern obtained under body force loading was similar to the stress pattern around a hole in a plate subject to external loading at lg except that, for the latter case, there is no stress gradient. As a consequence of the gradient in the centrifuged model, the stress trajectories were shifted downwards as compared to the externally loaded plate (see Fig. 2.11). As in the case of the circular opening, the stress gradient in the centrifuged model

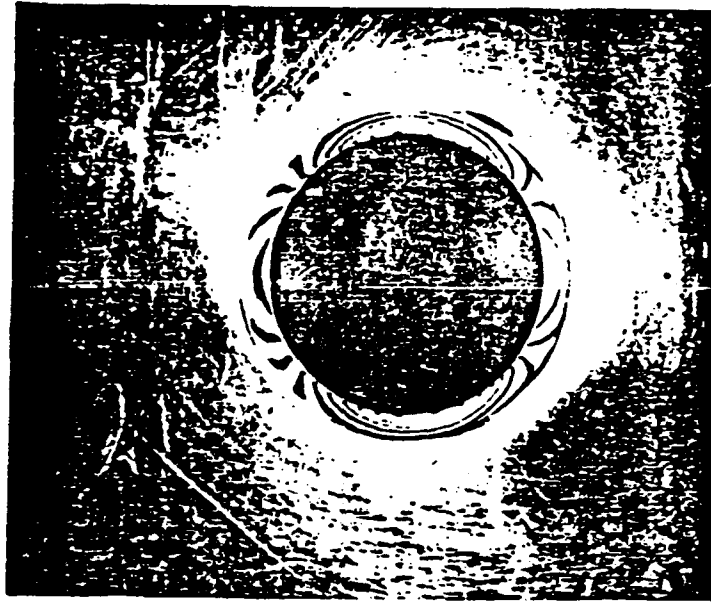


Fig.2.8. Stress pattern of rigid lining and weak plate.  
 $t/R = 0.177$ . From Clark (1981).



a) Lining thickness of 0.452 inches,  
 $t/R = 0.354$ .

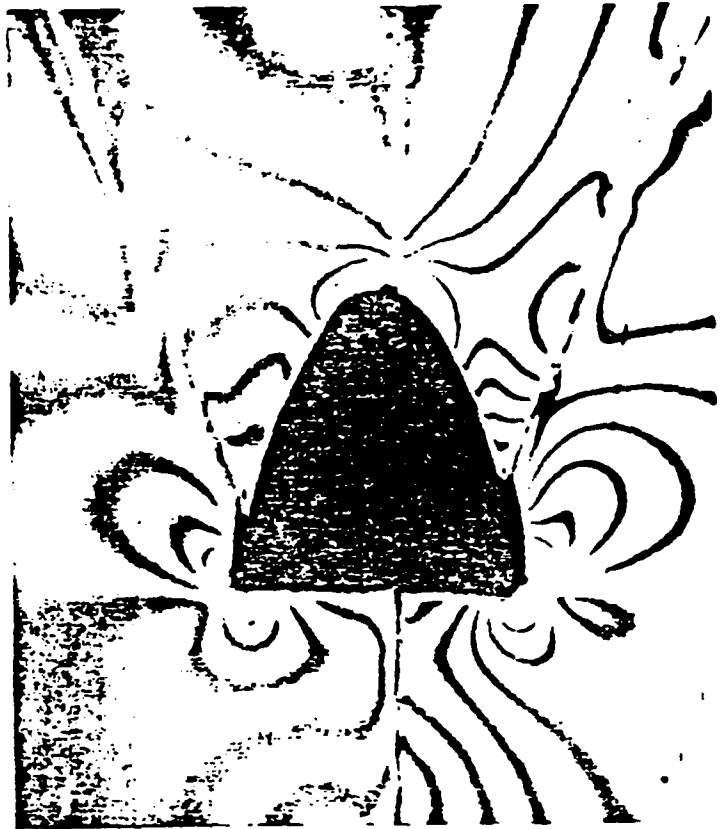


b) Lining thickness of 0.904 inches,  
 $t/R = 0.708$

Fig.2.9 Effect of varying liner thickness. From Clark (1981).



a) Stress pattern in rectangular opening.



b) Stress pattern in opening with high arch with fractures.

Fig.2.10. Stress distribution around typical openings studied. From Clark (1981).

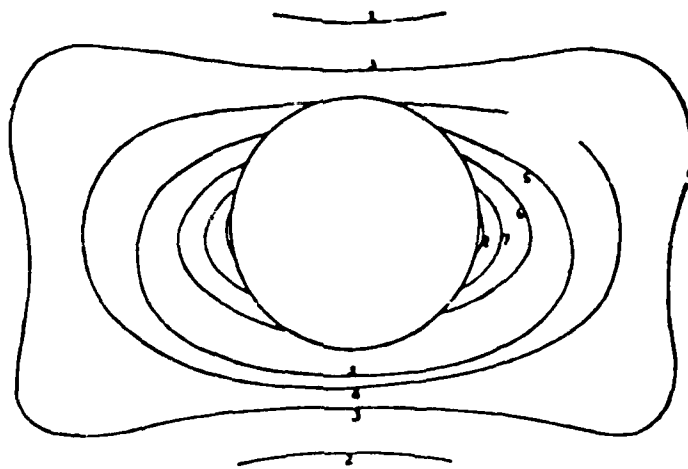


Fig.2.11. Calibration test stress distribution.  
From Clark (1981).

with the rectangular opening made the stress concentration slightly greater at the bottom of the opening than at the top. Introduction of the vertical fault and the oblique fractures caused very little change in the stress distribution patterns, compared with the stress distribution without fractures, as long as the stresses in the region with the fractures were compressive. The high arch openings with the same fracture pattern showed no tension existing about the opening, but there were stress concentrations at the bottom corners, at the top of the arch and in the wedges formed at the intersection of the fractures with the opening. A flatter parabolic arch with fractures has high stress concentrations only at the sides, with the vertical fault having only a small effect on the normal stresses.

The centrifuge has also been used to study openings in mines. In a classic paper, Hoek (1965) provided design details of a 9 foot diameter, 1000 g centrifuge that he used to test intact rock. He placed the centrifuge in an underground chamber for safety and lined the chamber with aluminum to reduce the turbulence. At the end of the fixed buckets, he mounted ovens with which he could heat the photoelastic models while spinning at the desired stress level. The softened model was spun until it came to equilibrium under the applied stress conditions, after which it was allowed to cool, thereby locking the stresses in the model and allowing the photoelastic analysis to be done at a later time. To check the accuracy of his technique, Hoek placed an epoxy resin disk standing on its edge in the centrifuge, spun it at 1000g, studied the resulting isochromatic pattern, and compared it with the theoretical pattern, with good results. Having established the accuracy of his technique, Hoek used it to study mining problems. Hoek (1965) demonstrated qualitatively the importance of body forces upon the fracture of rock around large mining excavations, using plaster of Paris models. One of two identical models was placed in a normal testing machine and subjected to a uniformly distributed edge load, until fracture occurred. The second model was spun in the

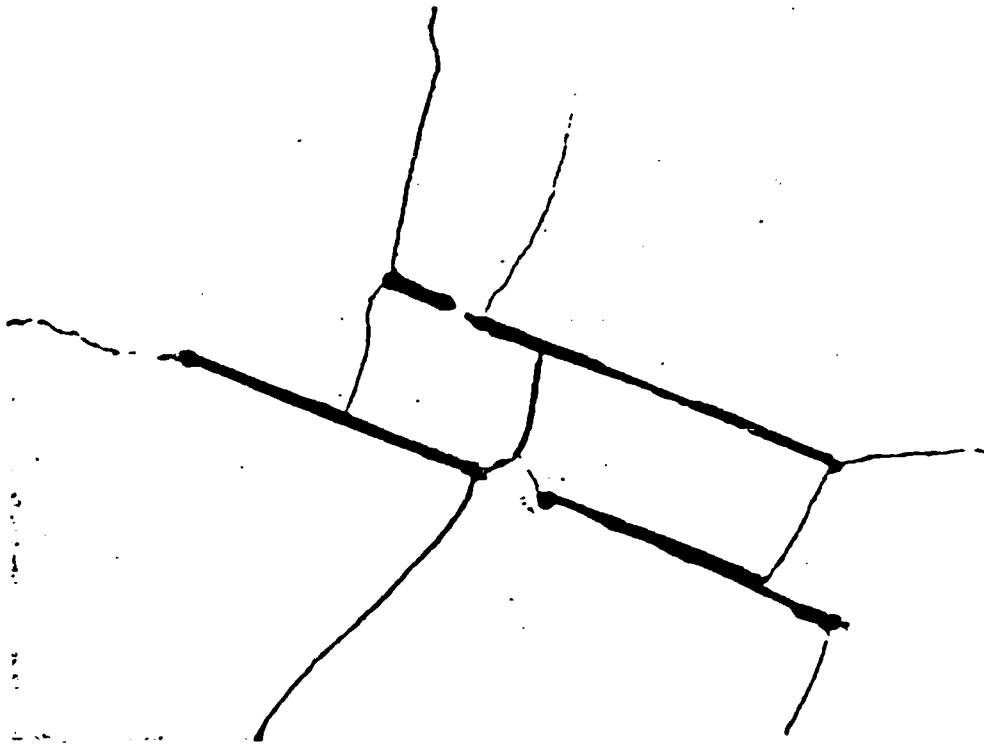
centrifuge until, at 600 g, failure occurred. In the two cases, the resulting fracture patterns were completely different as shown in Fig. 2.12, indicating the influence of the body forces. Hoek (1965) also studied the stress distribution around extensive stoping excavations on two horizons. Here, too, as shown in Fig. 2.13, stress distributions in the centrifuged model were quite different from the case where the model was loaded externally, indicating the importance of simulating the original stresses that exist in the rock mass. Like the previous case, the results were only qualitative. Hoek subsequently left for Imperial College, and thereafter not much work has been done on this machine.

Ramberg and Stephansson (1965) studied the static stability of excavations in rock using centrifuged models. The various types of excavations they studied are shown in column 1 of Table 2.1. The models were made up of cement, plaster of Paris, lime, sand and magnetite powder, which were mixed in various proportions so as to obtain the required density and strength. The models were placed in a small centrifuge and spun to as high as 3000 g's. The results of the various tests are shown in Table 2.1, where the column 'experimental a/g' gives the experimental ratio between the centripetal acceleration at the moment of collapse and the acceleration due to gravity. Similarly, the column 'theoretical a/g' gives the calculated ratio at failure based on the measured strength and density of the model material. The theoretical a/g values were calculated only for models K1, K2, K3, K4, K10 and K16. The last two columns give the dimensions of the equivalent prototypes made of granite or sandstone, that would theoretically collapse due to self-weight.

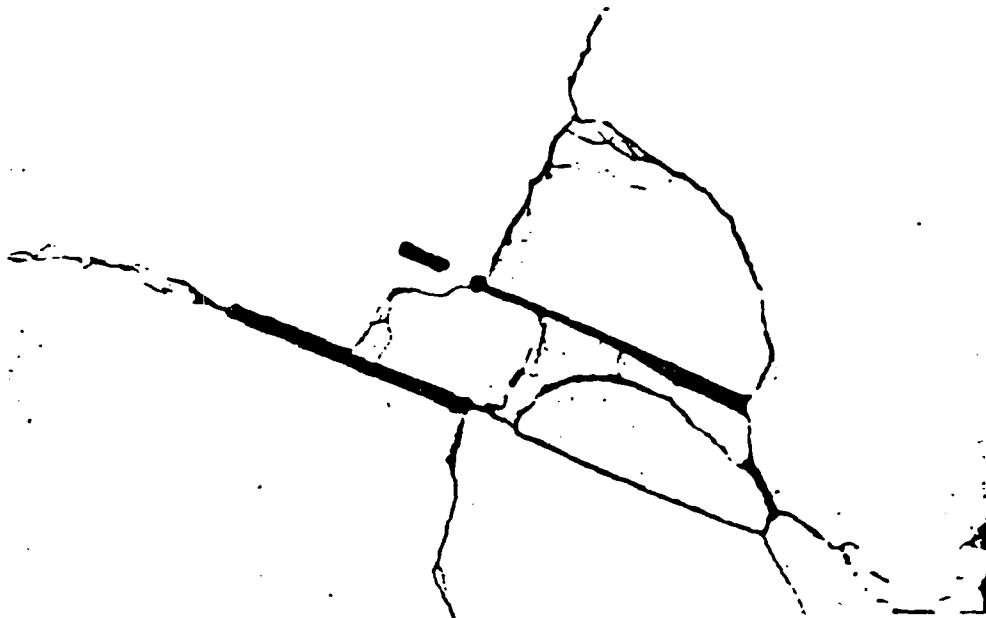
### 2.3.3 Slope Stability

Rock slopes also too have been studied with the centrifuge. The slopes studied were made up of photoelastic material or homogeneous artificial rock, either intact or with smooth joints. Rockfill dams also have been studied.





a) Plaster of Paris mine model loaded to fracture by uniformly distributed edge loads.



b) Plaster of Paris mine model loaded to fracture at 600 g in the centrifuge.

Fig. 2.12. Fracture patterns showing the importance of body forces in the fracture of large rock masses. From Hoek (1965).



a) Photoelastic pattern in a mine model subjected to uniformly distributed edge loading.



b) Photoelastic pattern in a mine model which had been stress-frozen under a centrifugal acceleration of 100 g.

Fig. 2.13. Comparison between photoelastic patterns under external and body force loading. From Hoek (1965).

Table 2.1. Investigation of models by means of a centrifuge. From Ramburg and Stephansson (1965).

Cross section of the model	Model no.	Total height (cm)	Height (cm)	Width (cm)	Height of opening (cm)	Length of opening (cm)	Radius of curvature (cm)	Pillar width (cm)	Inclination (°)	Density (g/cm³)	Tensile strength (kg/cm²)	Theoretical $\frac{\sigma}{\rho}$	Collapsing structure of granite with tensile strength $225 \cdot 10^3$ g/cm² and $\rho = 2.5$ g/cm³				Collapsing structure of sandstone with tensile strength $98 \cdot 10^3$ g/cm² and $\rho = 2.5$ g/cm³				
													Ratio $\lambda \cdot 10^3$	a (m)	b (m)	c (m)	Ratio $\lambda \cdot 10^3$	a (m)	b (m)	c (m)	
	K16	3.5	1.0	4.0	1.0	—	—	—	1.9	5.1	610	0.49	367	816	204	—	1.3	138	308	77	
	K22	3.4	1.1	1.0	0.6	—	—	—	1.8	5.2	2800	0.12	915	931	500	—	0.33	324	303	192	
	K14	3.1	1.3	2.1	1.1	0.5	1.5	—	1.9	5.1	900	0.33	392	635	322	—	0.88	148	239	125	
	K34	3.4	1.2	2.0	0.6	—	0.4	—	1.8	5.2	1300	0.24	500	934	250	—	0.86	182	303	91	
	K28	3.2	0.8	0.9	0.8	—	—	—	1.8	5.4	1300	0.25	320	360	360	—	0.89	118	122	122	
	K30	3.4	1.0	0.9	0.9	—	—	—	1.8	5.4	1400	0.24	416	375	375	—	0.83	159	163	163	
	K25	4.9	2.5	3.5	1.7	—	—	—	0	19	5.4	700	0.45	555	780	378	—	1.2	208	292	142
	K27	5.2	1.2	3.4	1.7	—	—	—	45	1.9	5.4	1300	0.24	866	1331	866	—	0.65	266	493	246
	K10	3.1	1.5	1.4	—	—	—	—	90	1.9	5.4	1900	0.17	705	2000	1000	—	0.44	273	773	386
	K23	3.1	1.8	2.1	—	5.7	—	—	40	1.9	3.9	1500	0.15	1000	931	—	0.41	366	341	—	
	K1	—	1.1	2.9	—	7.5	—	—	1.85	11.1	160	486	24	83	—	12.7	8.6	31	—		
	K2	—	0.5	4.0	—	7.5	—	—	1.77	8.2	72	70	63	50	—	21.4	2.3	19	—		
	K3	—	1.0	4.1	—	7.6	—	—	2.35	8.2	800	812	—	—	—	12.5	8.8	33	—		
	K4	—	0.8	3.9	—	7.6	—	—	2.54	2.25	1820	1875	16	71	—	—	—	—	—		

\* K3 - Sandstone, \*\* K4 - Granite

Gomah (1963) studied homogeneous intact rock slopes using 2-D slope models of photoelastic material to determine the stress distributions. The semi-cured models were spun in the centrifuge at the desired  $g$  level until curing was complete, and the stresses locked in the model. The model was then taken from the centrifuge and the fringe patterns studied under polarized light. Gomah studied the stress distributions in the slope as a function of the body stresses due to gravity, the angle of inclination of the slope and its height. Typical stress distributions are shown in Fig. 2.14. Loading, however, was not carried up to failure.

More recently, work has been done in Japan to study the behavior of rock slopes. Sugawara et al (1982) studied the progressive failure of rock slopes, using model slopes made up of a mixture of plaster, slaked lime, standard sand and water. Three materials made up of mixtures of the above materials were used to make model slopes, with slope angles ranging from 50 degrees to 80 degrees. A theoretical study of the slopes, using finite elements, was also made. Fig. 2.15 is the result of the finite element analysis and shows that if  $n = \frac{\gamma H}{c}$  is plotted against the normalized strain  $\epsilon/\epsilon_0$ , then the resulting curve is useful in studying progressive failure, where

$n$  = a dimensionless factor indicating the magnitude of gravitational loading

$\gamma$  = unit weight of the material

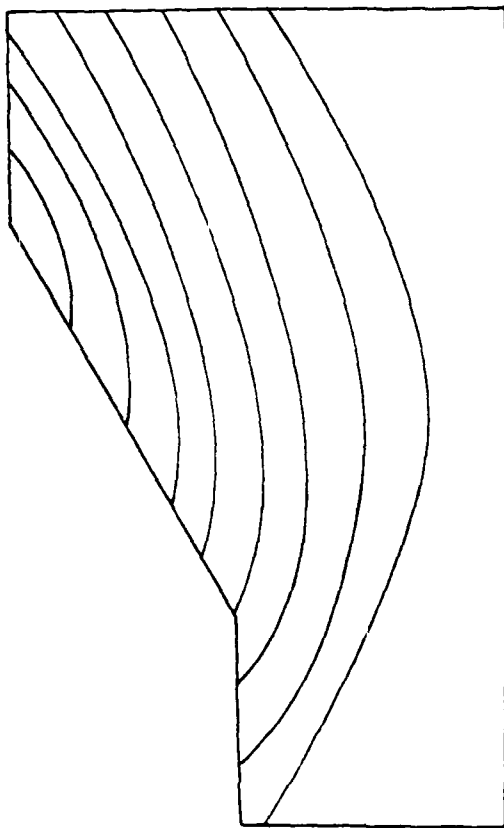
$H$  = height of slope

$c$  = cohesion of the material

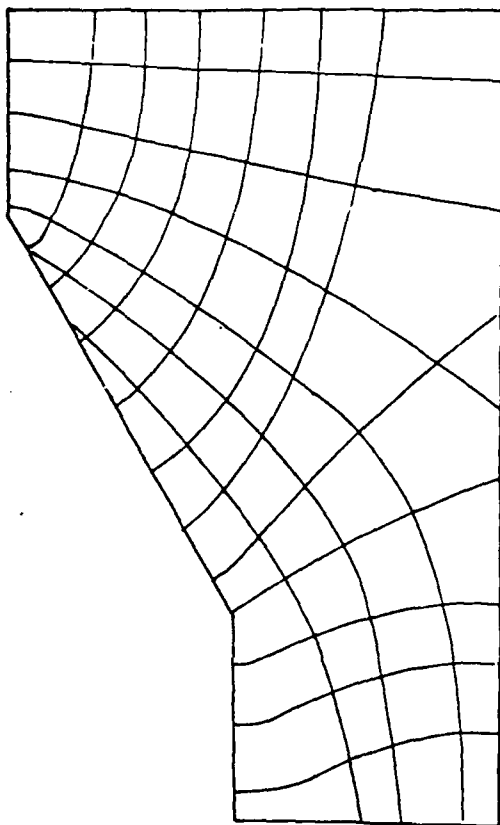
$\epsilon$  = strain measured on the rock surface

$\epsilon_0$  = material constant which is the elastic axial strain at the uniaxial compressive strength

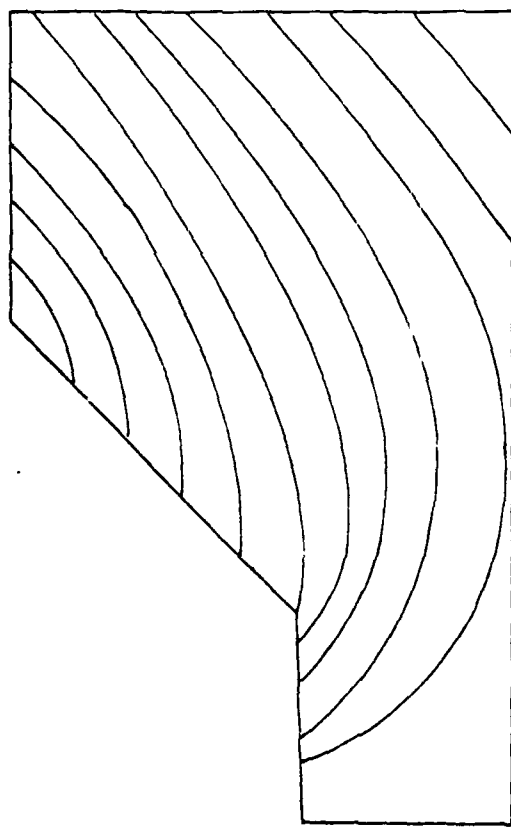
At  $n = n_i$ , failure initiates at the toe of the slope. At  $n = n_t$ , the strain increment on the surface of the slope changes from compression to tension, and at  $n = n_c$ , the strain increment becomes infinite which is the condition of limiting equilibrium.



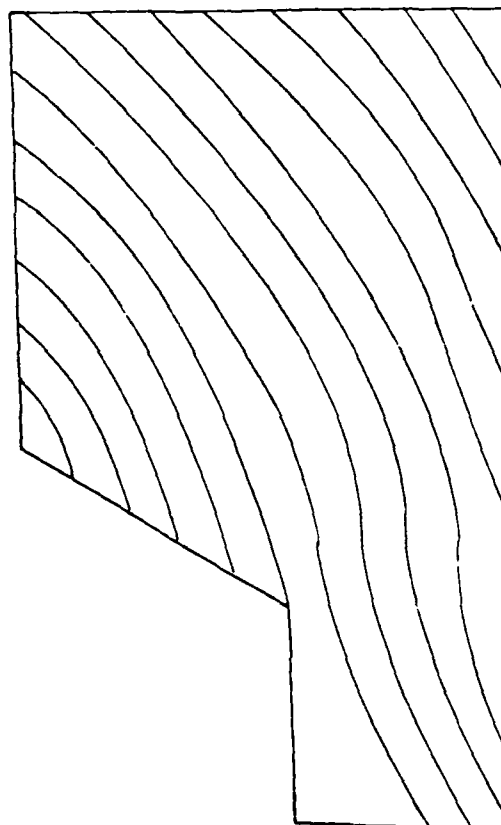
a) Maximum shear stress trajectories in 30° slope model.



b) Principal stress trajectories in 30° slope model.

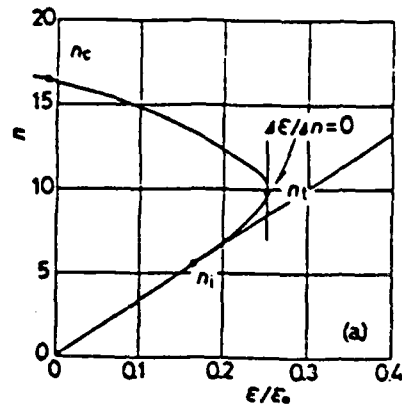


c) Shear stress trajectories in 45° slope model

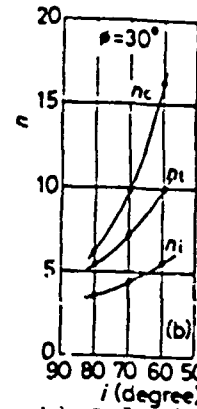


d) Shear stress trajectories in 60° slope model.

Fig.2.14. Stress trajectories obtained from centrifuge tests. From Clark (1981).

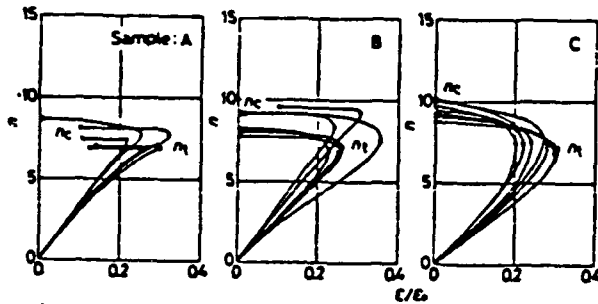


a) Relation between  $n$  and  $\epsilon/\epsilon_0$

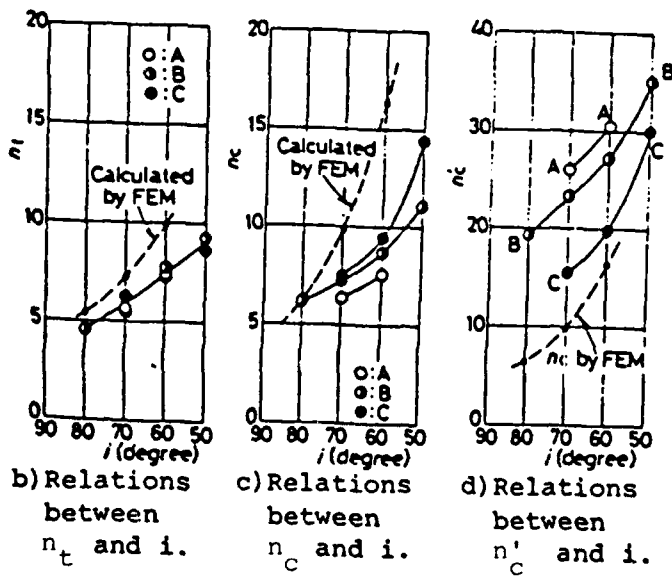
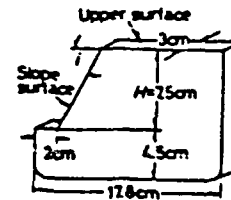


b) Relations between  $n_c$ ,  $n_t$ ,  $n_i$  and  $i$

Fig. 2.15. Results obtained by FEM analyses. From Sugawara et al (1982).



a) Relations between  $n$  and  $\epsilon/\epsilon_0$  at  $i = 60$  degrees.



b) Relations between  $n_t$  and  $i$ .

c) Relations between  $n_c$  and  $i$ .

d) Relations between  $n'_c$  and  $i$ .

Model	$\gamma$	$E$	$c_p$	$\phi_p$	$c_r$	$\phi_r$	$E/c_p$
A	140	80.5	137.0	30.0	34.0	29.0	588
B	142	60.8	97.9	30.0	31.0	29.0	621
C	145	40.3	71.3	30.0	34.0	29.0	565

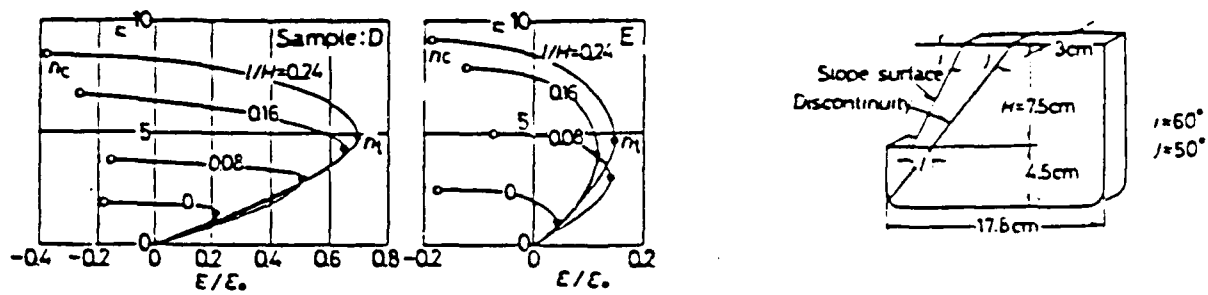
e) Model geometry and physical properties of materials.

Fig. 2.16. Results of centrifuge tests on intact rock slopes. From Sugawara et al (1982).

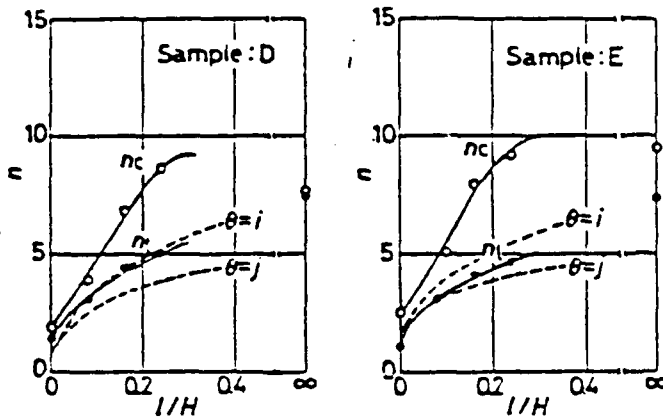
Sugawara et al suggested that the change from compression to tension of the strain increment measured on the surface was the result of progressive sliding on the slip lines, and that consequently  $n = n_t$  represented a stable-unstable transition. Progressive failure should be clearly detected at  $n > n_t$ .

The results from the centrifuge tests are shown in Fig. 2.16 and are similar to the finite element results. Also shown in Fig. 2.16 are the properties of the model materials, the model geometry and the relation between  $n_t$ ,  $n_c$  and  $n'_c$  ( $n'_c = \frac{c_{res}}{c}$  where  $c_{res}$  is the cohesion intercept of the residual strength) and the slope angle  $i$ . Sugawara et al showed that  $n_t$  was a linear function of  $i$  (Fig. 2.16). The value of  $n$  at which limiting equilibrium was reached was  $n = n_c$ . Based on their work, they suggested that using the peak shear strength of the rock mass to calculate the limiting slope height was unrealistic as strain softening is thereby ignored. On the other hand, using the residual shear strengths would be too conservative. Consequently they suggested that the analysis be based on the plot of  $n_t$  (the transition from stable to unstable conditions) vs.  $i$ .

Sugawara et al also analyzed a slope with a discontinuity. Fig. 2.17 shows the model geometry, material properties and results of the centrifuge tests, plotted as curves of  $n$  vs.  $\frac{l}{H}$ , for  $\theta = i$  and  $\theta = j$ . The terms  $l$ ,  $H$ ,  $\theta$ ,  $i$  and  $j$  are defined in Fig. 2.18. The theoretical analysis with which the experimental results were compared is also shown in this figure. The model assumes the simultaneous sliding of the failure wedge on both the potential slip plane GB in the intact rock and the joint surface DG. This assumption is valid only at the very start of sliding, or if the rock wedge is perfectly rigid, as otherwise movement on the two planes will not take place at the same time. In the experimental model (the material not being perfectly rigid), differences were observed between the test results and the results of the theoretical analyses. This is shown in Fig. 2.17



a) Relations between  $n$  and  $E/E_0$  at  $0 < l/H < 0.24$ .



b) Relation between  $n_c$ ,  $n_t$ , and  $l/H$ .

Model	Intact rock material				Joint surface	
	$c_p$	$\phi_p$	$c_t$	$\phi_t$	$c'$	$\phi'$
D	138.0	30.0	30.0	29.0	5.0	22.0
E	62.0	30.0	33.0	29.0	10.0	24.0

c) Model geometry and physical properties of materials.

Fig. 2.17. Results of centrifuge tests on jointed rock slopes. From Sugawara et al (1982).

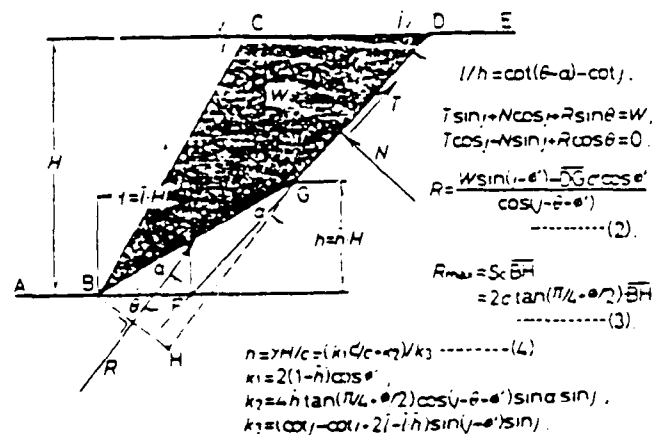


Fig. 2.18. A failure model of slope with a discontinuity. From Sugawara et al (1982).



where the dotted line is a plot of the theoretical value of  $n$  (calculated using Equation 4 in Fig. 2.18), plotted vs  $l/H$ . From the experimental results, it is seen that the theoretical analysis does not define the limiting equilibrium condition but corresponds to the stable-unstable transition. This is because the simultaneous sliding on the two planes as assumed in the theoretical analysis, is, for an imperfectly rigid material, valid only up till the stable-unstable transition. This test series showed clearly how theoretical modeling and centrifuge testing go hand in hand.

Mikasa et al (1982) ran stability tests on a rock fill dam using a centrifuge. The dam in question was a zoned dam with an inclined core and was to be built on unfavorable deposits, with its downstream zone made up of weak weathered material. They did not expect accurate results from finite element analyses and so decided to model the problem with the centrifuge. Eleven types of 2-D dam models were tested, of which the results of tests run on three models (models 7, 9 and 10) were presented. Details of these three models are shown in Fig. 2.19. For modeling the rock material, sandstone was pulverized to a maximum diameter of 4.8 mm, which was 1/150 the size of the prototype material. To model the core and the downstream material, particles of the core material from the site, under 2mm in size, were used. The model dimensions were made 1/150 those of the prototype and the model was centrifuged at 150 g. The tests were done in three stages. In the first stage, the g level was raised to 150 g over a period of 5 minutes. In the second stage, the upstream water level was raised from the base to 0.9 times the dam height, and then lowered back to the base. This cycle was repeated five and a half times so that, at the start of the third stage, the water level was near the dam crest. For the third stage, the model was inclined to the upstream side by 0.02 radians over a period of 6 seconds, and held in this position for 4 seconds, after which, it was brought to the vertical position again. The procedure was repeated until failure occurred, and was to simulate lateral earthquake action statically.

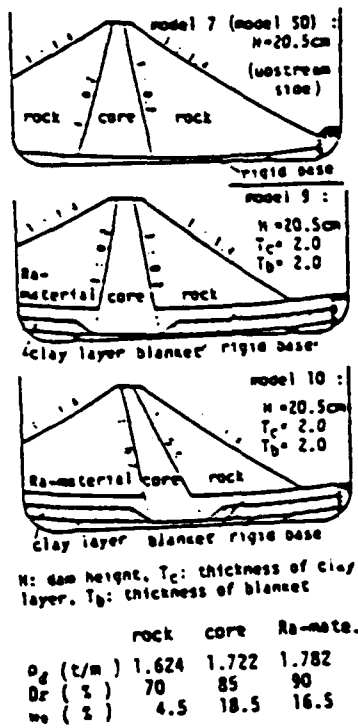


Fig. 2.19. The models studied.  
From Mikasa et al (1982).

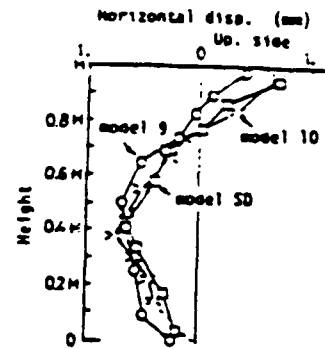


Fig. 2.20. Increment of horizontal displacement (2nd stage).  
From Mikasa et al (1982)

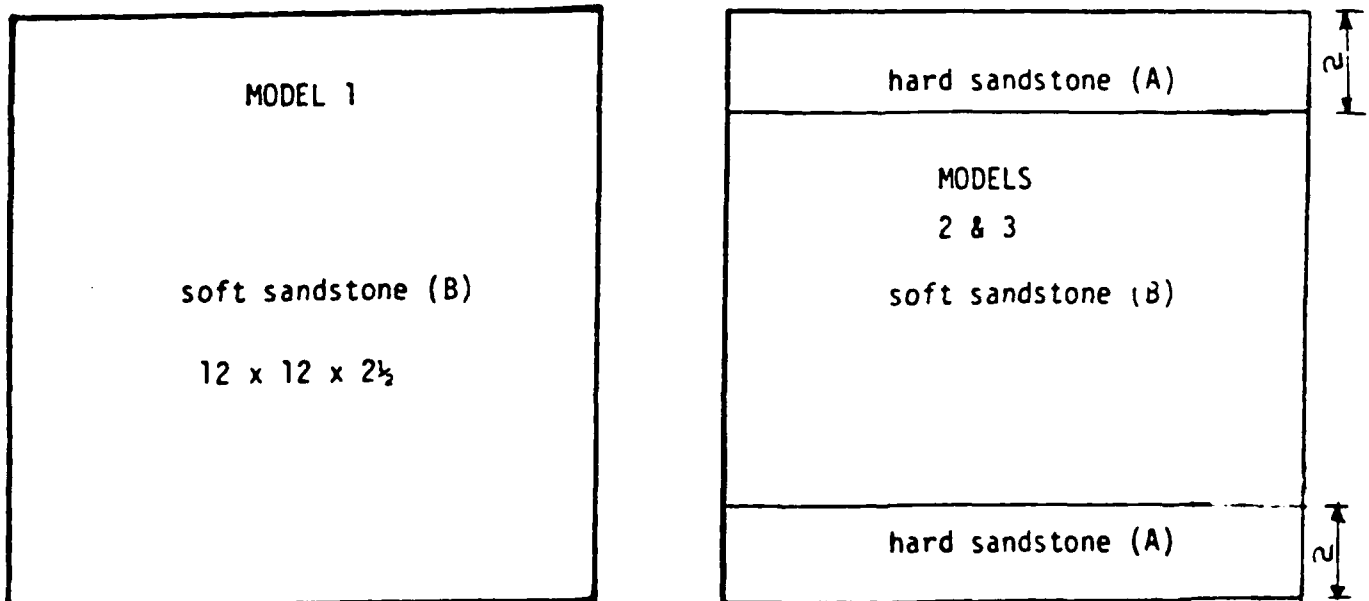


Fig. 2.21. Model configuration. From Clark (1981).

During Stage 1, Model 7 and Model 9 deformed symmetrically with respect to the core axis, even though Model 9 had an unsymmetrical arrangement of fill materials. Model 10 deformed unsymmetrically, with lateral movement to the upstream side. The cores for Models 7 and 9 moved slightly downstream, while for 10, it moved considerably upstream. Settlements were found to increase almost linearly with centrifugal acceleration. Though the core settled more than the shell, the transition was gradual, indicating that there was no slip between the two zones.

During the second stage, the deformations were much larger. The upstream slope settled considerably and the cores in all three cases bent like a bow, as shown in Fig. 2.20. Marsal (1967) observed this bending in an actual rock fill dam and suggested that it was caused by the settlement of the upstream face. Harada (1977) obtained the same bow-like bending from finite element analysis of a rock fill dam. For the models, the bow-like movement created a loosened area in the upstream shell, which ultimately resulted in slip failures on the upstream face of the dam.

For stage three, the angle of the slope surface at failure was found to be greater than the theoretical value, probably as a result of some cohesion in the model material. Since this cohesion was not expected to occur for the prototype material, it was neglected in the actual dam design. Based on these tests, the actual dam design was altered to one with a center core that was inclined slightly to the upstream side, as this was expected to be the most stable geometry.

#### 2.3.4 Miscellaneous

This section deals with research in rock mechanics using the centrifuge that cannot be grouped in one of the previous categories.

The material properties of small cores of rock are not the same as those of larger specimens of massive rock unless the rock is ideally uniform, homogenous and isotropic. Scale factors have been proposed and used for coal, to extrapolate the results of small scale tests to prototypes. Clark (1980) ran centrifuge tests with

flat sandstone slabs cut with the large faces normal to the bedding planes. The slab dimensions were 12 inches x 12 inches x 2 1/2 inches. In order that stresses be evenly distributed, the slabs were surface ground on all the outside surfaces. As most rocks in large masses are not uniform in properties or composition, no attempt was made to select a slab of exceptional uniformity.

Two sandstones - sandstone A and sandstone B - were used to make three models of a large intact rock slab. Sandstone A had a higher modulus of elasticity than sandstone B. Fig. 2.21 shows the models that were tested. Model 1 was made entirely of sandstone B, while Models 2 and 3 had layers of sandstone A of different thicknesses at the top and bottom. The layered models were placed in the centrifuge bucket and spun to check whether any effects due to bedding would become evident during testing, and whether these effects scaled with the g level. Strain gages were mounted at various points on the surface of the sandstone. The gages showed a wide range of readings with some gages even indicating that yield had occurred, i.e. the stress-strain properties of the rock appeared to vary with position. This shows that it would be desirable to consider the properties of a rock as a function of position, for input into theoretical models.

Clark (1981) has suggested that the centrifuge can play an important role in studying explosive cratering in rock. Schmidt and Holsapple (1980) modeled cratering in sand using small amounts of explosive in a multiple gravity field. They developed a unified theory for cratering dynamics in terms of source characteristics, energy and specific energy, soil strength, gravity, time and the range over which debris were distributed. The equations were applied to the case of an explosive detonated on the surface of a deformable soil medium with the space above the medium being filled with gas. Schmidt et al identified eight independent variables that they thought controlled cratering phenomena, and, by using dimensional analysis, obtained five  $\pi$  terms, one of which showed that the

yield of an explosion scaled at  $N^3$  i.e.  $\frac{E_m}{E_p} = N^3$ , where  $E_m$  is the energy yield of the model explosion and  $E_p$  is the yield of the prototype explosion. There has been some discussion as to whether the energy yield scales at the third power or fourth power of  $N$ , or at some value in between. Using the Boeing centrifuge, they were able to successfully simulate explosions in a range of soil types, with the values of the dimensionless terms chosen so as to cover the equivalent of twelve orders of magnitude of explosive energy. Schmidt and Holsapple (1980) suggested that by modifying the variables to account for the properties of rock, it would be possible to run the same types of tests to study cratering phenomena in rock. The relative cost of experimental prototype scale cratering is several orders of magnitude greater than that of an equivalent small scale test as the centrifuge, clearly showing the cost effectiveness of the centrifuge in studying prototype behavior.

Early centrifuge work dealt with problems involving rock. Most of the centrifuge work in the fifties and sixties too dealt with rock. In the latter half of the sixties, more interest was shown in studying soil problems in the centrifuge, until, in the seventies, very little work if any, was done on rock problems. In the eighties, there has been a renewed interest in studying problems dealing with rock. From the previous sections, it is clear that centrifuge testing is a technique that can be used to advantage in rock mechanics to study a wide range of problems. Most of the work described previously deals only with intact rock material, with little or no work done with jointed rocks or rock masses. The centrifuge technique could possibly be of considerable use in investigating this area. A second report will explore these possibilities.

#### 2.4 Ice Mechanics

Oil exploration is being carried out from off-shore structures in Arctic areas. For the efficient design of structures in these areas, an idea about the ice forces

exerted by the surrounding ice fields on these structures is required. Vinson (1982) proposed the use of a centrifuge to study these forces. Of interest were the magnitudes of the forces exerted on the structure, the failure mechanisms and details on factors influencing general ice behavior. The variables of interest suggested were the ice temperature, thickness and salinity, the flow velocity and the angle of incidence of impact with the structure.

Clough et al (1986) describe the development of a program to test ice behavior in the centrifuge. Four components were involved: 1) the insulated strong box to contain the model, 2) a system for forming the ice sheet, 3) a drive system to pull a structure through the ice sheet (effects similar to a sheet moving past the structure) and 4) the instrumentation. The various components are shown in Fig. 2.22. The model strong box was build of aluminum, lined on the insides with 1/4 inch acrylic plastic and on the outside by 1 inch thick polystyrene foam. By doing this, the heat flow was made essentially unidirectional, with the heat flow through the sides and the base only 1% of the flow through the ice covered surface. To form the ice sheet, liquid nitrogen was injected through holes along a circular boundary ring (Fig. 2.22). The nitrogen vapor was held in the container by an acrylic plastic cover held in place by a wing nut. Using this system it was possible to create a fairly uniform ice sheet. A motor placed on the centrifuge platform, with its shaft passing through the container wall and connected to a worm drive through a flexible coupling (Fig. 2.23), was used to pull a 1 inch diameter aluminum rod, mounted on a base plate, through the ice sheet. Feedback loops were used to maintain temperatures at desired levels and also to control the velocity of movement of the structure. Temperatures were monitered at different spots using thermistors. Movement of the structure was measured with LVDT's. Loads on the structure were measured by strain gauges attached to the bottom of the aluminum rod. The entire system was found to work well and data from centrifuge tests compared well with the results of in-situ tests reported in the literature.

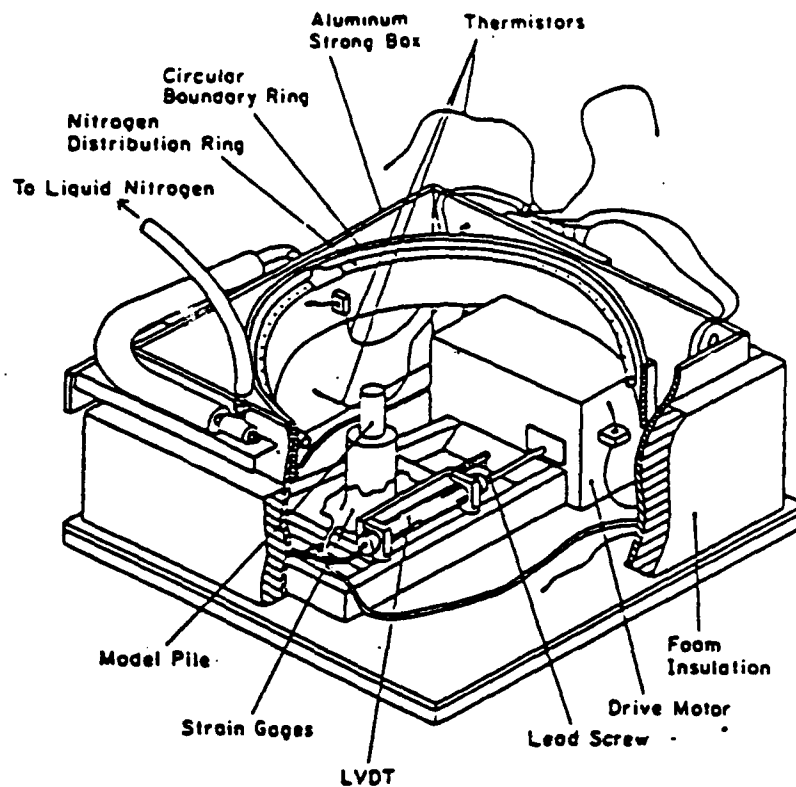


Fig. 2.22. Sectional view of model test container. From Clough et al (1986).

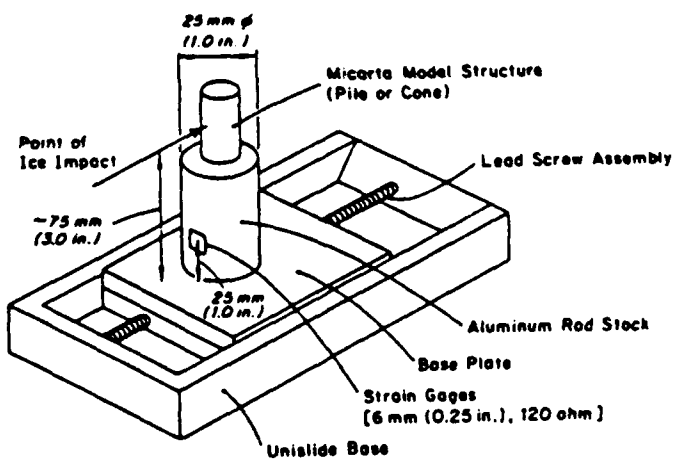


Fig. 2.23. Model structure assembly. From Clough et al (1986).

Clough and Vinson (1985) studied the ice forces on vertical structures using the apparatus described above. From a dimensional analysis they obtained five dimensionless products which they used to conduct the centrifuge model tests. Based on their results, they concluded that small scale tests, if properly interpreted, can describe large scale forces for the crushing mode of failure. They found that centrifuge modeling of ice-structure interaction is valid, and provides a way of scaling self-weight forces of the ice, for gravity dependent problems. For the crushing mode of failure in thin ice sheets, a small scale model will accurately describe the prototype if the model dimensions are at least thirteen times the average ice crystal size. The normalized force on the structure for the crushing mode of failure is constant for a ductile type failure, in accordance with plasticity theory, but for some reason rises to a peak in the transition from ductile to brittle failure. The normalized force on a frictionless conical structure for the bending mode of failure is proportional to the tangent of the cone angle, linearly dependent on the normalized inertial acceleration (centrifugal acceleration) and independent of the normalized velocity for normalized velocity values less than or equal to  $1 \times 10^{-3}$ . Measured horizontal forces agree well with theoretical predictions. Lastly, they concluded that the small scale modeling technique was valid for the crushing model of ice-structure interaction investigated and that the results of their study could be used to predict ice forces due to ice crushing on rigid isolated vertical structures in either fresh or saline ice.

Professor Schofield at Cambridge University, England, has modeled ice on the centrifuge. Lovell and Schofield (1986) detail the procedure used to form the ice sheets. Sixty-five litres of water with a salinity of 3% is cooled by liquid nitrogen. The nitrogen boils steadily for 4 1/2 hours due to heat entering the nitrogen. The cold gas falls to the surface of the water, extracts the heat and rises to leave the package. It was found that the time to develop an ice sheet of



25 mm at 60 g was just over an hour. The time required at 1 g to form a sheet of equivalent thickness ( $60 \times 25 = 1500$  mm) is about 6 months. It was found that the grain size of the salt ice scales to the correct order of magnitude. Also, appropriate scaling of the random, transition and columnar zones as in the first year sea-ice was obtained. It was also found that the rate of increase of horizontal crystal diameter with depth of the ice was in good agreement with that of first year sea-ice. The ice sheets were tested under vertical static loads, by layering dead weights onto the ice at the center of the sheet. Comparison of the breakthrough loads with recommended loadings showed the results to be of the same order as those expected. Further studies involving lateral loads, various scales and loading rates were proposed. A drum centrifuge capable of 500 g is to be built, with which bigger ice sheets can be modeled.

## 2.5 Tectonics

The centrifuge has also been used in experimental tectonics. Ramberg (1963) started a project modeling tectonic processes at the University of Chicago. He then went to Uppsala, Sweden where the method was further developed to the point where it was considered a routine method of testing. The centrifuge at Uppsala that Ramberg used could accelerate a mass of 1.5 kg to 3000 g.

Tectonic processes are difficult to model at 1g. The prototype structures are so large (ranging from hundreds of meters to hundreds of kilometers) that gravity effects play a role in their evolution. In a scaled model the self weight stresses at 1g are very small. Also, due to the high strength and viscosity of the material, prototype structures deform very slowly. Consequently, in order that deformations develop reasonably quickly under the low stresses that exist at 1 g, the model material should be made far weaker than the prototype material. True similarity at 1g requires model material that is so weak that it is often impossible to construct models from these materials. In his pioneering work in modeling tectonic processes,

Ramberg (1963) overcame this problem by subjecting his models to an elevated gravity field, using the centrifuge. By increasing self-weight stresses, he was able to satisfy similitude requirements using stiffer and more viscous model materials. Commonly used model materials included: 1) silicone putty of various viscosities, either pure, or mixed with fine powder of magnetite or tungspar (or both) to obtain the desired density, 2) painters putty with a plastic base, 3) mixtures of collophony and ethylene phthalate, 4) modeling clay or plasticene, 5) oil-wax mixtures and 6)  $K Mn O_4$  solutions.

Various prototype tectonic processes which are driven and controlled by gravity have been successfully modeled in the centrifuge. Ramberg (1968 a, 1968b, 1972) studied the formation of mantled domes (Fig. 2.24), extrusion of lava, folding of layered complexes, subsiding bodies, and other processes powered by gravitational instability. He was also able to model continental drift.

Dixon and Summers (1982) used a centrifuge capable of reaching 20,000g, at the Experimental Tectonics Laboratory at Queens University in Ontario, Canada, to model tectonic processes. The centrifuge consists of a 33 inch diameter disc of solid aluminum, 3.25 inches thick, and provided with two diametrically opposed cavities to hold the samples. The general types of problems they studied were the convective overturn of unstable density stratification, and the gravitational collapse and lateral spreading of a rock mass elevated with respect to the gravitational equipotential surface. Specific problems that were examined were the progressive evolution of mantled Gneiss Domes [Dixon (1975)], the internal geometry, strain distribution and progressive deformation of simple Greenstone Belts [Dixon and Summers (1980), (1981)] and folding and faulting in layered materials [Dixon and Summers (1982)]. Quantitative data concerning the strain distribution within the structure were obtained by constructing the model in two halves, with passive internal layering. The layering is horizontal in one half and vertical in the other

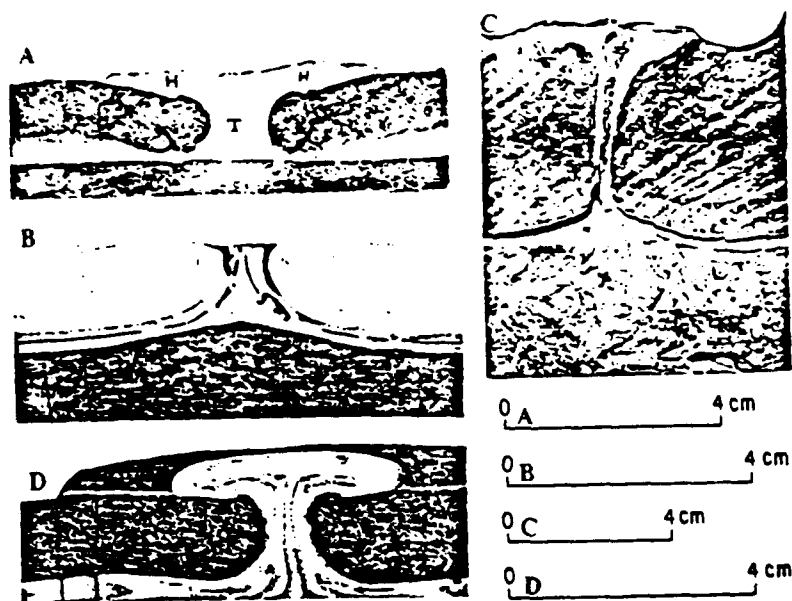


Fig. 2.24. (A) Dome of silicone putty ( $\rho = 1.14 \text{ g/cm}^3$ ) having penetrated overburden of painters putty ( $\rho = 1.87 \text{ g/cm}^3$ ) during centrifugation. Initial structure consisted of horizontal parallel and continuous layers. H = hat of dome, T = trunk. Arrows indicate rim syncline. (B) Silicone-putty dome (light gray, with thin, dark sheet that has broken into boudins) rises through painter's putty overburden. Substratum (black) consists of heavy silicone putty mixed with powder of magnetite. Note bulge on substratum below dome. Original layering horizontal. (C) Layer of light silicone putty that has risen through overburden of painter's putty, spread across the surface, and sucked up the heavy substratum almost to the surface. (D) Model indicating direction of flow in source layer and dome. The initially evenly thick horizontal source layer consisted of alternating strips of dark and light colored silicone with square cross section as indicated by two vertical lines on left side of photo. Present pattern indicates movement. Note that horizontal flow in source layer has passed underneath the rim syncline. From Ramberg (1972).

as shown in Fig. 2.25, so that, when two layers in the undeformed model - one from each half - are superimposed, a square grid is obtained. After deformation, two corresponding sections, similarly superimposed, will yield a deformed grid. By comparing the deformed grid with the undeformed grid, the orientation and magnitude of maximum deformation in each grid element can be obtained, as shown in Fig. 2.26. A grid of lines can also be drawn on the surface of the model to study surface deformations. The advantage of this method is that information regarding large deformations, which would cause a break down of numerical schemes, can be obtained. Also, this method provides a detailed three-dimensional picture of the evolution of the structure.

Large scale tectonic processes are complex in terms of configuration, rheological properties, boundary stresses, displacement conditions, significant local heterogeneities in the displacement field, and finite strains. Consequently, they are difficult to model correctly using current numerical methods. Physical modelling using the centrifuge offers an additional tool, for obtaining information about these processes.

## 2.6 Conclusion

This section briefly summarizes the work done in geotechnical engineering using the centrifuge and also suggests areas in rock mechanics where the technique will be of use.

At present, the most frequent application of the centrifuge in geotechnical engineering is in soil mechanics. Centrifuges in various countries are being used to study a wide range of problems involving soil. The work being done can be considered as falling under one of the following headings - the flow of water through soils, soil-structure interaction, dynamics, underground construction and other uses such as slope stability, embankments, penetrometer studies, etc.

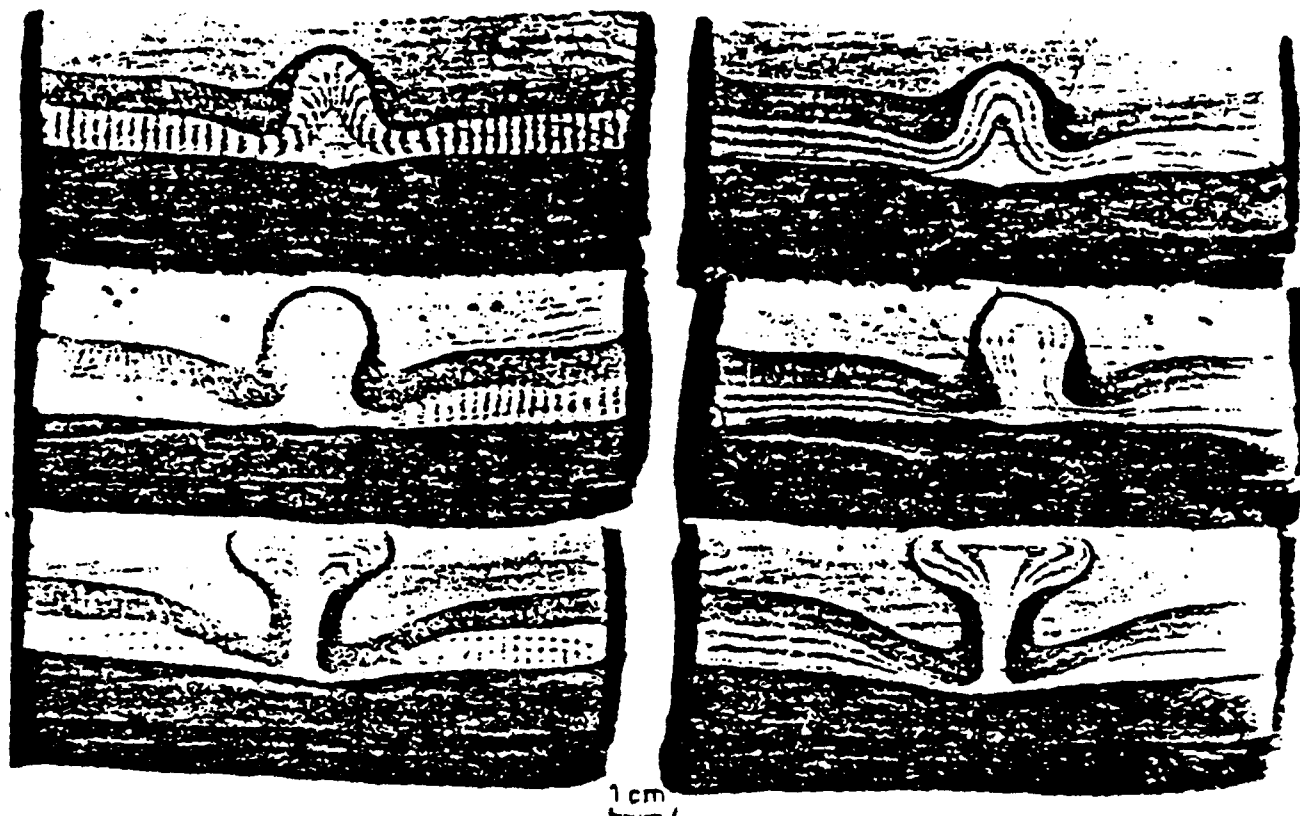


Fig.2.25. Three stages in the development of a Mantled Gneiss Dome. Top row: two sections through model WD-4. Note that in one section the striped pattern in the buoyant layer and in the immediate overburden was initially vertical, and in the other section, horizontal. If the two striped patterns are superimposed, the deformed grid of Fig.2.26 is produced. Middle and bottom rows: two more advanced stages of growth of the dome (models WD-2 and WD-3). (Models described in detail in Dixon, 1975). From Dixon and Summers (1982).

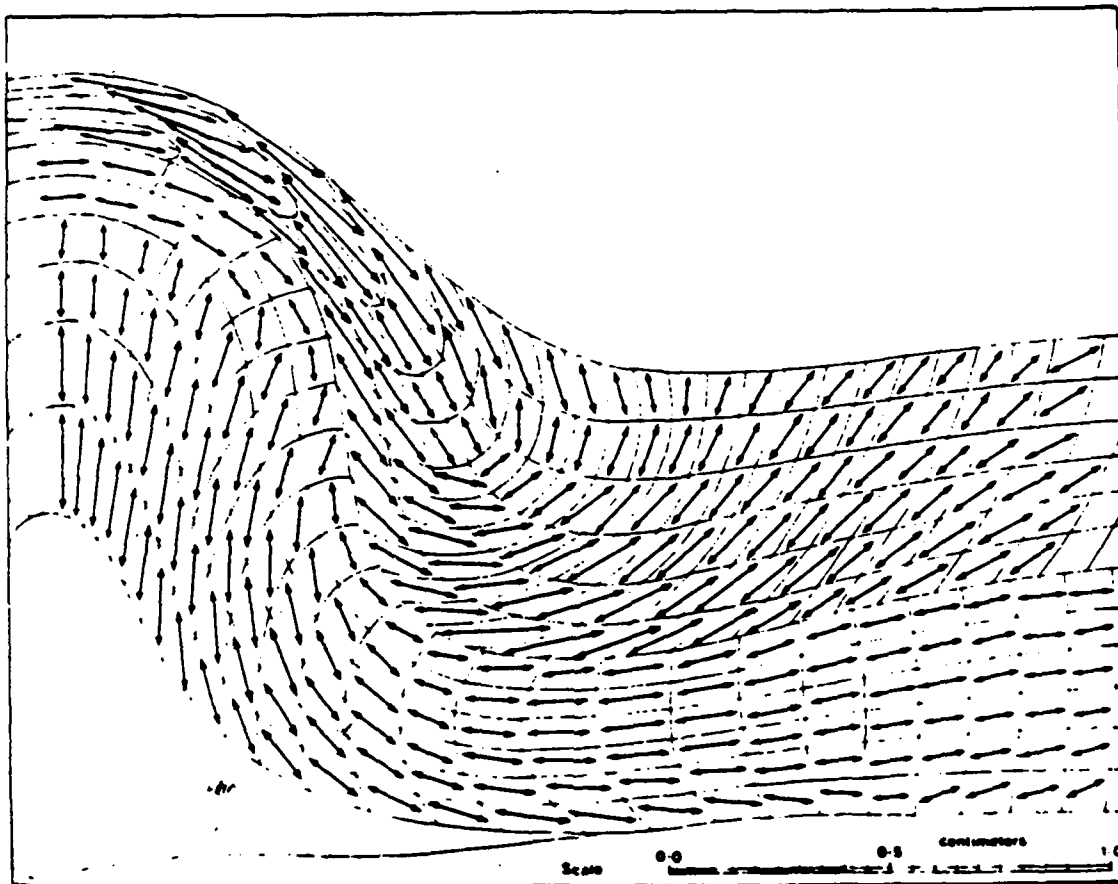


Fig.2.26. Deformed grid elements of Mantled Gneiss Dome model WD-4 (Dixon, 1975), showing the orientation and relative magnitude of the axis of maximum finite elongation in each grid element. From Dixon and Summers (1982).

In rock mechanics research, the centrifuge was quite frequently used in the late fifties and in the early sixties. Subsequent to this there was not much centrifuge work until the eighties when some work seems to have started. Most of the earlier work dealt with intact rock and consequently required relatively high g fields. The models were made up either of natural rock or of artificial materials. A common technique used then to study stress distributions within the material was photoelasticity, with the stresses being frozen into the photo elastic model. The work done in centrifuge testing involving rock can be grouped under the headings:

- 1) simple beams and unsymmetrical beams, 2) layered roof, subsidence problems, underground openings and excavations 3) rock (intact and jointed) slopes, rock fill dams and 4) miscellaneous problems like large rock specimens and explosive cratering.

The centrifuge technique has offered considerable insight into these areas. As described previously, it has also been applied to study problems in ice and tectonics.

It is clear that the centrifuge can be applied to a wide range of problems in areas associated with geotechnical engineering. In rock mechanics, Clark (1982) suggested that the centrifuge can be used in the following areas:

"1) Simple body force loading

- a) Intact rock of various sizes and types
- b) Structures in intact rock

2) Fracture due to body force loading

- a) Beams and similar structures
- b) Geologic structures, surface and underground
- c) Manmade underground structures, slopes, power stations, etc.

3) Slopes

- a) Stress distribution
- b) Failure surfaces vs. maximum shear stress

- c) Rock slides
- d) Fractured solid rock slopes, stress and stability
- 4) Behavior of rock masses with and without similitude (qualitative studies)
- 5) Mechanics of caving, with and without similitude (qualitative studies)
- 6) Many other types of investigations where body forces are dominant."

Most, if not all of the research described previously deals with intact rock. Problems involving sliding along the discontinuities have not been modeled with the centrifuge. The reason is that the shear behavior of a joint may be governed by the magnitudes of absolute displacement. If this is the case, then scaling may result in a loss of similitude as regards displacement related behavior. A future report will deal in detail with the scaling relations for both intact rock and jointed rock. Also included in that report will be suggestions for future research in rock mechanics (including problems in jointed rock masses), using the centrifuge.



### References

- Al-Hussaini, M.M., Goodings, D.J., Schofield, A.N. and Townsend, F.C. (1981), "Centrifuge Modeling of Coal Waste Embankments," ASCE, Journal of the Geotechnical Engineering Division, Vol. 107, No. GT 4, April.
- Almeida, M.S.S. and Parry, R.H.G., (1984), "Penetrometer Apparatus for Use in the Centrifuge During Flight," Proceedings of the Application of Centrifuge Modelling to Geotechnical Design, Editor W. H. Craig, University of Manchester.
- Almeida, M.S.S., Davies, M.C.R. and Parry, R.H.G. (1985), "Centrifuge Tests of Embankments on Strengthened and Unstrengthened Clay Foundations," Geotechnique, Vol. 35, No. 4, pp. 425-441.
- Andersen, G.A., (1987), "Tilting Response of a Centrifuge Model Gravity Retaining Wall to Seismic Shaking," Masters Thesis, M.I.T., Cambridge, Massachusetts.
- Anandrajah, A., Arulanandan, K. and Hutchinson, J.R. (1985), "Difficulties in the Simulation of Dynamic Events in a Centrifuge," Second Symposium on the Interaction of Non-Nuclear Munitions with Structures, Panama City, Florida.
- Arulanandan, K., Anandarajah, A., Abghari, A. (1982), "Centrifugal Modelling of Soil Liquefaction Susceptibility," ASCE, Journal of Geotechnical Engineering, Vol. 109, No.3, March.
- Barton, Y.O. (1984), "Response of Pile Groups to Lateral Loading in the Centrifuge," Proceedings of the Application of Centrifuge Modelling to Geotechnical Design, Editor W. H. Craig, University of Manchester.
- Bloomquist, D.G., Davisdon, J.L., and Townsend, F.C. (1984), "Platform Orientation and Start-up Time During Centrifuge Testing," Geotechnical Testing Journal, GTJ00J, Vol. 7, No. 4, Dec. 1984, pp. 195-199.
- Bolton, M.D. (1984), "The Development of Multi-Anchor Earth Retention Systems," Proceedings of the Application of Centrifugal Modelling to Geotechnical Design, Editor W. H. Craig, University of Manchester.
- Bolton, M.D. and Steedman, R.S. (1982), "Centrifuge Modelling of the Response of Microconcrete Retaining Walls subjected to Shaking." Proc. Conf. Soil Dynamics and Earthquake Eng., Southampton, 13-15 July, pp. 311-329.
- Bolton, M.D. and Steedman, R.S. (1984), "The Behavior of Fixed Cantilever Walls Subject to Lateral Shaking," Proceedings of the Application of Centrifuge Modelling to Geotechnical Design, Editor W. H. Craig, University of Manchester.
- Bucky, P.B. (1931), "Use of Models for the Study of Mining Problems," American Institution of Mining and Metallurgical Engineers, Tech. Pub. 425, 3-28.
- Cargill, K.W. and Ko, H.Y. (1984), "Centrifugal Modelling of Transient Water Flow," ASCE, Journal of Geotechnical Engineering, Vol. 109, No.4.

Caudel, R.D. and Clark, G.B. (1955), "Stresses Around Mine Openings in Some simple Geologic Structures," University of Illinois Engineering Experimental Standard Bulletin 430.

Chan, S.M.C. (1960), "Physical Properties Tests of Rock, Centrifugal Tests and the Design of Mine Openings," M.S. Thesis, University of Missouri School of Mines.

Cheney, J. (1982), "Introduction to Geotechnical Centrifuge Modelling," Proceedings of a Workshop on High Gravity Simulation for Research in Rock Mechanics, Colorado School of Mines, Department of Mining Engineering, Golden, Colorado.

Clark, G.B. (1980), "Investigation of Effects of Sample Size on Compressibility Coefficients," Report for Sandia Laboratories, New Mexico.

Clark, G.B. (1981), "Geotechnical Centrifuges for Model Studies and Physical Property Testing of Rock and Rock Structures," Colorado School of Mines Quarterly, Vol. 76, No. 4.

Clough, H.F., Vinson, T.S. (1985), "Ice Forces on Vertical Cylindrical Structures," Draft of Paper.

Clough, H.F., Wurst, P.L., Vinson, T.S. (1986), "Determination of Ice Forces with Centrifuge Models," Geotechnical Testing Journal, GTJODJ, Vol. 9, No. 2, 1986, pp. 49-60.

Craig, W.H. and Al-Saoudi, N.K.S. (1981), "The Behaviour of Some Model Off-shore Structures", Tenth ICSMFE, Vol. 1, pp. 83-88, Stockholm.

Craig, W.H. (1984), "Installation Studies for Model Piles," Proceedings of the Application of Centrifuge Modelling to Geotechnical Design, Editor W.H. Craig, University of Manchester.

Croce, P., Pane, V., Znidarcic, D., Ko, H.Y., Olsen, H.W. and Schiffman, R.L., (1984), "Evaluation of Consolidation Theories by Centrifuge Modelling," Proceedings of the Application of Centrifuge Modelling to Geotechnical Design, Editor, W.H. Craig, University of Manchester.

Davidenkova, N.N. (1936), "A New Method of Using Models for the Study of Equilibrium of Structures," Technical Physics of the USSR, Vol. III, No. 1, 1936, pp. 131-136.

Davis, M.C.R., and Parry, R.H.G. (1983), "Shear Strength of Clay in Centrifuge Models," ASCE, Journal of Geotechnical Engineering, Vol. 109, No. 10, October.

Dixon, J.M. (1975), "Finite Strain and Progressive Deformation in Models of Diapiric Structures," Tectonophysics, No. 26, pp. 89-124.

Dixon, J.M. and Summers, J.M. (1980), "A Centrifuged Model Study of the Tectonic Development of Archean Greenstone Belts," Geoscience Research Grant Program Summary of Research, 1979-80, Ontario Geological Survey, MP 93, pp. 58-71.

Dixon, J.M., and Summers, J.M. (1981), "A Centrifuged Model Study of the Tectonic Development of Archean Greenstone Belts," Geoscience Research Grant Program Summary of Research, 1980-81, Ontario Geological Survey MP 98, pp. 54-66.

Dixon, J.M. and Summers, J.M. (1982), "High-G Centrifuge Modelling of Geological Structures," Proceedings of a Workshop on High Gravity Simulation for Research in Rock Mechanics, Colorado School of Mines, Department of Mining Engineering, Golden, Colorado.

Esser, R.H.K, (1962), "A Model Study of the Application of Roof Bolts Under Unsymmetrical Loading Conditions," M.S. Thesis, University of Missouri School of Mines.

Ferguson, K.A., and Ko, H.Y. (1984), "Application of Centrifugal Modelling to Cone Penetrometer Technology," Proceedings of the Application of Centrifuge Modelling to Geotechnical Design, Editor, W.H. Craig, University of Manchester.

Fragaszy, R.J. and Cheney, J.A. (1981), "Drum centrifuge Studies of Overconsolidated Slopes", ASCE, Journal of the Geotechnical Engineering Division, Vol. 107, No. GT7, July.

Finn, W.D.L., Barton, Y.O., Tolohata, I. (1984), "Dynamic Lateral Response of Pile Foundations: Centrifuge Data and Analysis, " Proceedings of the Application of Centrifugal Modelling to Geotechnical Design, Editor, W.H. Craig, University of Manchester.

Gemperline, M.C. and Ko, H.Y. (1984), "Centrifugal Model Tests for Ultimate Bearing Capacity of Footings on Steep Slopes in Cohesionless Soils," Proceedings of the Application of Centrifugal Modelling, to Geotechnical Design, Editor, W.H. Craig, University of Manchester.

George, P.J. and Shaw, P.G.H. (1976), "Certification of Concrete Gravity Platforms in the North Sea", Offshore Technology Conference Paper OTC 2436.

Goodings, D.J. (1979), "Centrifugal Modelling of Slope Failures," Ph.D. Thesis, Cambridge University.

Goodings, D.J. (1984), "Relationships for Modelling Water Effects in Geotechnical Models," Proceedings of the Application of Centrifuge Modelling to Geotechnical Design, Editor, W.H. Craig, University of Manchester.

Gomah, A.H. (1963), "An Application of Photoelasticity to the Stability of Slopes," M.S. Thesis, University of Missouri School of Mines.

Halliday, D. and Resnick, R. (1981), "Fundamentals of Physics," John Wiley and Sons, Inc. pp. 816.

Harada, T. (1977), "A Study on Stability Analysis, Design and Construction of Rockfill Dams," Doctoral Thesis, Osaka City University.

Haycocks, C. (1962), "Mechanics of a Voussoir Arch," M.S. Thesis, University of Missouri School of Mines.

Hoek, E. (1965), "The Design of a Centrifuge for the Simulation of Gravitational Force Fields in Mine Models," Journal of South African Institute of Mining and Metallurgy, Vol. 65, No. 9.

Kimura, T., Kusakabe, O., Saitoh, K. (1984), "Undrained Deformation of Clay of which Strength Increases Linearly with Depth," Proceedings of the Application of Centrifugal Modelling to Geotechnical Design, Editor:, W.H. Craig, University of Manchester.

Kimura, T., Kusakabe, U., Saitoh, K. (1985), "Geotechnical Model Tests of Bearing Capacity Problems in a Centrifuge," Geotechnique, Vol. 35, No. 1, pp. 33-45.

Ko, H.Y., (1982), "Centrifuges and Soil Mechanics", Proceedings of a Workshop on High Gravity Simulation for Research in Rock Mechanics, Colorado School of Mines, Dept. of Mining Engineering, Golden, Colorado.

Kusakabe, O. (1982), "Stability of Excavations in Soft Clay," Ph.D. Thesis, University of Cambridge.

Kutter, B.L. (1982), "Centrifugal Modelling of the Response of Clay Embankments to Earthquakes," Ph.D. Thesis, Cambridge University.

Langhaar, H.L. (1951), "Dimensional Analysis and Theory of Models," John Wiley and Sons, New York.

Laut, P. (1975), "Application of Centrifugal Model Tests in Connection with Studies of Flow Patterns of Contaminated Water in Soil Structures," Geotechnique, Vol. 25, pp. 401-406.

Lyndon, A., Pearson, R. (1984), "Pressure Distribution on a Rigid Retaining Wall in Cohesionless Material," Proceedings of the Application of Centrifugal Modelling to Geotechnical Design, Editor, W.H. Craig, University of Manchester.

Mair, R.J. (1979), "Centrifugal Modelling of Tunnel Construction in Soft Clay," Ph.D. Thesis, University of Cambridge.

Mair, R.J., Phillips, R., Schofield, A.A.N. and Taylor, R.N. (1984), "Application of Centrifuge Modelling to the Design of Tunnels and Excavation in Soft Clays," Proceedings of the Application of Centrifugal Modelling to Geotechnical Design, Editor: W.H. Craig, University of Manchester

Malushitsky, Y.N. (1981), "The Centrifugal Model Testings of Waste Heap Embankments," English translation of Russian, 1975 edition, Cambridge University Press.

Marsal, R.J., Arellano, L.R. (1967), "Performance of El Infiernillo Dam," ASCE, SM4, pp. 265-297.

Mikasa, M., Mochizuki, A. and Matumoto, T. (1982), "Stability Test of a Rockfill Dam by Centrifuge," International Conference on Soil Mechanics and Foundation Engineering, pp. 475-478.

Nakase, A., Kusakabe, O., Wong, S.F. (1984), "Centrifuge Model Tests on Bearing Capacity of Clay," ASCE, Journal of Geotechnical Engineering, Vol. 110, No. 12, pp. 1749-1765.

Nunez, I.L. and Randolph, M.F. (1984), "Tension Pile Behavior in Clay - Centrifuge Modelling Techniques," Proceedings of the Application of Centrifugal Modelling to Geotechnical Design, Editor: W.H. Craig, University of Manchester.

Oldham, D.C.E. (1984), "Experiments with Lateral Loading on Single Piles in Sand," Proceedings of the Application of Centrifugal Modelling to Geotechnical Design, Editor: W. H. Craig, University of Manchester.

Oudenhoven, M.S. (1962), "A Model Study of the Behavior of Elastic Liners in Shallow Underground Openings," M.S. Thesis, University of Missouri, School of Mines.

Ovesen, N.K. (1975), "Centrifugal Testing Applied to Bearing Capacity Problems of Footings on Sand", Geotechnique, Vol. 25, No. 2, 394-401.

Padfield, C.J. and Schofield, A.N. (1983), "The Development of centrifugal Models to Study the Influence of Uplift Pressures on the Stability of a Flood Bank," Geotechnique, Vol. 33, No. 1, pp. 57-66.

Panek, L.A. (1949), "Design of Safe and Economical Structures," Transactions of the American Institute of Mining and Metallurgical Engineers, Vol. 181, pp. 371-375.

Panek, L.A. (1952a), "Centrifugal-Testing Apparatus for Mine-Structure Analysis," U.S. Bureau of Mines Report of Investigations 4883.

Panek, L.A. (1952b), "Centrifugal-Testing Apparatus for Mine-Structure Stress Analysis," U.S. Bureau of Mines Report of Investigations 4884.

Panek, L.A. (1956a), "Theory of Model Testing as Applied to Roof Bolting," U.S. Bureau of Mines Report of Investigations 5154.

Panek, L.A. (1956b), "Design of Bolting Systems to Reinforce Bedded Mine Roof," U.S. Bureau of Mines Report of Investigations 5155.

Panek, L.A. (1956c), "Principles of Reinforcing Bedded Mine Roof with Bolts," U.S. Bureau of Mines Report of Investigations 5156.

Panek, L.A. (1962a), "The Effect of Suspension in Bolting Bedded Mine Roof," U.S. Bureau of Mines Report of Investigations 6138.

Panek, L.A. (1962b), "The Combined Effects of Friction and Suspension in Bolting Bedded Mine Roof," U.S. Bureau of Mines Report of Investigations 6139.

Panek, L.A. (1982), *Proceedings of a Workshop on High Gravity Simulation for Research in Rock Mechanics*, Colorado School of Mines, Dept. of Mining Engineering, Golden, Colorado.

Phillips R. (1869), "Comptes Rendus de l'Academie des Sciences," Paris, Jan-June, p. 68.

Phillips, R., (1982), "Trench Excavations in Clay," M. Phil. Thesis, University of Cambridge.

Phillips, R. (1984), "Forthcoming Ph.D. thesis," University of Cambridge.

Pokrovsky, G.I. (1933), "Zeitschrift for Technische Physics," Vol. 14, No. 4.

Pokrovsky, G.I. and Fyodorov, I.S. (1936), "Studies of Soil Pressures and Deformations by Means of a Centrifuge," *Proceedings, 1st. Int. Conf. on Soil Mech.*, Vol. 1., No. 70.

Prevost, J.H. Cuny, B. and Scott, R.F. (1981), "Offshore Gravity Structures: Centrifugal Modeling," *ASCE, Journal of the Geotechnical Engineering Division*, Vol. 107, No. GT2.

Ramberg, H. (1968a), "Instability of Layered Systems in the Field of Gravity, I." *Phys. Earth Planet Int.*, V.1, pp. 427-447.

Ramberg, H. (1968b), "Instability of Layered Systems in the Field of Gravity, II." *Phys. Earth Planet, Int.*, V. 1, p. 448-474.

Ramberg, H. (1972), "Inverted Density Stratification and Diapirism in the Earth: *Journal of Geophysical Research*, Vol. 77, p. 877-989.

Rowe, P.W. (1975), "Displacement and Failure Models of Model Offshore Gravity Platforms founded on Clay", *Conf. Offshore Europe 75*, pp. 218, 1-17, Spearhead Publications, Aberdeen.

Rowe, P.W. and Craig, W.H. (1976), "Studies of Offshore Caissons founded on Oosterschelde Sand", *Conf. on Design and Construction of Offshore Structures*, pp. 49-55, Inst. of Civil Engineers, London.

Rowe, P.W. and Craig, W.H. (1978), "Predictions of Caisson and Pier Performance by Dynamically Loaded Centrifugal Models", *Symp. on Foundation Aspects of Coastal Structures*, Paper IV.3, pp. 1-16.

Rowe, P.W. and Craig, W.H. (1980), "Application of Models to the Prediction of Offshore Gravity Platform Foundation Performance", *Int. Conf. on Offshore Site Investigation*, pp. 269-281, Graham and Trotman, London.

Sabagh, S.K. (1984), "Cyclic Axial Load Tests on Piles in Sand," *Proceedings of the Application of Centrifugal Modelling in Geotechnical Design*, Editor: W.H. Craig, University of Manchester.

Schmidt, R.M. and Holsapple, K.A. (1980), "Theory and Experiments on Centrifuge Cratering," *J. Geophysics. Res.* 85(B1), 235-252.

Scott, R.F. (1979a), "Cyclic Lateral Loading of Piles, Analysis of Centrifuge Tests," Research Program for API-OASAPR, Project 13. Calif. Inst. Tech.

Scott, R.F. (1979b), "Cyclic Static Model Pile Tests in a Centrifuge," Proc. 11th Offshore Technology Conference, pp. 1159-1168, Paper OTC 3492.

Scott, R.F. (1981), "Pile Testing in a Centrifuge," Proc. 10th Int. Conf. on S.M.F.E., Stockholm, Vol. 2, pp. 839-842.

Stephansson, O. (1971), "Stability of Single Openings in Horizontally Bedded Rock," Engineering Geology, Vol. 5, pp. 5-71.

Stephansson, O. (1982), "Stability of Single Openings in Horizontally Bedded Rock," Proceedings of a Workshop on High Gravity Simulation of Research in Rock Mechanics, Colorado School of Mines, Department of Mining Engineering, Golden, Colorado.

Sutherland, H.J. (1982), "Centrifuge Simulations of the Subsidence Over Coal Mines and the Stability of Tailings Dams," Proceedings of a Workshop on High Gravity Simulation for Research in Rock Mechanics, Colorado School of Mines, Department of Minings Engineering, Golden, Colorado.

Sutherland, H.J. and Rechard, R.P. (1984), "Centrifuge Simulations of Stable Tailing Dam," ASCE, Journal of Geotechnical Engineering, Vol. 110, No. 3, March.

Tan, T.F. and Scott, R.F. (1985), "Centrifuge Scaling Considerations for Fluid-Particle Systems," Geotechnique, Vol. 35, No. 4, pp. 461-470.

Taylor, R.N. (1979), "Stand-up of a Model Tunnel in Silt," M. Phil. Thesis, University of Cambridge.

Taylor, R.N. (1984), "Grand Movements associated with Tunnels and Trenches," Ph.D. Thesis, University of Cambridge.

Trott, J.J., Taylor, R.N. and Symons, I.F. (1984), "Tests to Validate Centrifuge Modelling of Flexible Pipes," Proceedings of the Application of Centrifugal Modelling to Geotechnical Design, Editor: W.H. Craig, University of Manchester.

Vinson, T. S. (1982), "Ice Forces on Offshore Structures," Proceedings of a Workshop on High Gravity Simulation for Research in Rock Mechanics, Colorado School of Mines, Department of Mining Engineering, Golden, Colorado.

Wang, C.S., Boshkov, S.H. and Wane, M.T. (1967), "The Application of Barodynamic Photostress Techniques to the Study of the Behavior of Rock Beams Loaded by Their Own Weight," 9th Symp. on Rock Mech., Am. Inst. of Metallurgical Engineers.

Whitman, R.V. (1984), "Experiments with Earthquake Ground Motion Simulation," Proceedings of a Symposium on the Application of Centrifuge Modelling to Geotechnical Design, Editor: W. H. Craig, University of Manchester.